UCLouvain

AGRO LOUVAIN

Faculté des bioingénieurs

Assessing Land Use/Land Cover Change Detection Algorithms using Sentinel-2 Satellite Time Series from 2018 to 2022

Auteur : Sraboni Sarker

Promoteur (s) : Pierre Defourny

Co-promoteur (s): Céline Lamarche

Audric Bos

Lecteur(s) : Sophie Bontemps

Quentin Ponette

Année Académique : 2023 - 2024

Mémoire de fin d'études présenté en vue de l'obtention du diplôme de Master SAIV – MSc Erasmus+ GEM : Geo-information Science and Earth Observation for Environmental Modelling and Management

Acknowledgement

First and foremost, I am profoundly grateful to God for being my constant source of strength, inspiration, wisdom, and knowledge throughout my academic journey. His unwavering presence has guided me every step of the way.

I would like to express my profound sense of gratitude to my respected supervisor Professor Pierre Defourny, for his indispensable and expert guidance, direct concern, constructive criticism, and inspiration throughout this thesis. Then, I would like to express my immense gratitude to my co-supervisors Céline Lamarche and Audric Bos for their continuous support, prompt replies, technical expertise, and pragmatic look which made it possible to develop the framework of this research.

I would like to thank Erasmus Mundus Joint Masters scholarship for hosting me conducting my master's under the GEM program. I am grateful to my current institution 'Université Catholique de Louvain' and my former educational institution 'Lund University' for providing the foundation in geo-informatics, including GIS/geospatial analysis, remote sensing, and ecosystem modelling and dynamic process-based spatial models.

I am deeply grateful to my beloved parents and sister for their continuous mental support and motivation throughout this journey. Despite not being physically present with me during my studies abroad, their love, understanding, and unwavering support have been my constant motivation.

Later, I want to thank my colleagues in the GEM program for their friendship, intellectual discussions, and the sense of community we shared. Their support and friendship made the journey more enjoyable and enriched my learning experience.

Finally, I am particularly grateful to myself for the passion, dedication and perseverance I put into this research. Without my self-motivation and commitment, completing this thesis would be difficult.

Table of Contents

List of Figures

List of Tables

List of Acronyms

ARD	Analysis Ready Data
BFAST	Breaks For Additive Seasonal and Trend
BFASTm	Breaks For Additive Seasonal and Trend Monitor
CCDC	Continuous Change Detection and Classification
CEOS	Committee on Earth Observation Satellites
CMFDA	Continuous Monitoring of Forest Disturbance Algorithm
CMFDA	Continuous Monitoring of Forest Disturbance Algorithm
COLD	Continuous Monitoring of Land Disturbance
CONUS	Conterminous United States
EEA	European Environment Agency
EIONET	European Environment Information and Observation Network
EO	Earth Observation
ERIC	European Research Infrastructure Consortium
EWMACD	Exponentially Weighted Moving Average Change Detection
FAO	Food and Agriculture Organization
FN	False Negative
FP	False Positive
GAUD	Global Annual Urban Dynamics
GEE	Google Earth Engine
GIS	Geographic Information System
GMW	Global Mangrove Watch
LandTrendr	Landsat-based Detection of Trends in Disturbance and Recovery
LCMAP	Land Change Monitoring, Assessment, and Projection
LPV	Land Product Validation
LULC	Land use/land cover
LULUCF	Land-Use Change and Forestry
MLC	Maximum Likelihood Algorithm
MODIS	Moderate Resolution Imaging Spectroradiometer
NAFD	North American Forest Dynamics
NAIP	National Agricultural Imagery Program

NDVI	Normalized Difference Vegetation Index
NIR	Near Infra-Red
NN	Neural Networks
OA	Overall Accuracy
OB	Object-based
OB-COLD	Object-Based Continuous monitoring of Land Disturbance
PA	Producers' Accuracy
PLCC-INSPIRE	INSPIRE Pure Land Cover Components
RF	Random Forest
RMSE	Root Mean Squared Error
SAR	Synthetic Aperture Radar
SCL	Scene Classification
SVM	Support Vector Machines
TN	True Negative
TOA	Top-Of-Atmosphere
TP	True Positive
TSCCD	Time-Series Classification approach based on Change Detection
UA	Users' Accuracy
UN	United Nations
VCT	Vegetation Change Tracker
VNIR	Vegetation Red Edge

Chapter 1: Introduction

Globally, environmental issues have grown significantly since the Industrial Revolution. Land use/land cover (LULC) changes are the most basic and prominent landscape characteristic describing the impact of anthropogenic disturbance on the surface of the Earth and play an important role in the studies of regional and global environmental changes (Quintero-Gallego et al., 2018). Alterations in land conditions, whether from human activities or climate change, subsequently influence regional and global climates (Shukla et al., 2019). Historical land cover changes have contributed to the increase in atmospheric CO_2 content and thus to global warming (Jia et al., 2020). The terms "land use" and "land cover" have varying degrees of significance. The term "land cover" refers to the physical cover that is observed on the surface of the earth, which includes both naturally occurring and artificially created vegetation (FAO, 2024). According to the United Nations (UN) framework, land cover is important because it affects disaster risk reduction, food security, biodiversity conservation, sustainable development, and climate change. Land use categories are defined as the activities that occur on the land that reflect the properties' current use, such as built-up institutions, shopping malls, parks, and reservoirs (Fonji and Taff, 2014).

Over the last few decades, the use of GIS and remote sensing technologies has increased the significance of LULC change assessment (Reid et al., 2000). Due to the importance of monitoring change in Earth’s surface features, research of change detection techniques is an active topic, and new algorithms are constantly being developed. Good change detection algorithms can provide information about the area change and change rate and the spatial distribution of changed types. In evaluating these surface alterations on Earth, the selection of the most suitable method and algorithm for change detection is not easy in practice (Lu et al., 2004). Different change detection algorithms have been introduced in the past, depending on the remote sensing imagery (Weng, 2001; Araya and Hergarten, 2008; Franklin et al., 2015).

The Landsat program is the longest-running enterprise for the acquisition of satellite imagery of Earth, which eventually provided better spatial and temporal resolution data. After that, the Copernicus programme, launched the multispectral instruments Sentinel-2 satellites, which provides high-resolution satellite data with higher spatial and temporal resolution for LULC monitoring, climate change and disaster monitoring (Phiri et al., 2020). So, having both high spatial and temporal resolution makes it easier to track accurately, and understand how

land cover changes over time while accounting for both detailed spatial details and observation frequency.

Nevertheless, free and open access remote sensing data, such as the Landsat archive is freely available since 2008, enabling dynamic analysis in both space and time, allowing multidimensional data-based and then Sentinel-2 satellite data to escalate the process. Since then, research to detect changes in LULC has increased based on time series of satellite images (Wulder et al., 2012; Lunetta et al., 2006). Many time series based change detection have been developed using Landsat images focusing on LULC changes (Verbesselt et al., 2010; Jin et al., 2013; Hilker et al., 2009; Zhu et al., 2020).

Most of the time-series analysis-based LULC change algorithms proposed in the remote sensing community perform well on datasets for which they were designed, but their effectiveness on datasets selected at random from around the world has not been investigated (Saxena et al., 2018). According to European statistics (EEA, 2017) only 1.6% of land cover type has changed during the 2006–2012 period. This number covers 39 countries which span over 5.86 million km^2. Statistically, Belgium has one of the lowest mean annual land cover rates in all of Europe. Only about 30 km^2, or 0.1% of the total area, is changed to a different land cover class each year (EEA, 2017). A study was carried out in Wallonia, Belgium by Radoux et al. (2022) using orthophotos data to produce a dataset to provide land cover information through 13 classes. However, LULC information was not used to cross the dataset, and orthophotos could have been replaced as they are not frequently acquired. There is no comprehensive study implemented in the Wallonia region, Belgium, where different LULC change detection algorithms have been performed together and benchmarked.

In this context, this master thesis aims to select a couple of state-of the-art LULC change detection algorithms and explore the potential of Sentinel-2 data from 2018 to 2022 for testing the accuracy. This work will explore the performances of the algorithms in a local context in Wallonia, Belgium. It will review relevant scientific literature, and describe the materials and methods used to achieve the better-performing algorithm. As a final result, LULC change maps of Wallonia from different LULC change detection algorithms will be presented, discussed and evaluated following accuracy assessment protocol both qualitative and quantitative to ensure their validity.

Chapter 2: Literature Review

This chapter will provide an overview of the current state-of-the-art scientific knowledge about LULC change and different change detection algorithms. LULC classification techniques are reviewed in Section 2.1. In section 2.2, different LULC change detection algorithms are reviewed briefly. Finally, accuracy assessment procedures for the validation will be discussed here in section 2.3.

2.1. Land Use Land Cover Classification Techniques

The LULC classification is the process of appointing LC classes to pixels and categorizing them like water, urban area, woodland, shrub land, agriculture, grasslands, mountains, etc. (Anderson, 1976). In addition to single-date LULC classification, it is necessary to observe the continuous process of LULC patterns over an extended period (Hamad, 2020).

2.1.1. Maximum Likelihood Supervised Classification

Chughtai et al. (2021) reviewed many papers on LULC classification methods and concluded that the Maximum likelihood classification algorithm (MLC) was the mostly used by researchers (69%), followed by object-based (13%), minimum distance (5%), Support Vector Machine (5%) and others. MLC is one of the most popular supervised classification methods used with remote sensing image data. This method is based on the probability that a pixel belongs to a particular class (Rawat and Kumar, 2015).

Different studies have been conducted using the MLC technique to classify the LULC changes. Dewan and Yamaguchi (2009) used the MLC technique to derive LULC classification in a multi-temporal approach to detect LULC changes in Dhaka Bangladesh. MLC was subsequently applied to each image which has generally been proven to obtain the best results from remotely sensed data. Abd El-Kawy et al. (2011) used MLC, which was applied to four Landsat images collected over time (1984, 1999, 2005, and 2009) that provided recent and historical LULC conditions for the western Nile delta. Few studies found that urban expansion has increased causing loss to other land cover types, where MLC has been used for image classification to observe the expanded urban areas (Rahman et al., 2012; Fichera et al., 2012; Prabu and Dar, 2018). However, traditional techniques, such as a MLC, have failed to produce a product with sufficient accuracy with high-resolution data (Balha and Singh, 2023; Otukei and Blaschke, 2010).

2.1.2. Random Forest Classification

The Random Forest (RF) method can produce a highly accurate classification compared with other commonly used methods (McInerney and Nieuwenhuis, 2009; Rodriguez-Galiano et al., 2012). Even it outperforms other classification approaches, like Support Vector Machines (SVM), and Neural Networks (NN) (Balha and Singh, 2023; Dye et al., 2011). Besides, it is more robust to outliers and noise (Gislason et al., 2006; Breiman, 2001).

Halmy et al. (2015) used the RF method to classify the Thematic Mapper Landsat 5 data and ancillary data for predicting future changes in the north-western coastal desert of Egypt. The performance of the classification was with an overall accuracy of more than 90%. Moreover, the RF classifier predicted the LULC distribution effectively before and after LULC changes. Svoboda et al. (2022) tested the RF classifier for Land Use, Land-Use Change and Forestry (LULUCF) classification in Czechia. The RF classifier was able to correctly classify the surfaces with an OA of 89.1%. The developed method is based on the classification of Sentinel-2 data using the RF classifier in the cloud-based platform Google Earth Engine (GEE).

RF classification generally provides better results for high-resolution data. Hayes et al. (2014) conducted a study using the ensemble RF classifier to classify land cover at 1 m resolution using 2009 National Agricultural Imagery Program (NAIP) imagery in south-eastern Wyoming. The performance was evaluated by an OA of 81% and a kappa coefficient of 79%. Apart from them, it has also been used in different time-series LULC change detection algorithms mentioned in the next section, where this classifier got higher accuracy (Wu et al., 2020; Zhu et al., 2019; Zhu and Woodcock, 2014).

2.2. LULC Detection Algorithms

2.2.1. Image Differentiating Change Detection Algorithms

The early common methods, which are quite simple and straightforward, include image differencing, principal component analysis, post-classification comparison, and change vector analysis (Bruzzone et al., 2004; Lu et al., 2004). These techniques work on the basis that changes are typically identified by comparing the variations between image reflectance taken at two distinct times. The post-classification methods, which compare the class maps from independent classification, are more popular in practical applications (Ahlqvist, 2008; Yuan et al., 2005). Chughtai et al. (2021) reviewed different papers based on post-classification change detection methods at a regional level.

The authors mentioned that Kusimi (2008) assessed LULC change in the Wassa West district of Ghana. Supervised classification MLC was used to perform the post-classification change detection technique and found the reduction of primary forest which covered 88% of the study area was reduced to 69% during the study period. Weng (2001) evaluated urban expansion and its impact on surface temperature in the Zhujiang Delta, China. Post-classification change detection was proposed to identify qualitative and quantitative change. Supervised classification MLC was used for urban expansion. Shen et al. (2011) analyzed urban LULC changes in Beijing, China during the study period using supervised classification MLC to extract quantitative LULC information. The post-classification change detection technique was applied to detect LULC changes resulting in the reduction of water due to climate, hydrology, and urbanization during the study period. Petit et al., (2001) quantified the LULC changes and future prediction of LULC changes in the region of Lusitu, southern province of Zambia. Multispectral spot satellite imagery was used to observe land cover information using post-classification. This study results in a huge expansion in the agriculture sector after implementing the MLC. The overall accuracy for almost all of the studies using Post-classification approaches to detect LULC changes reviewed by Chughtai et al. (2021) was higher than 80% (Fichera et al., 2012; Halimi et al. 2018).

Although most of the available change detection algorithms are pixel-based, change detection has also been approached using object-based logic (Araya and Hergarten, 2008). Object-based (OB) change detection techniques are more frequently used because of their advantages over the other techniques in the analysis of high-resolution images. Accuracy assessment and the results using OB change detection techniques are quite prominent (Albrecht et al., 2010, Hernando et al., 2012, Lein, 2012). Desclée et al. (2006) used the OB-Reflectance method which is object-based and statistically driven to identify forest land cover changes in both deciduous and coniferous stands in the Eastern part of Belgium using three SPOT-HRV images. It was found that the OB methods were higher than pixel-based methods. The results proved the method very efficient with higher overall accuracy (> 90%) and Kappa (> 0.80). Then, Bontemps et al. (2009) also tested the OB change detection algorithm through a multi-year application on the tropical forest of Borneo, using SPOT-VEGETATION time series from 2000 to 2008 and concluded that this algorithm can efficiently monitor forest changes at a global scale on a yearly basis.

2.2.2. Time Series Analysis based Land Use/Land Cover Change Detection Algorithms

Verbesselt et al. (2010) proposed a generic change detection approach named Breaks For Additive Seasonal and Trend (BFAST) to detect and characterize time series. BFAST iteratively estimates the time and number of changes and characterizes change by its magnitude and direction. In this study, the approach was validated by simulating 16-day Normalized Difference Vegetation Index (NDVI) time series from 2000 to 2008 in forested regions of southeastern Australia, which are dominated by temperate broadleaf forests. BFAST performed well in decomposing the NDVI time series and fitted seasonal, trend and remainder components. Forest plantation changes can be identified using BFAST. It remained unaffected by variations in the seasonal component's amplitude and is resistant to noise. It was proposed that various kinds of remotely sensed time series could be analyzed using BFAST (Landsat).

In a review paper, Zhu (2017) mentioned that a modified version named BFAST Monitor (BFASTm) algorithm has been applied to Landsat time series for detecting forest change (DeVries et al., 2015; Dutrieux et al., 2015; Reiche et al., 2015). Then, the BFASTm was used to detect drought-related vegetation disturbance in near real-time using MODIS time series (Verbesselt et al., 2012).

Wu et al. (2020) found that the BFAST algorithm was able to capture well the changes related to the Donting Lake region, the second-largest freshwater lake and one of the major grain production areas in China. In this study, monthly Landsat NDVI time series were used. Then, spatiotemporal variations of forests were also investigated between 2000 and 2018. Here, the RF classifier was used to classify the LULC classes before and after the changes. The result showed that the forest change is more frequent in the core zone than in the transition zone, and most changes occurred in the areas with DEM ranging from 20 to 40 m. The performance of the algorithm was assessed using an error matrix, where the Producers' Accuracy and Users' Accuracy were 90.7% and 84.3%, respectively with 87.8% of OA.

Another interesting LULC change detection algorithm was introduced and named the Landsat-based Detection of Trends in Disturbance and Recovery (LandTrendr) in the LULC change detection research. The core of the algorithm is a temporal segmentation of Landsat time series allowing the extraction of spatial patterns of land cover change magnitude, change duration, and year of change. The LandTrendr algorithm was initially tested in forest disturbance and recovery detection in the Pacific Northwest of the United States of America, western Oregon, and Washington by Kennedy et al. (2010). The findings of their study confirmed that the model

outperformed the bi-temporal change detection previously carried out by Cohen et al., (1998) in tracking forest disturbance and detecting other trends related to forest phenology and regrowth in the same study area. A growing number of studies have subsequently proven the effectiveness of LandTrendr algorithms in investigating the patterns of forest disturbance and recovery (Fragal et al., 2016; Cohen et al., 2018). Furthermore, trends in mining-induced land cover change based on GEE-LandTrendr were successfully tracked respectively in Richards Bay Minerals Site, South Africa (Yang et al., 2018), and in central east Queensland, Australia (Mugiraneza et al., 2020).

Mugiraneza et al., 2018 tested a GEE-LandTrendr cloud-computing framework based on Landsat time series and LandTrendr stacked bands and indices for reconstructing annual land cover maps in Kigali, Rwanda. A SVM classification was first performed on the two Landsat scenes, respectively, acquired in 1987 and 2019. A scheme of five different land cover classes was selected to understand the urbanization phenomena. They explored that reconstructed land cover based on Landsat time series and GEE-LandTrendr was considerably cost-effective for continuous urban land cover change monitoring, especially for sub-Sahara Africa where data is sparse, and concerns are high regarding EO data affordability.

Zhu et al. (2019) applied the LandTrendr algorithm to monitor long-term (1998–2018) cropland change patterns in Dongting Lake, China, in which original lake areas reclaimed for cropland were converted back to lake or cultivation areas. It played an important role in identifying cropland abandonment and re-cultivation based on annual time series of cropland probabilities. LandTrendr based on GEE detected cropland change more efficiently with the advantages of cloud computing offering an opportunity to map large-scale cropland change (Schneibel et al., 2017; Dara et al., 2018; Shelestov et al., 2017). Zhu et al., (2019) detected and mapped using RF classification the conversion of cropland to lake and poplar cultivation with overall accuracies of 87.0% and 83.8%.

Zhu et al., (2012) developed a change detection algorithm at high temporal frequency particularly for continuous forest disturbance using all available Landsat 7 images, named Continuous Monitoring of Forest Disturbance Algorithm (CMFDA). CMFDA uses Landsat images to estimate surface reflectance model for each pixel. Here two different approaches (single-date and multi-date differencing) have been used regarding how many dates, or comparisons, to use at a Savannah River site sharing border between Georgia and South Carolina with a variety of land covers. Due to the higher spatial and temporal accuracies, the

multi-date differencing algorithm was chosen as the final CMFDA product. It determines a disturbance pixel by the number of times “change” is observed consecutively. Pixels showing change for one or two times will be flagged as the probable change and if a third consecutive change is found, the pixel is assigned to the “change” class. The algorithm performance was assessed with an error matrix with 99.76% overall accuracy.

Zhu and Woodcock (2014) introduced to Continuous Change Detection and Classification (CCDC) algorithm to detect different kinds of continuous land cover changes using all available Landsat images. It is a time series model which is updated every time a new image is collected. Generally, three different categories of surface change, intra-annual, gradual inter-annual and abrupt changes are captured by different components of trend, seasonality and breaks. In this algorithm, if a pixel is observed to change in three consecutive observations, the pixel is defined as a “change” class. The Root Mean Squared Error (RMSE) is computed for each spectral band, and the difference between observations and model predictions for each Landsat band is normalized by three times the RMSE. CCDC algorithm classifies land cover before and after the change occurred using the RF classifier. It uses the coefficients of time series models as the inputs for land cover classification. The performance of CCDC was assessed using a random stratified sample design with 97.72% producer accuracy and 85.60% user accuracy. CCDC has been used and combined with other methods and algorithms in different research, as it is one of the most widely used algorithms to determine land cover changes (Awty-Carroll et al., 2019; Tollerud et al., 2023).

Another algorithm was introduced by Brown et al. (2020) based on CCDC to monitor land surface changes called Land Change Monitoring, Assessment, and Projection (LCMAP) using Landsat ARD. The main objective of developing this algorithm was to address several challenges of the CCDC algorithm (Zhu and Woodcock, 2014) to meet the goals of robust, repeatable, and geographically consistent monitoring results from it over six diverse study areas across the United States. In LCMAP, the CCDC was modified so that change detection can be dependent on the observational frequency and can improve its ability to characterize gradual land surface changes. Besides, to improve the representativeness of training data, the RF classifier was replaced with a boosted decision tree and got overall agreement from 85% to 90%.

Recently, Zhu et al. (2020) introduced an algorithm named Continuous Monitoring of Land Disturbance (COLD) using Landsat time series to detect different kinds of land disturbances in

the forest areas in the US. COLD is also developed upon the CCDC algorithm. In this algorithm, time series from Landsat ARD provides comparatively better detection results. The algorithm got higher accuracy when the consecutive anomaly observations increased from four to six and decreased when consecutive anomaly observations increased to seven. Therefore, six consecutive anomaly observations are used to confirm a change. COLD showed reliable performance with 73% producer accuracy and 72% user accuracy against different land disturbance types.

Awty-Carroll et al. (2021) used the COLD algorithm in five different mangroves throughout the world. The study aimed to identify whether the approach was transferable for the long-term monitoring of mangrove extent and trend despite having limited data availability from satellites due to cloud cover. In this study, the Global Mangrove Watch (GMW) Version 2.0 dataset was used for data validation. The GMW provides a highly accurate global mangrove baseline for 2010 (Bunting et al., 2018). The performance of the algorithm was assessed by the OA of 92.7% with a UA of 77% for the mangrove class. Therefore, the COLD approach outperformed in mapping historical mangrove extent globally along with providing high-quality mapping summarized on an annual basis while also accounting for seasonal changes.

Generally, it makes sense to assume that, in the event of a disturbance, a pixel undergoing spectral changes will be accompanied by synchronized spectral changes in its neighboring pixels, forming a change object. Ye et al. (2023) succeeded in developing a novel algorithm named “Object-Based Continuous monitoring of Land Disturbance” (OB-COLD) identifying land disturbances. This algorithm has been tested in the United States and may be able to better utilize spatial contexts, which are frequently disregarded, for dense time-series analysis. The LCMAP reference dataset was used for validation, as this dataset (Stehman et al., 2021) has no bias for specific land cover types. According to the accuracy assessment, the OB-COLD achieved a producer accuracy of 76.9%, which is 16.3% higher than COLD (Zhu et al., 2020). Besides, user accuracy was also comparable between OB-COLD and COLD approaches with 58.7% and 57.8%, respectively.

An advanced framework of the multifaceted view of land change through the lens of remote sensing was proposed by Zhu et al. (2022). The first two facets of “Time” and “Location” provide information on the detection and monitoring of land change, and the other three facets of “Target”, “Metric”, and “Agent” are related to the characterization of land change. The

impacts of spatial, spectral, temporal, and angular domains of the remotely sensed data on the observation, monitoring, and characterization of land change were also evaluated.

In this paper, Zhu et al. (2022) mentioned that most of the large-scale land change products in the case of high resolution (10-30m) are only focusing on a single change target, such as changes in forest, urban, or water. For example, Hansen et al. (2013) created the 2000–2019 global 30-m forest cover and forest cover change (i.e., forest loss and forest grain) products based on time series spectral metrics of Landsat data and a supervised classification approach. The North American Forest Dynamics (NAFD) project implemented the Vegetation Change Tracker (VCT) algorithm (Huang et al., 2010) to produce annual forest disturbance maps for the conterminous United States (CONUS) from 1986 to 2010 based on annual Landsat time series data (Zhao et al., 2018). Liu et al. (2020) created a 30-m Global Annual Urban Dynamics (GAUD) dataset to provide information on urban expansion and green recovery from 1985 to 2015 based on existing global urban extent maps and Landsat time series data. Only a few products can provide information on land change on different kinds of land surfaces. Recently, Friedl et al. (2022) have also created annual global land cover change maps between 2000 and 2020 based on the Landsat time series. Among all these products, LCMAP (Brown et al., 2020), and LANDFIRE (Rollins, 2009) are some of the few land change products that not only can provide change location and time, change target, but also land change metrics, or even land change agent information.

A different kind of project named “MapBiomas” (Brasil) was launched in July 2015, aiming to develop a fast, reliable, collaborative, and low-cost method to process large-scale datasets and produce an annual time series of Brazil's land cover and land use maps. The LULC annual maps produced in this project were based on the Landsat archive available in the GEE platform, encompassing the years from 1985 to the present. Here, a RF classifier was used for each year (Breiman, 2001) for the entire territory based on the training dataset of that year. Post-classification was also performed to create the final product. The accuracy was assessed by following the good practices proposed by Olofsson et al. (2014).

A few comparative studies have been conducted based on different time-series algorithm to assess their performances. Yan et al., 2019 proposed a Time-Series Classification approach based on Change Detection (TSCCD) for rapid LULC mapping and compared the results with BFAST, LandTrendr, and CCDC. TSCCD outperformed these three algorithms in detecting large and subtle changes, overall in time-series change detection with high overall accuracy.

Another study was conducted by Saxena et al., 2018, where the performance of a TSA-based 'polyalgorithm' for LULCC including three algorithms (BFAST, Exponentially Weighted Moving Average Change Detection (EWMACD), and LandTrendr) were assessed against these algorithms individually. The polyalgorithm yields more accurate results than EWMACD and LandTrendr alone, but counterintuitively not better than BFAST alone.

Radoux et al., (2022) designed a database for Wallonia, Belgium using remote sensing images (orthophotos and Sentinel-1&2) at 2 m resolution. The dataset was created as part of Belgium's Lifewatch-ERIC, the European Research Infrastructure Consortium, contributing to ecosystem and biodiversity research. Apart from that, the monitoring of small-scale forest plantations was reported to be successful using Sentinel-2 in the Tanintharyi region in Myanmar (Nomura and Mitchard, 2018). Giannetti et al. 2021 estimated Windstorm Damaged Forest Area in Italy Using Time Series Sentinel-2 Imagery and Continuous Change Detection Algorithms and got an overall accuracy of more than 89.7%. Close et al. (2021) also tested the most commonly used change detection techniques to evaluate the capability of Sentinel-2 data in analyzing land conversion associated with LULC. The study was carried out in Wallonia, Belgium and they mentioned that Sentinel-2 has great potential for LULC change detection analysis.

However, Landsat has a longer historical archive that is useful for long-term research and trend analysis. Ultimately, the choice between Sentinel-2 and Landsat depends on the specific requirements of the land cover change detection algorithms, including the magnitude of change, desired level of detail, and required time frequency of monitoring. Most of the time series-based LULC change detection algorithms were developed using Landsat time series. Sentinel-2 has higher spatial resolution, which helps to detect small changes and obtains more detailed information about LULC at a fine scale. Therefore, higher temporal resolution can play an important role in monitoring dynamic changes such as seasonal variations and rapid changes in land cover. In addition, Sentinel-2 has improved cloud detection and atmospheric correction capabilities.

2.3. Accuracy Assessment

Classification accuracy assessment is important in LULC change detection because it ensures the change detection in different LULC classes with precision. Besides, it can help in understanding how changes are happening and affecting the overall environmental health. Overall, it enhances the reliability of the algorithms for detecting the LULC changes.

Statistically robust and transparent approaches for assessing accuracy and estimating areas of change are critical to ensure the integrity of land change information. All papers related to LULC and LULC changes follow the validation guidelines of the Committee on Earth Observation Satellites (CEOS). CEOS Land Validation subgroup (of the Working Group Calibration and Validation) provides a hierarchy of validation stages which are used for assessing the data products developed from EO (CEOS, 2023). The highest validation stage was reached for satellite-derived land cover products.

Olofsson et al. (2014) recommended good practices for the accuracy assessment of a change map and estimating area based on the reference sample data based on The CEOS Land Product Validation (LPV) subgroup. Here accuracy assessment methodology was separated into three major components, the response design, sampling design, and analysis. The objectives of sampling design commonly specified are to estimate OA, UA (or commission error), PA (or omission error), and the area of each class. A recommended good practice sampling design stratified random sampling is a practical design that satisfies the basic accuracy assessment objectives and most of the desirable design criteria.

In the context of studies of land change, there are two key objectives of the analysis: 1) accuracy assessment of the change classification, and 2) estimation of the area of change. In this case, the error matrix plays a crucial role. The error matrix is a simple cross-tabulation of the class labels allocated by the classification of the remotely sensed data against the reference data for the sample sites. The cell entries and marginal values of the error matrix are fundamental to both accuracy assessment and area estimation.

Table 1: Error matrix with p_{ij} representing the proportion of area in the mapped land cover category i and the reference land cover category j (Source: Liu et al., 2007)

Classified	Reference				
	1	2	…	*m*	Total
1	p_{11}	p_{12}	…	p_{1m}	p_{1+}
2	p_{21}	p_{22}	…	p_{2m}	p_{2+}
.	.	.	…	.	.
.	.	.	…	.	.
m	p_{m1}	p_{m2}	…	p_{mm}	p_{m+}
Total	p_{+1}	p_{+2}	…	p_{+m}	

From the error matrix, several measures of classification accuracy can be calculated using Equations. (1)–(6) (Maxwell and Warner, 2020). Besides, the area of each class according to the classification determined from the reference can be estimated.

Overall Accuracy = $\frac{Number\ of\ correctly\ classified\ samples}{Number\ of\ Total\ samples}$ …… (1)

Producer's Accuracy = $\frac{Number\ of\ correctly\ classified\ samples\ in\ category}{Number\ of\ samples\ from\ reference\ data\ in\ category}$ …… (2)

User's Accuracy = $\frac{Number\ of\ correctly\ classified\ samples\ in\ category}{Number\ of\ samples\ classified\ to\ that\ category}$ ……..... (3)

Commission Error = 1 - User Accuracy ……...(4)

Omission Error = 1- Producer Accuracy ……..……....(5)

The Kappa is the proportion of agreement after chance agreement is removed (Rosenfield & Fitzpatrick-Lins, 1986).

Kappa Statistic = $\frac{Overall\ Accuracy - Estimated\ Chance\ Agreement}{1 - stimated\ Chance\ Agreement}$ ……..... (6)

Chapter 3: Research Objectives

The main objective of the study is to assess the accuracy and reliability of different LULC change detection algorithms, while comparing their performance using established accuracy statistics and reference datasets to determine their effectiveness using Sentinel-2 imagery at 10 m resolution applied to the Wallonia region, Belgium.

To achieve the main objective, this study seeks to answer the following research question:

How to determine the efficacy of different LULC change detection algorithms and standardize them using Sentinel-2 satellite time series in the Wallonia region, Belgium?

To accomplish the goal of this study, the following steps are outlined:

1. Selecting and implementing different types of LULC change detection algorithms using 10 m Sentinel-2 data from 2018 to 2022,

2. Evaluating the strength and weaknesses of the respective algorithms in the context of multiclass classification,

3. Estimating different performance metrics such as accuracy, precision, and error matrix to quantitatively assess the algorithms' performance based on the LULC classification.

Chapter 4: Materials

This chapter provides background information regarding the study area and the datasets used in this research. Section 4.1 provides a comprehensive description of the study area with context. Furthermore, section 4.2 delves into the data sources utilized and outlines the various data types employed.

4.1. Study Area

The research is carried out in the Wallonia region of Belgium, located in the Southern part of Belgium (50.5°N, 4.75°E) as shown in Figure 1. The region covers an area of 16,901 km^2 with a population of over 3.6 million. The Walloon region has almost 530,000 hectares of forest that covers 30% of its territory.

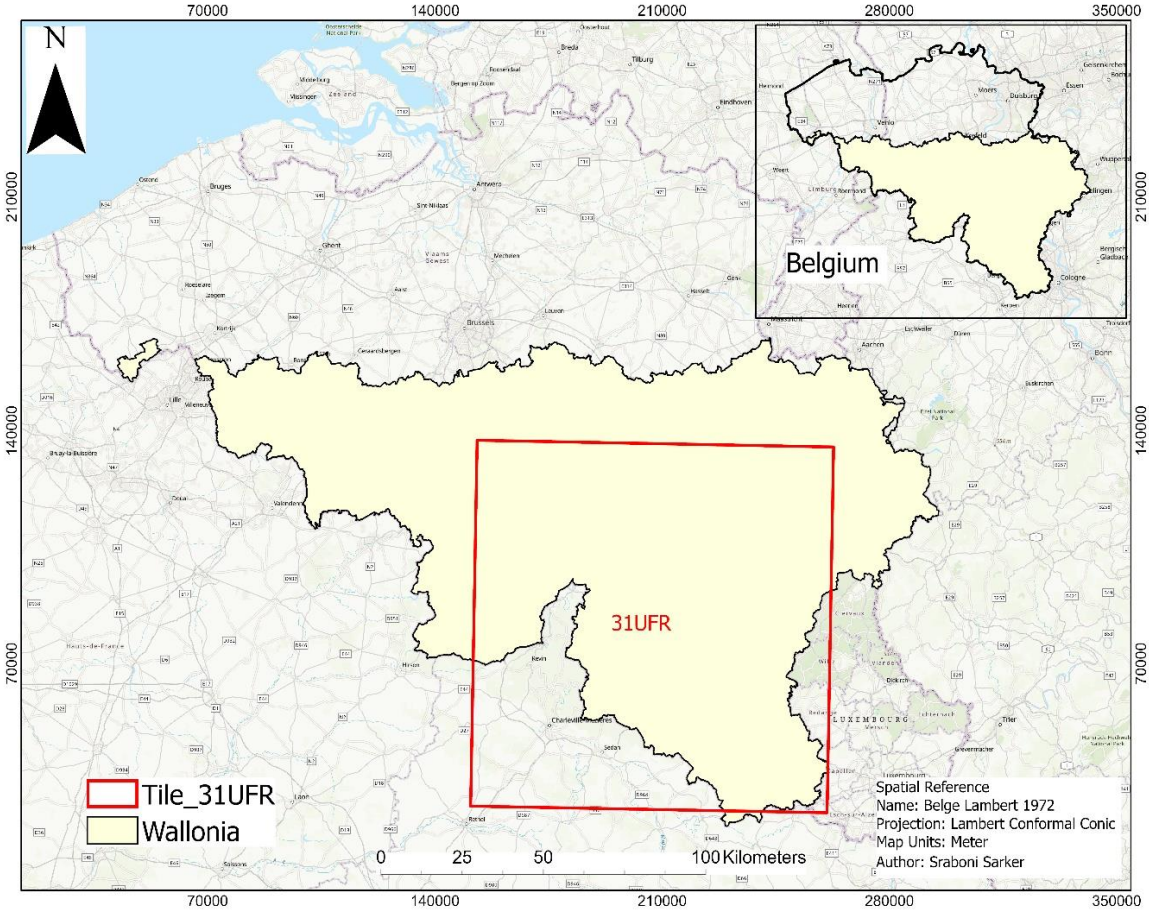

Figure 1: Study area map (Wallonia region, Belgium) with the Sentinel-2 tile selected for LULC change detection algorithms

Wallonia is the most wooded region, representing around 80% of the total Belgian forest (reforestACTION, 2024). In 2004, it consisted of 544,800 ha, which corresponds to a woodland

cover of 32.3% (Rondeux et al., 2010). In Wallonia, broadleaved forests (53%) and needle-leaved forests (44%), make up the majority of the country's forest cover. The remaining 3% is made up of mixed forests (Brogna et al., 2018). In this area, major LULC changes are related to the clear-cut of forest and cropland conversion from grassland, and vice versa. Most of the clear-cut are implemented at in the end of each year.

4.2. Data Sources

The current study utilized two different types of data including in-situ and remote sensing. The in-situ data was acquired from the European Lifewatch infrastructure. The remote sensing data was taken from Sentinel-2 of the Copernicus program. The data description for each type are explained below:

4.2.1. In-situ Data

For the study's calibration and validation dataset, the Lifewatch data for the years 2018 through 2022 were used. Using topography and remote sensing data as input variables, the landscape was automatically delineated into ecotopes and stored in this database (Radoux et al., 2022). A main source for ecotopes is 25 cm orthophotos and the LIDAR to automatically define the LC classes. The land surface were classified at 2 m resolution into 13 land cover classes. So the ecotopes at 2 m resolution layer, was used to calculate the percentage of each class. In addition to the airborne datasets, images from the Sentinel-1 and 2 satellites provided information about temporal dynamic LC features (grassland in rotation, difference between broadleaved and coniferous trees). The C-Band SAR instrument obtained Sentinel-1 10 m resolution images every 2 to 6 days, while the Sentinel-2 instrument recorded multispectral reflectance at 10 and 20 m resolution every 3 to 5 days. A total of 16,902 km^2 were mapped. It is stored in Geo-TIFF format with geo-referencing information (Belgian Lambert 2008 projection).

The definition of the classes is compatible with the guidelines of the European Environment Information and Observation Network (EIONET), which is a partnership network of the European Environment Agency (EEA) and its 38 member and cooperating countries (Radoux et al., 2022). The legend of this data is a pure land cover legend, derived from the INSPIRE Pure Land Cover Components (PLCC-INSPIRE) legend.

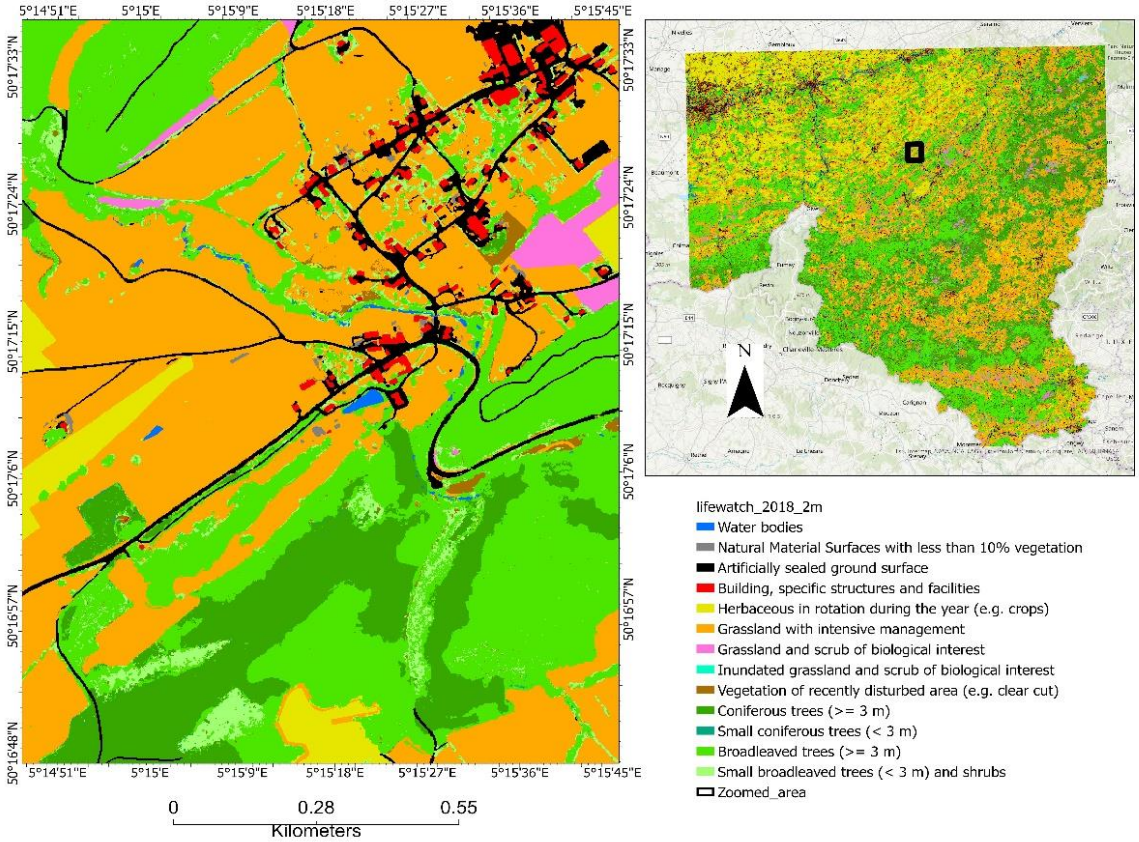

Figure 2: Lifewatch map of 2018 with 13 different LULC classes in 2m resolution

The two-meter layer has been validated by photointerpretation consolidated on the field when necessary. Approximately 93% of the total accuracy is achieved using 1200 randomly distributed points. A few aliases used by the geodatabase file are visible in certain software. The ratios are expressed as "per thousand," with 0 denoting no land cover type and 1000 denoting a pure ecotope for that type of land cover. Wallonia has those layers for 2006, 2010, 2015, 2018, 2022 (Lifewatch, 2024). A point-based accuracy assessment was carried out on the input land cover data. The OA for the years 2006, 2015, 2018, and 2019 was 93.1%, 92.6%, 94.8%, and 93.9% +/− 1.3%, respectively (Radoux, n.d.).

The strength of this mapping study lies in the generation of extremely accurate land cover dataset at very high resolution for each class, which is made possible by a thorough mapping effort at 2m and a statistically sound confusion matrix based on reliable visual interpretation. This precision and quality provide a unique validation dataset to benchmark LULC change detection algorithms.

4.2.2. Remote Sensing Data

In this study, Sentinel-2 images were downloaded from the Copernicus Open Access Hub. Sentinel-2 is a sun-synchronous optical remote sensing mission that consists of two polar-orbiting satellites. It makes available EO data in 13 spectral bands at three different spatial resolutions (10, 20, and 60 meters) and a five-day revisit period (ESA, 2015). As part of its twin-satellite capability, the Sentinel-2 mission supports land services by providing frequent and systematic coverage for mapping land cover, creating change and classification maps, and accurately assessing geophysical parameters (Copernicus, 2023).

Sentinel-2 images are provided in tiles through the Copernicus programme. To cover the whole of Wallonia, eight tiles were required. For this methodological research one tile was used, 31UFR as shown in Figure 1. The properties of the S2 spectral band are shown in Table 2.

Table 2: Sentinel-2 spectral bands properties (Source: Weiss et al., 2020; ESA, 2015)

Band Number	Band Names	Central Wavelength (nm)	Spatial Resolution	Possible Applications
1	Coastal Aerosol	443	60	Atmosphere
2	Blue	490	10	Atmosphere
3	Green	560	10	Vegetation
4	Red	665	10	Vegetation
5	VNIR	705	20	Vegetation
6	VNIR	740	20	Vegetation
7	VNIR	783	20	Vegetation
8a	NIR	842	10	Vegetation
8b	VNIR	865	20	Vegetation
9	Water vapour	945	60	Atmosphere
10	SWIR Cirrus	1375	60	Atmosphere
11	SWIR	1610	20	Vegetation
12	SWIR	2190	20	Vegetation

Chapter 5: Methods

This chapter presents a comprehensive overview of the methodology used for benchmarking two LULC change detection algorithms. Section 5.1 describes data preprocessing of in-situ and remote sensing data. In section 5.2, the methodology for the two different algorithms are thoroughly discussed. Then, in section 5.3, the LULC classification is explained. Furthermore, section 5.4 briefly describes the quantitative assessment of these two algorithms used to identify the most accurate one based on the year-to-year validation approach.

5.1. Data Preprocessing

5.1.1. In-situ Data Preparation

Lifewatch dataset has 13 different land cover classes at 2m resolution. In this study, these 13 land categories have been reclassified into seven categories of land (Table 3). These may be considered as top-level categories for representing land areas within a country. Six of the categories are consistent with the IPCC Guidelines and the requirements of Articles 3.3 and 3.4 of the Kyoto Protocol. It is recognized that the names of these land categories are a mixture of land cover (e.g., Forest land, Grassland, Wetlands) and land use (e.g., Cropland, Settlements) classes (Penman et al., 2003). Here, disturbed areas (clear cut of vegetation) has been categorized as a class, which is not included in IPCC categories.

Table 3: Reclassified Lifewatch categories to IPCC land categories

IPCC Categories	Lifewatch Categories
Wetland	Water bodies, Inundated grassland and scrub of biological interest
Settlements	Artificially sealed ground surface, Building, specific structures and facilities
Cropland	Herbaceous in rotation during the year (e.g. crops)
Grassland	Grassland with intensive management, Grassland and scrub of biological interest
Forest	Coniferous trees (>= 3 m), Small coniferous trees (< 3 m), Broadleaved trees (>= 3 m), Small broadleaved trees (< 3 m) and shrubs
Other land	Natural Material Surfaces with less than 10% vegetation
Disturbed Area**	Vegetation of recently disturbed area (e.g. clear cut)

The reclassification for each year from 2018 to 2022 were performed in Python. Here, reclassified Lifewatch map of 2018 is shown in Figure 3.

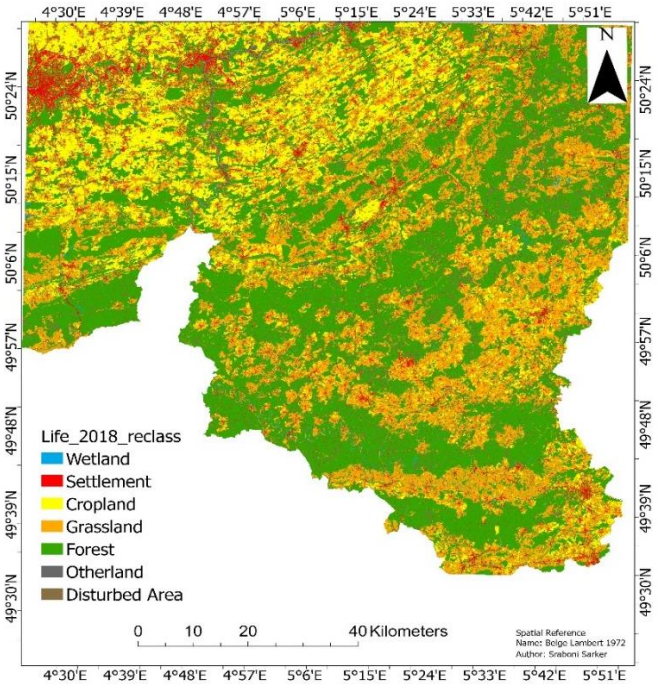

Figure 3: Reclassified Lifewatch map of 2018 with seven new LULC classes

The reclassified images were resampled to 10m resolution using Python, where mode was used as the resampling technique (Figure 4).

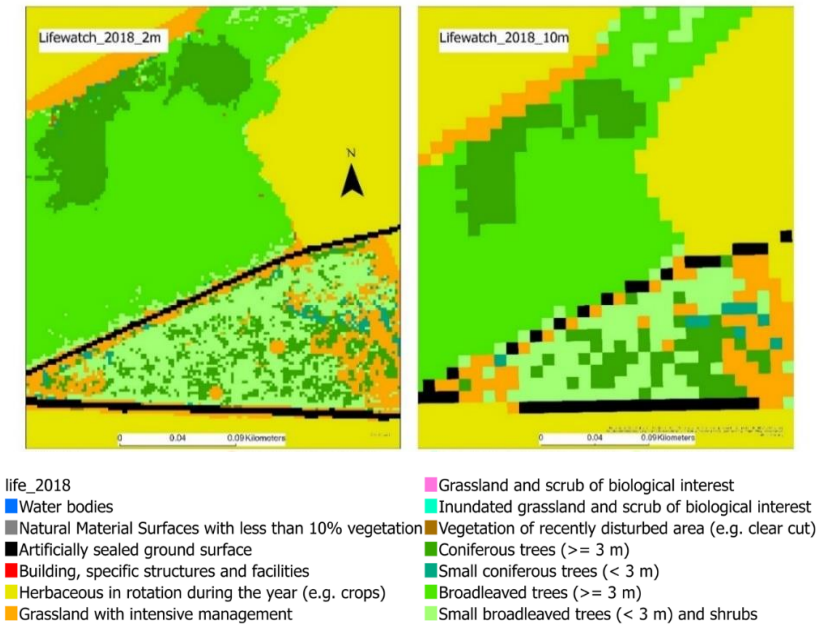

Figure 4: Resampled Lifewatch data of 2018 to 10m

5.1.2. Remote Sensing Data Preparation

The image dataset utilized for this study comprises Sentinel-2 Level 2A data, accessed through the Copernicus Open hub. These data provide valuable insights into land cover dynamics, facilitated by the Scene Classification (SCL) algorithm. The Sentinel-2 Level 2A prototype

processor (Sen2Cor) processes Top-Of-Atmosphere (TOA) Level 1C ortho-image reflectance products, alongside SCL. The SCL algorithm enables the identification of clouds, snow, and their shadows, yielding a comprehensive classification map consisting of distinct categories for various environmental features, including clouds (cirrus cloud), shadows, vegetation, non-vegetated areas, water bodies, and snow cover (Sentinel Online, 2024). Effective cloud screening is imperative for accurate atmospheric and surface parameter retrieval during subsequent atmospheric correction procedures. Utilizing the Sentinel-2 SCL, clouds were initially masked, effectively mitigating outlier influences.

Subsequently, the Normalized Difference Vegetation Index (NDVI) was computed, given its pivotal role in change detection and forest monitoring endeavors. NDVI quantifies the disparity in reflectance between Near-Infrared (NIR) and RED spectral bands, with higher values indicative of healthier vegetation cover.

$$\text{NDVI} = \frac{(\text{NIR} - \text{RED})}{(\text{NIR} + \text{RED})} = \frac{(\text{B08} - \text{B04})}{(\text{B08} + \text{B04})}$$

To ensure the utilization of high-quality NDVI data, a smoothing process was applied to the raw NDVI time-series dataset on GEE. This process aimed to rectify outliers and ensure temporal coherence within the annual frequency. Smoothing involved resampling the Sentinel-2 NDVI time-series to daily frequency data, harmonizing it with other temporal datasets, and interpolating missing values through linear interpolation techniques. Throughout this research, NDVI serves as a foundational component within the algorithms evaluated across the Wallonia region, underpinning robust analysis and insights into land cover dynamics and changes.

5.2. Selection of Land Use/Land Cover Change Detection Algorithms

5.2.1. CCDC Algorithm

5.2.1.1. Overview of CCDC

After the Landsat archive opened in 2008, CCDC was created to enhance the monitoring of land cover and changes in a given area. The ability to detect change detection with each new image that is collected is what is meant to be understood by the term "continuous" here. The method gets closer to almost real-time change detection if it is updated as new images are gathered. Since a LC map can be created for any point in time within the time span covered by images, the word "continuous" is also used in the algorithm's name. This algorithm can identify a wide range of changes in the LC. Using all of the available Landsat data, CCDC fits harmonic regression models to each pixel reflectance on NDVI over time. A break is identified if the observed data deviates from the expected signal for all observations within a moving window

period by more than a predetermined threshold when compared to the new observations predicted by the current model. A RF classifier is then used to classify land cover using the model fits as inputs. Hence, classification has not been performed in this study.

Three types of land surface changes are typically identified by the CCDC algorithm: (a) abrupt changes caused by urbanization, fires, floods, deforestation, and other factors; (b) gradual changes caused by vegetation growth, climate variability, and/or gradual changes in land management or degradation; and (c) intra-annual changes caused by vegetation phenology driven by seasonal patterns of environmental factors such as temperature and precipitation.

The CCDC algorithm was utilized for detecting land cover change, operated by analyzing a series of dates collectively. This approach mitigates transient effects, enhancing the likelihood that a pixel showcasing alterations across multiple successive images indeed signifies a substantive change in land cover. Consequently, pixels demonstrating change in only one or two consecutive instances are tentatively categorized as "potential change." However, if a third consecutive alteration is detected, the pixel is definitively classified into the "changed" category.

5.2.1.2. CCDC Parameters

There are nine different parameters which are essential to get the CCDC temporal segmentation result. The parameters are explained in Table 4:

Table 4: CCDC temporal segmentation parameters (Source: GEE Documentation, 2024; SEPAL Cookbook, 2024)

Parameters	Details
collection	Collection of images on which to run CCDC.
breakpointBands	The name or index of the bands to use for change detection. If unspecified, all bands are used.
tmaskBands	The bands selected here are used for additional multi-temporal filtering of cloud-affected pixels that have not been identified as such throughout the pre-processing of single images.
minObservations	This is the number of observations needed before a break is actually confirmed based on its temporal behavior. A low number will lead to more changes and reduce the gaps between two temporal segments. Higher numbers will lead to more confidence in the observed change; however, in cloud-prone regions, higher numbers might lead to long gaps between two temporal segments.

chiSquareProbability	The Chi-Square test will check whether an observation is part of the general statistical distribution of the time series. A low value of Chi-Square probability will favor the rejection of the null-hypothesis (i.e. being part of the statistical distribution), therefore flagging it as possible change. Ultimately, a lower value leads to more breaks detected, which favors omission over commission error. A high value allows for more noise in the time series, and less changes will be detected, therefore lowering the commission error rate.
minNumOfYearsScaler	This parameter determines the minimum length of any inner-temporal segment.
dateFormat	The time representation to use during fitting: 0 = jDays, 1 = fractional years, 2 = unix time in milliseconds. The start, end and break times for each temporal segment will be encoded this way.
lambda	The LAMBDA parameter is part of the LASSO regression used for modelling the time series. It is used to generalize the model, thereby improving its predictive power. More specifically, it is controlling the weight of each of the parameters, and might even result in the annulation of some parameters. In practical terms, an initial third-order harmonic model might shrink to a first-order harmonic, if this provides the best generalized fit. Setting LAMBDA to 0 will lead to a regular Ordinary-Least-Square regression, not providing any generalization. Instead, a higher value will provide a more generalized model.
maxIterations	The iterations for the maximum number of runs for LASSO regression convergence. If set to 0, regular OLS is used instead of LASSO.

5.2.1.3. Calibration of Parameters

In this algorithm, the tuning of parameters plays a crucial role in optimizing output quality. For optical data from Landsat and Sentinel-2, the GREEN and SWIR1 bands are recommended. In case of minObservations, usually a number between 4 and 8 is recommended (SEPAL Cookbook, 2024). Besides, if LAMBDA is set too high, the model will under fit, which is not desired. Since a value of 50 has been found to provide a generally good performance in this case study, the spot of neither overfitting nor under fitting will be around this number.

In this study, the values of parameters have been set as shown in Table 5 to get the optimized performance. The CCDC results were derived using GEE.

Table 5: CCDC temporal segmentation parameters calibrated values

Parameters	Type	Values
collection	ImageCollection	S2 images
breakpointBands	List	B2, B3, B4, B8, , B12, NDVI

tmaskBands	List	B3 and B12
minObservations	Integer	6
chiSquareProbability	Float	0.99
minNumOfYearsScaler	Float	1.33
dateFormat	Integer	2
lambda	Float	50
maxIterations	Integer	10000

A single change index with a predetermined threshold is adequate to identify specific land cover changes, such as changes in forests (Zhu et al., 2012). More spectral bands are required in order to detect a wide variety of land cover changes, since changes in land cover that are evident in one spectral band (or index) may be more challenging to detect in other spectral bands (or indices). Furthermore, the cutoff point for classifying a change may vary depending on the type of land cover change.

5.2.1.4. Flowchart

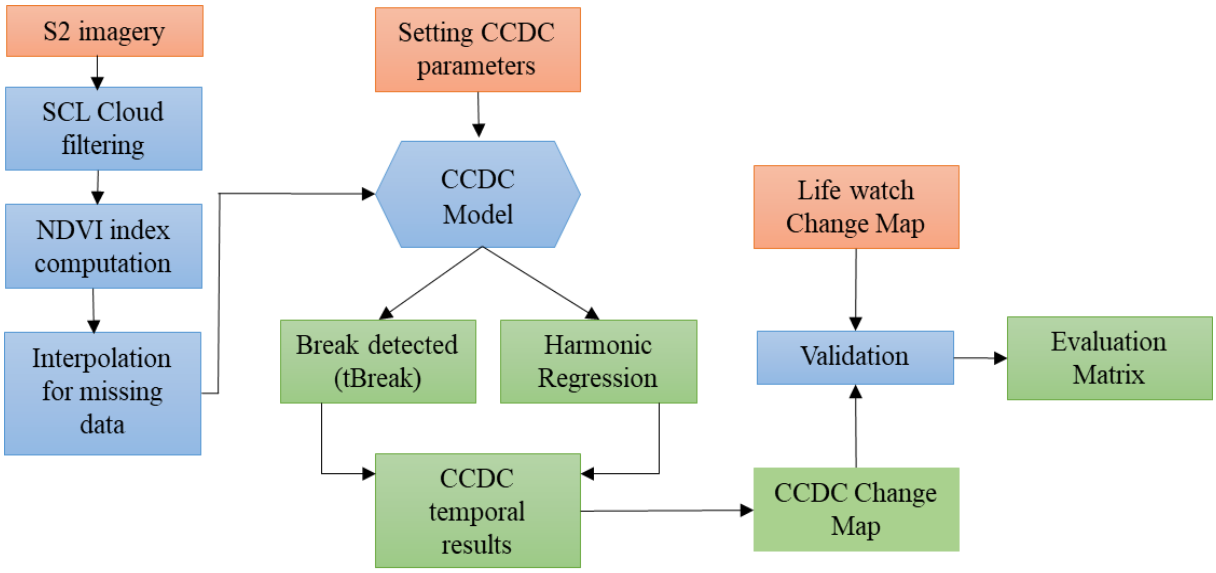

Figure 5: Schematic workflow of CCDC algorithm

Figure 5 presents the methodology of CCDC algorithm implemented in this study. CCDC operates by fitting a harmonic regression model to the temporal data, enabling the detection of breaks within the time series. These breaks delineate distinct segments of regression, with the number of segments determined by the identified breaks. Each segment is characterized by several parameters, including its start and end dates, as well as the number of observations contained within the segment. This approach allows for the segmentation of the time series data into meaningful intervals, facilitating the identification and analysis of temporal changes in land cover dynamics.

```
▾ tBreak: [1628592431885,0]
    0: 1628592431885
    1: 0
▾ tEnd: [1626864432672,1695552432764]
    0: 1626864432672
    1: 1695552432764
▾ tStart: [1535712013458,1628592431885]
    0: 1535712013458
    1: 1628592431885
```


Figure 6: CCDC temporal segmentations based on the number of detected changes

For each pixel in the image collection the CCDC algorithm generates information about the segments before and after a break – tBreak (Figure 6). Here, "tBreak" is the exact time of the break points in the CCDC time series, which can be more than one. The number 1628592431885 appears to be a Unix timestamp in milliseconds. It represent the number of milliseconds that have elapsed since January 1, 1970 (known as the Unix epoch). So, 1628592431885 represents the date and time of Tuesday, August 10, 2021 10:47:11.885 AM in GMT. In this study, the last break was taken into account to produce the change map. CCDC is similar to BFAST Monitor's season-trend model but includes modifications to improve its performance. It adapts to minimize overfitting and capture seasonal dynamics effectively. Unlike BFAST, which uses a fixed number of coefficients, CCDC dynamically fits second, third, or fourth-order harmonic models based on available observations. To prevent overfitting, CCDC employs LASSO regression instead of Ordinary Least Squares (OLS) regression during model fitting. LASSO regression restricts the absolute value of coefficients, reducing overfitting effectively (Awty-Carroll et al., 2019). Within this realm, harmonic regression emerges as a sophisticated technique with profound implications, particularly in the detection of break points within temporal data. By fitting sine and cosine functions to the data, harmonic regression can effectively model periodic or cyclic patterns inherent in many time series datasets. Figure 7 presents the harmonic regression fit before and after a change was detected in 2020.

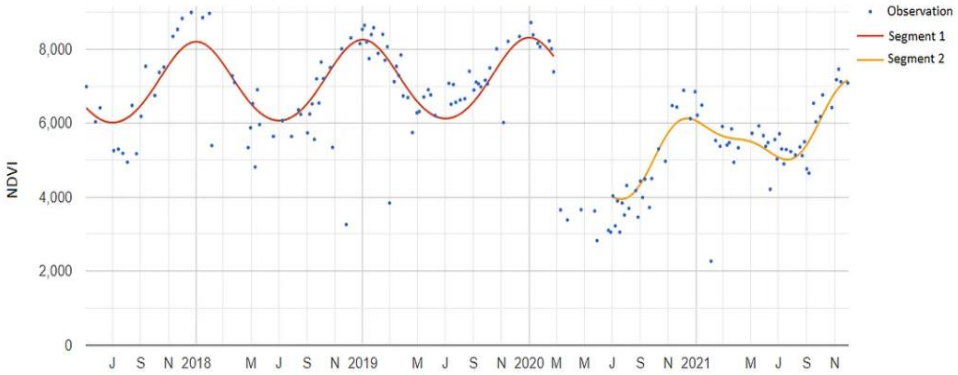

Figure 7: CCDC harmonic regression fit based on the number of detected changes

5.2.1.5. Software tools

The following platforms were used in processing the dataset:

- Google Earth Engine - GEE (Gorelick et al., 2017)
- QGIS version 3.34.4 (Sherman, 2002)
- ArcGIS Pro version - 2.7.0 (2020)

5.2.2. BFASTm Algorithm

5.2.2.1. Overview of BFASTm

Breaks for Additive Seasonal and Trend (BFAST) method was developed to analyze the dynamics of time series using the MODIS 16-day NDVI product. High temporal resolution allows for the decomposition of the time series into trend, seasonal, and remainder components, from which the time and number of changes can be identified. In this study, Sentinel-2, a 5-day NDVI, was used. Using a segmentation algorithm, it can identify breakpoints and estimate segments in Trend to describe the duration and extent of changes in vegetation trends from NDVI time series.

The BFAST algorithm doesn't inherently handle missing values. Therefore, linear interpolation between adjacent time points is commonly employed to fill in missing values due to its simplicity and effectiveness (Fang et al., 2018). In contrast, the BFASTm algorithm takes a different approach to break detection. It aims to identify a single break at the end of a time series, making it suitable for near real-time monitoring. Developed by Verbesselt et al. (2012), BFASTm involves several steps, including fitting a season-trend model and detecting structural changes and their magnitudes. Unlike BFAST, BFASTm does not attempt to separate seasonal and trend changes. This approach enables the algorithm to detect disruptions efficiently in time series data.

For BFASTm to operate effectively, the time series is partitioned into two segments: a monitoring period, wherein the algorithm searches for breaks, and a stable history period characterized by typical variability. The stable history period, extrapolated over the monitoring period, is modeled using a linear model. Subsequently, predictions derived from this model are compared against the actual data from the monitoring period. BFASTm has demonstrated its capability to detect multiple breaks in the past. This was achieved by iteratively running the algorithm with progressively extended monitoring intervals (Masiliūnas et al., 2016). Such an approach enables the algorithm to adapt to different temporal patterns and effectively identify significant disruptions in the time series data. BFASTm works better for inter-annual changes. This methodology was originally developed on Landsat and MODIS data, but can also be

applied to other optical satellite data. In our case, the methodology was adapted for time series analysis of S-2 images.

BFASTm was implemented using the GEE package (https://github.com/bfast2/geeBfastMonitor), utilizing a stable history period of one year, which could have potentially been extended for more comprehensive analysis. The decision to employ a second-order harmonic model for BFASTm was influenced by the complexity supported by the simulations used in the analysis. This choice aimed to strike a balance between computational efficiency and model accuracy, optimizing performance within the limitations of available data and computational resources.

5.2.2.2. BFASTm Parameters

There are different parameters which are crucial to get the BFASTm temporal segmentation result. The parameters are explained below:

Table 6: BFASTm temporal segmentation parameters (Source: R Documentation, 2024)

Parameters	Details
roi	region of interest as a Feature
historyStart	The starting date of the stable period
historyEnd	The end date of the stable period
monitoringStart	The starting date of the monitoring period
monitoringEnd	The end date of the monitoring period
h	Numeric scalar from interval (0,1) specifying the bandwidth relative to the sample size in MOSUM monitoring processes
period	Maximum time, relative to the history period, that should be monitored.
alpha	Significance level of the monitoring procedure
magnitudeThreshold	Threshold for magnitude level for which a change should be considered
harmonics	Order of the harmonic term

5.2.2.3. Calibration of Parameters

Effective tuning of parameters is essential for optimizing the output quality of the algorithm. In case of 'period' the default is 10 times the history period. In this algorithm, second order harmonics has been used to fit the NDVI values. The values of parameters have been calibrated as shown in table 7. In this study, GEE was utilized to obtain the BFASTm results.

Table 7: BFASTm temporal segmentation parameters calibrated values

Parameters	Values
roi	Wallonia region, Belgium (31UFR)
historyStart	01-01-2017

historyEnd	31-12-2017
monitoringStart	01-01-2018
monitoringEnd	31-12-2022
h	0.25
period	10
alpha	0.001
magnitudeThreshold	-0.0015
harmonics	2

5.2.2.4. Flowchart

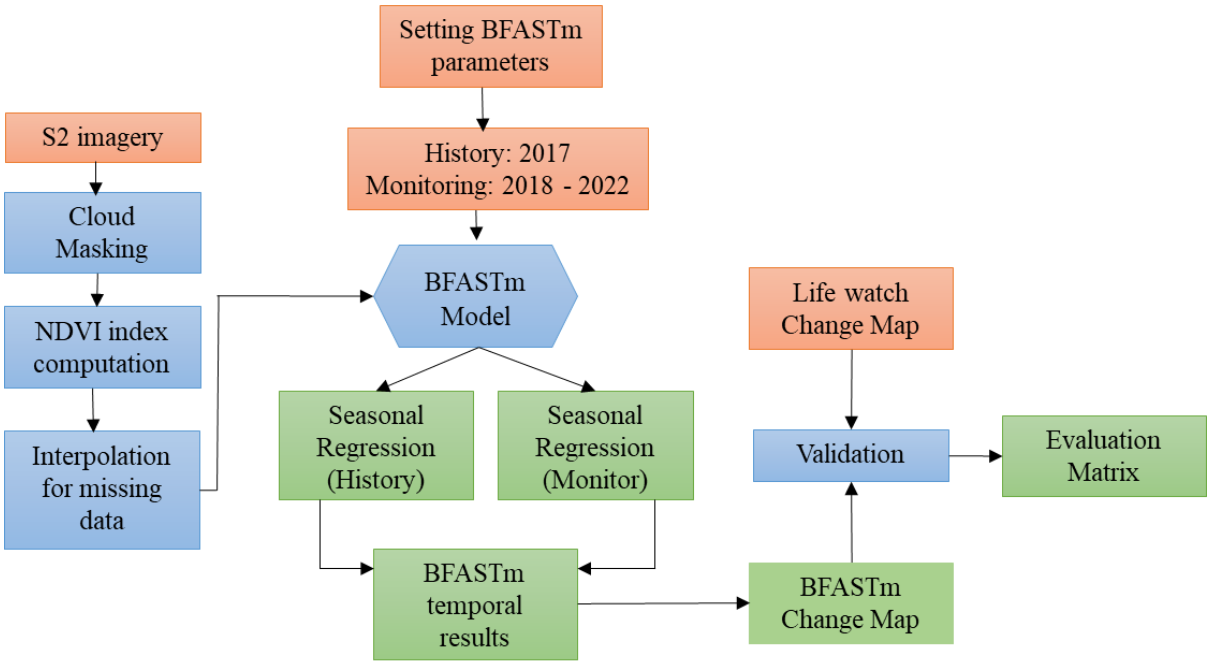

Figure 8: Schematic workflow of BFASTm algorithm

Figure 8 presents the methodology of BFASTm algorithm implemented in this study. The BFASTm identifies unusual observations within a monitoring period by establishing a stable history period. Initially, the start of the monitoring period is determined, followed by the automatic selection of a stable history period using the reversed-ordered-cumulative sum (CUSUM) of residuals. Subsequently, a regression model, typically a linear harmonic regression model, is fitted based on the history period. During the monitoring period, the moving sums (MOSUM) of residuals are computed, with the bandwidth defined by the parameter 'h', to assess the stability of the model with new observations. A break is identified when the absolute value of the moving sums surpasses a predefined probability threshold. The magnitude of change is quantified as the median of the difference between the observed data and the model prediction in the monitoring period. As BFASTm requires only a single

observation to exceed the threshold, it is susceptible to false positives (Awty-Carroll, 2019, Ghaderpour and Vujadinovic, 2020) and magnitude thresholds are often applied to minimize those (Gao et al., 2021, Hamunyela, 2017).

5.2.2.5. Software tools

The following platforms were used in processing the dataset:

- Google Earth Engine - GEE (Gorelick et al., 2017)
- QGIS version 3.34.4 (Sherman, 2002)
- ArcGIS Pro version - 2.7.0 (2020)

Both algorithms were processed on GEE platform. Computing capability, such as the cloud-computing technology with the GEE platform, has been greatly improved in the last few years. GEE synchronously archives the Sentinel data from Copernicus and effectively performs data processing by using the cloud computing technology through utilizing millions of servers worldwide. This technology shows potentials and prospects of the emerging GEE platforms in large regional and long temporal scales for land cover change research, and several studies have proved its feasibility (Pérez-Cutillas et al., 2023).

5.4. Accuracy Assessment

5.4.1. LULC Change Detection Algorithms Validity Assessment

The optimal source for accuracy assessment of LULC change detection is the Lifewatch dataset (Figure 4). According to Olofsson et al. (2014), the number of sample size was determined based on equation 1.

$$n = \frac{\left(\sum W_i S_i\right)^2}{\left[S\left(\hat{O}\right)\right]^2 + (1/N)\sum W_i S_i^2} \approx \left(\frac{\sum W_i S_i}{S\left(\hat{O}\right)}\right)^2 \qquad (7)$$

Here,

n = sample size

W_i = the mapped proportion of area of stratum i

S_i = is the standard deviation of stratum i

S ($o^{\wedge}$) = the standard error of the estimated overall accuracy

A target standard error for overall accuracy of 0.01 was specified. A random stratified samples design were using QGIS Actmata plugin (QGIS version 3.34.4). A total of 1228 reference pixels were selected for four different strata. 307 pixels were selected for each stratum:

Agreement, BFASTm, CCDC, and No Change based on the equal strategy. The "Agreement" stratum represents pixels where both CCDC and BFASTm detected changes. The "CCDC" stratum includes changes detected only by CCDC, while the "BFASTm" stratum represents changes detected only by BFASTm. The "No Change" stratum includes pixels where no changes were detected by either algorithm.

In the response design phase, these 1228 pixels were labeled using Lifewatch. For the response window views, the CCDC change map with two classes (change and no change) was used as the thematic map, and the Lifewatch change map served as the reference map for the time series. During the analysis phase, these 1228 labeled pixels were used as a sampling file, with a simple/systematic estimator applied to calculate the error matrix, including the weight of each class. The same procedure was followed for the BFASTm algorithm to derive the error matrix from the 1228 labeled pixels.

Lastly, it should be mentioned that neither of these two algorithms was used for any classification. Based on Lifewatch data, 400 points were produced for each algorithm to evaluate the LULC classes' accuracy. To assess accuracy, user-based accuracy was created for every of the seven distinct LULC classes.

This matrix was utilized as a quality assessment tool for change mapping, comparing the changes to the reference change map. The accuracy matrix comprises True Positive (TP), True Negative (TN), False Positive (FP), and False Negative (FN) values, derived from the comparison between actual and predicted values (Table 8). TP and TN denote accurately changed pixels, while FP and FN represent unchanged pixels. Subsequently, PA and UA were computed from this matrix to assess the performance.

Table 8: Accuracy assessment matrix for CCDC algorithm

CCDC/ BFASTm Change Map	**Reference Change Map**		
		Change	No change
	Change	TP (True positive)	FP (False positive)
	No Change	FN (False negative)	TN (True negative)

The OA of classification is determined by dividing the sum of TP and TN by the total number of validation points. F-score, another performance indicator, is calculated from UA and PA. In some cases, accuracy may be misleading, potentially resulting in poor representation of changed pixels. F-score addresses this imbalance by combining UA and PA into a single

metric, providing a more balanced evaluation. Table 9 outlines the performance indicators utilized in this study along with their respective formulas.

Table 9: Performance indicators used in this study (Fawcett, 2006)

Performance indicator	Formula
PA of the change pixel	TP / (TP + FN)
PA of the stable pixel	TN / (TN + FP)
UA of the change pixel	TP / (TP + FP)
UA of the stable pixel	TN / (TN + FN)
Overall accuracy (OA)	(TP + TN) / Total sample size
F-score of each class	2/{(1/UA)+(1/PA)}

Here, two types of errors are considered. Omission error indicates the reference pixel that was omitted from being detected as a change (100% - PA) and commission error indicates the pixels that were wrongly detected as a change (100% -UA).

5.4.2. Benchmarking of Algorithms

The accuracy results of the both confusion matrix analysis were thoroughly examined to determine which algorithm demonstrated superior performance in accurately identifying land cover changes. Finally, based on the findings, the preferred algorithm was selected for further analysis and interpretation.

Chapter 6: Results

6.1. CCDC Algorithm

6.1.1. Change Map Analysis

Interpreting change maps is considered crucial for understanding the evolution of LULC over time. These maps play a pivotal role in providing vital insights into various shifts, such as vegetation disturbances, agricultural expansion and others. By analyzing them, areas experiencing different changes can be identified, and the underlying reasons for these shifts can be understood.

CCDC possesses the capability to detect multiple changes within a time series, encompassing diverse types of alterations. Figure 9 illustrates the most recent change that occurred in each pixel. A significant observation is that the majority of pixels have undergone more than one change. These earlier breaks might not provide the necessary context for current LULC conditions, as the most recent changes are often more critical. By mapping the latest detected break, the map will showcase the most recent changes, providing a current snapshot of land cover or land use dynamics. It has been found that a substantial portion of pixels experienced their most recent changes in 2021 and 2022. Conversely, changes observed in 2019 and 2020 are minimal.

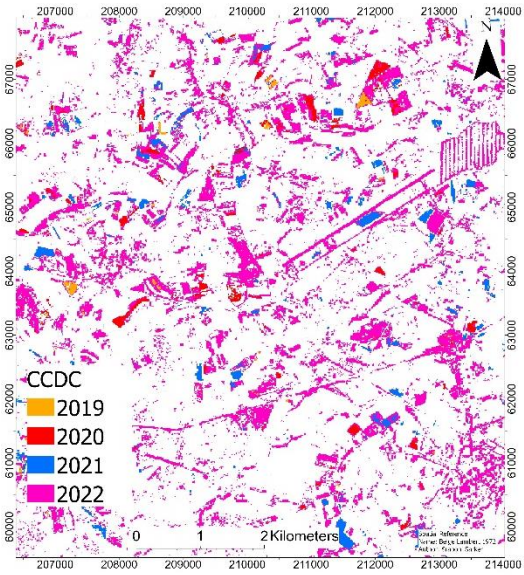

Figure 9: CCDC LULC Change Map

Figure 10 displays a map featuring a zoomed-in pixel highlighting the change detected in 2021. This visual representation is further reinforced by Sentinel-2 imagery (Figure 10b), providing additional validation. The area under scrutiny, once grassland in 2018, now exhibits evident signs of conversion to cropland by 2021 (Figure 10a). Notably, the CCDC analysis accurately

captures this transformation, demonstrating its efficacy in detecting and documenting temporal changes in land cover dynamics (Figure 10d).

6.1.2. Time Series Analysis

Time series analysis plays a pivotal role in various fields, offering valuable insights into the temporal behavior of phenomena.

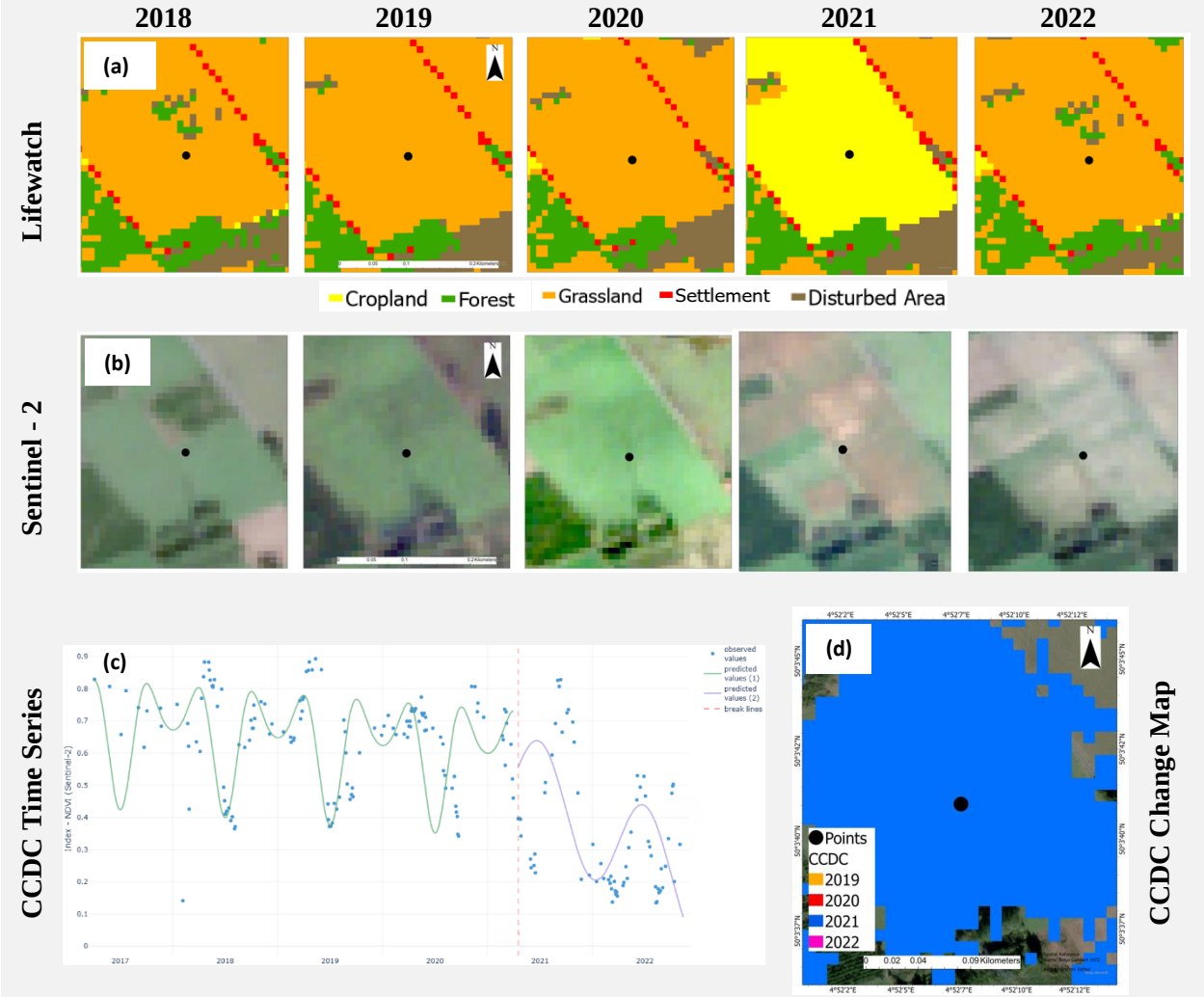

Figure 10: CCDC time series (c) comparison with Lifewatch data (a), sentinel – 2 images (b) along with CCDC change map (d)

Figure 10 (c) presents the harmonic regression of the time series, highlighting the break point where a change occurred. Notably, the time series unmistakably indicates a notable change occurring in 2021, which aligns effortlessly with the Sentinel-2 images and CCDC Change Map analysis. This convergence underscores the accuracy and reliability of the harmonic regression method in detecting and documenting temporal changes in land cover dynamics.

6.2. BFASTm Algorithm

6.2.1. Change Map Analysis

Unlike CCDC, which is designed to detect multiple changes throughout a time series, BFASTm aims to identify a single break at the end of a time series, rendering it suitable for near real-time monitoring. This approach allows the algorithm to be adaptable to various temporal patterns and to effectively identify significant disruptions in the time series data. Figure 11 presents the change map generated by the BFASTm algorithm.

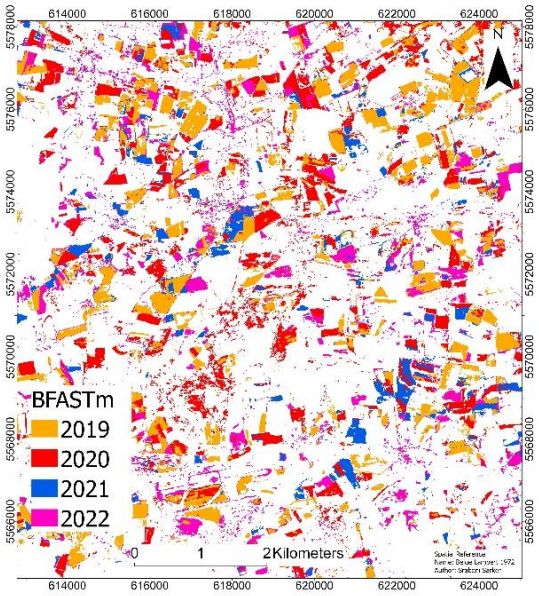

Figure 11: BFASTm LULC Change Map

In Figure 12, a detailed map focuses on a zoomed-in area, highlighting the most recent change detected using the BFASTm algorithm. This visual presentation is complemented by Sentinel-2 imagery (Figure 12b), providing extra validation and context. Previously covered in grassland from 2018 to 2021, the area shows noticeable signs of converting to cropland by 2022 (Figure 12a). The BFASTm analysis accurately identifies this transformation in land cover over time (Figure 12d).

6.2.2. Time Series Analysis

BFASTm is suitable for observing the change in near real-time monitoring. It does not attempt to separate seasonal and trend changes like traditional BFAST. This approach enables the algorithm to detect disruptions efficiently in time series data. A break is identified in the time series when the predictions are derived from the model and compared against actual data from the monitoring period. Figure 12 (c) visually represents the shift from grassland to cropland in 2022 as indicated by the reference data, and a change was accurately identified by both the

BFASTm time series and change map. Notably, the detection of the break precisely in 2022 aligns completely with the temporal patterns observed in the Sentinel-2 images.

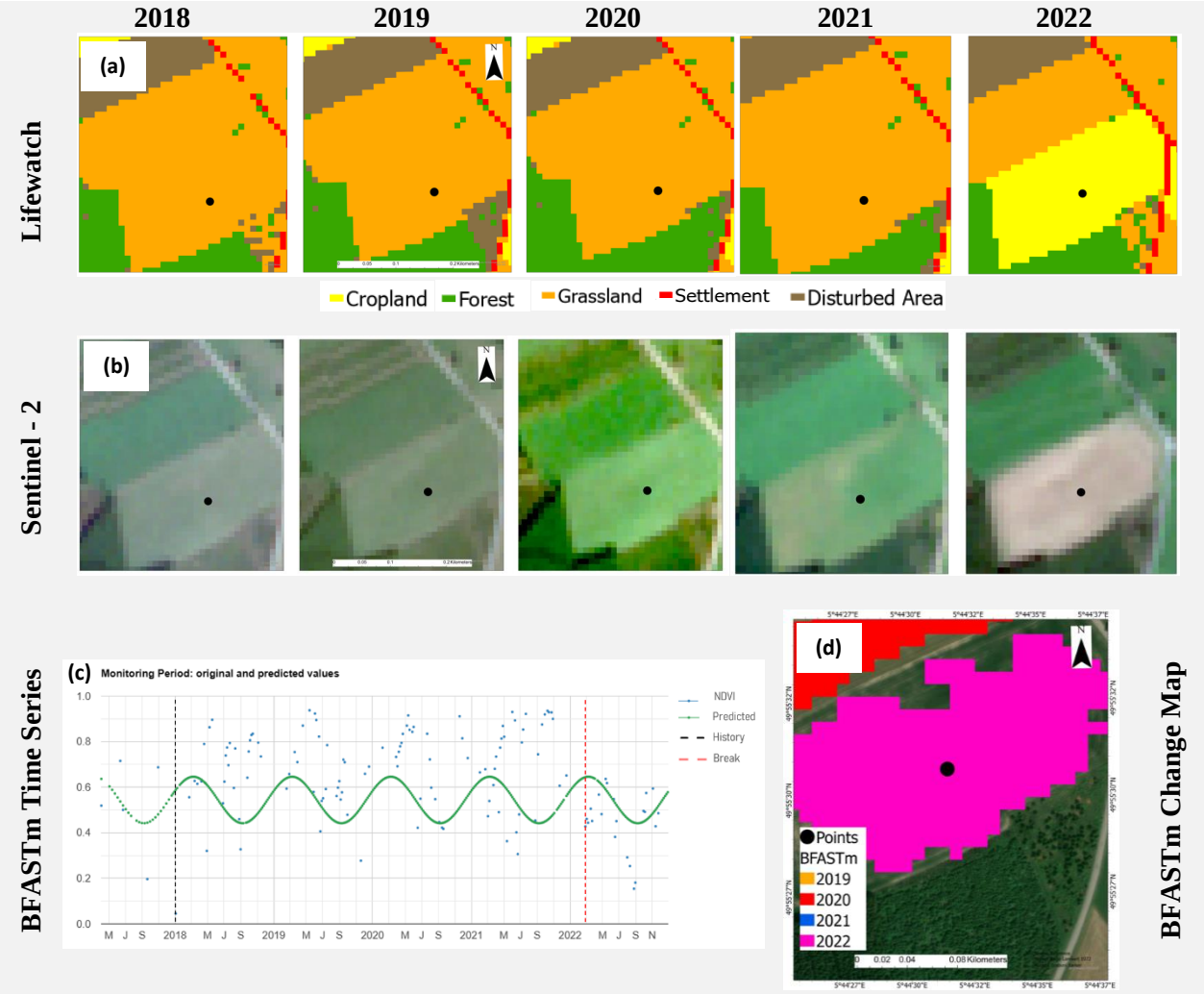

Figure 12: BFASTm time series (c) comparison with Lifewatch data (a), Sentinel-2 images (b) along with BFASTm change map (d)

6.3. Comparing CCDC and BFASTm algorithms

6.3.1. Correct Change Detections

The CCDC algorithm demonstrates commendable accuracy in detecting changes in land cover dynamics. Through rigorous analysis, a significant portion of the detected changes aligns with ground truth data and corroborating evidence from satellite imagery. These correctly identified changes provide valuable insights into temporal variations in land cover categories**.**

6.3.1.1. Forest Land Change

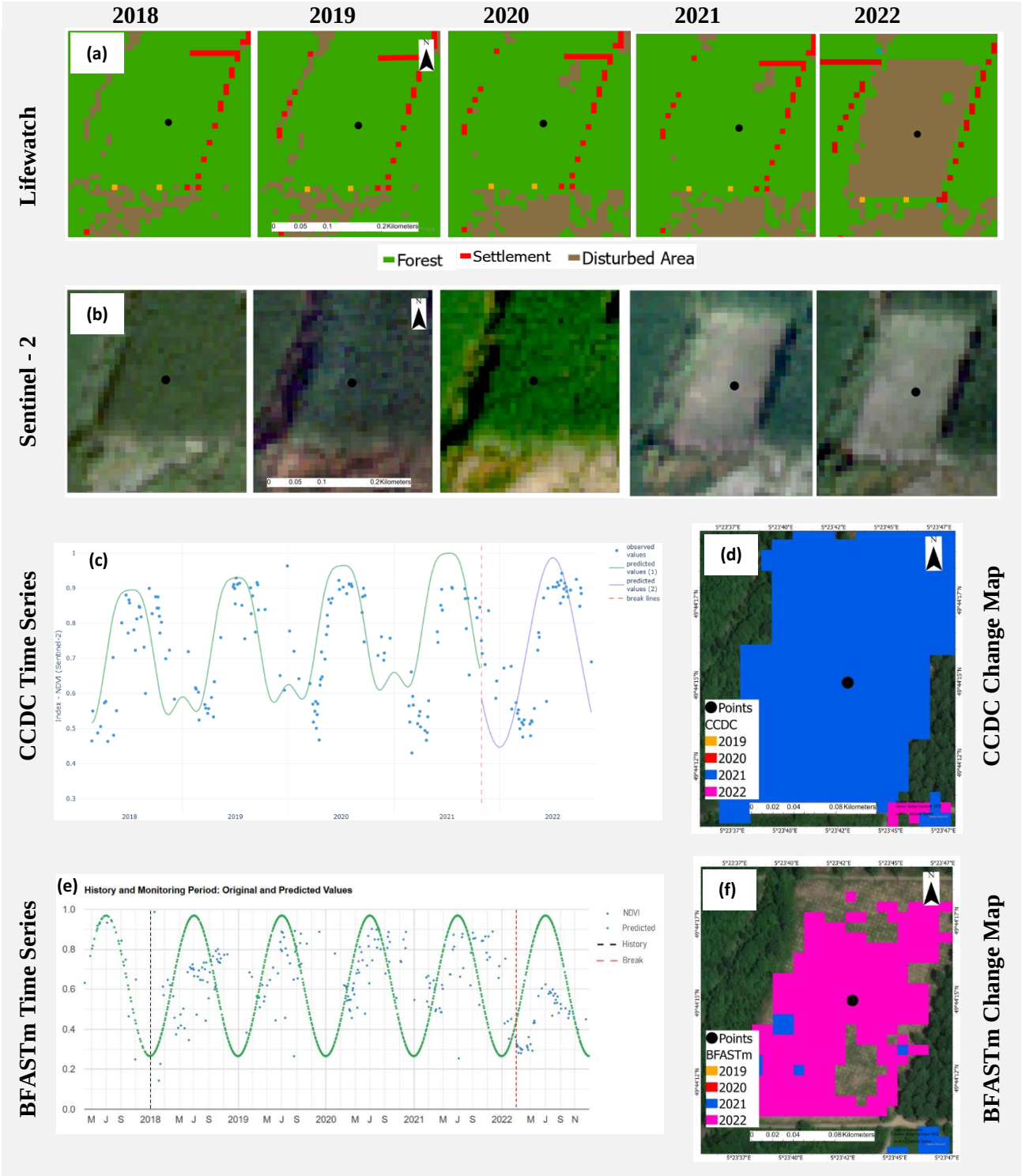

Figure 13: CCDC and BFASTm change detection algorithm comparison in forest land area based on Lifewatch data (a), sentinel – 2 images (b), CCDC time series (c) and change map (d) indicating break in 2021, BFASTm time series (e) and change map (f) indicating a break in 2022

In Figure 13, the transformation of forest land over a five-year span is depicted, offering insights into temporal shifts within the designated area. Until 2020, the pixel in focus remained steadfast as forest land. However, a notable vegetation disturbance emerged in 2021, as

corroborated by Sentinel-2 imagery (Figure 13b). Impressively, both the CCDC time series analysis and change map accurately identified this transition, specifying the precise date in 2021 in the CCDC time series. Furthermore, BFASTm seasonal analysis also detected a change towards the close of 2021. Yet, the BFASTm change map indicates that the change took place in 2022. This variance may be attributed to the algorithm's training on end-of-year changes, potentially delaying detection until 2022.

6.3.1.2. Cropland Change

In Figure 14, the evolution of cropland changes over the study period is illustrated. The latest change is accurately detected by CCDC, as depicted in the CCDC change map for the year 2021 (Figure 14d) and, it also produced a lot of pseudo changes or pepper and salt noises in the surrounding areas. Furthermore, both changes are effectively captured by the CCDC time series, accurately identifying the transitions in 2019 and 2021, respectively (Figure 14c). In contrast, a single change throughout the entire period is identified by BFASTm, with the transition in 2021 reflected in the BFASTm change map (Figure 14f). In the BFASTm time series, there is a break detected at the end of 2021 (Figure 14e). Overall, the ability of both algorithms to correctly detect the changes is demonstrated, underscoring their efficacy in land cover change detection.

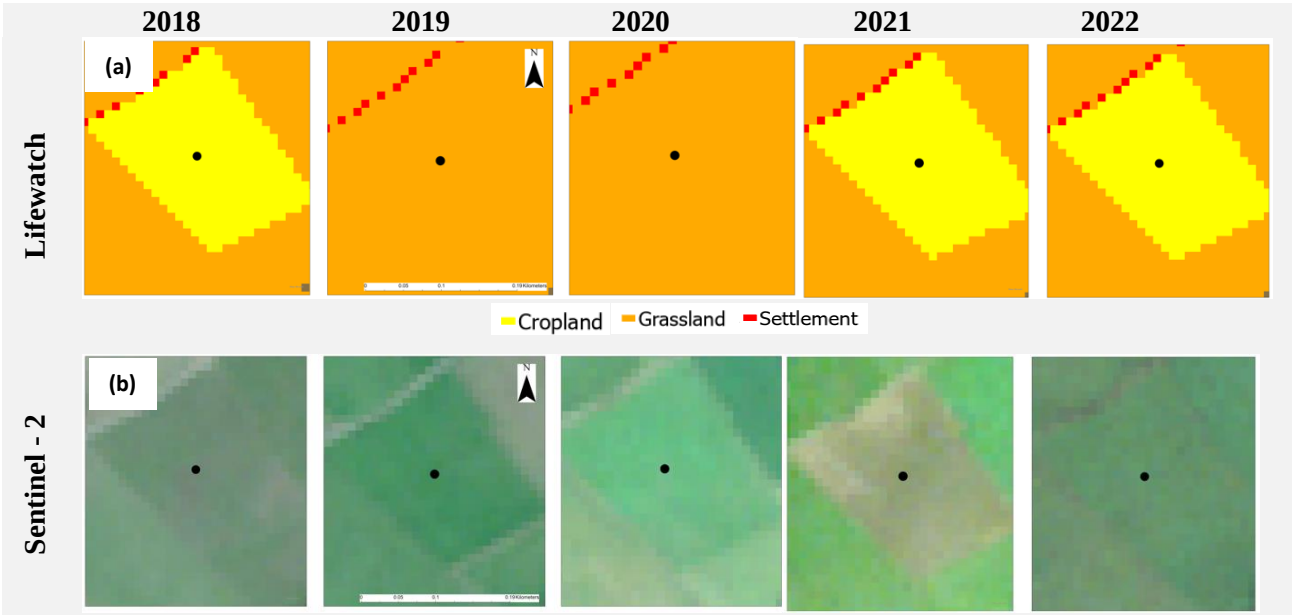

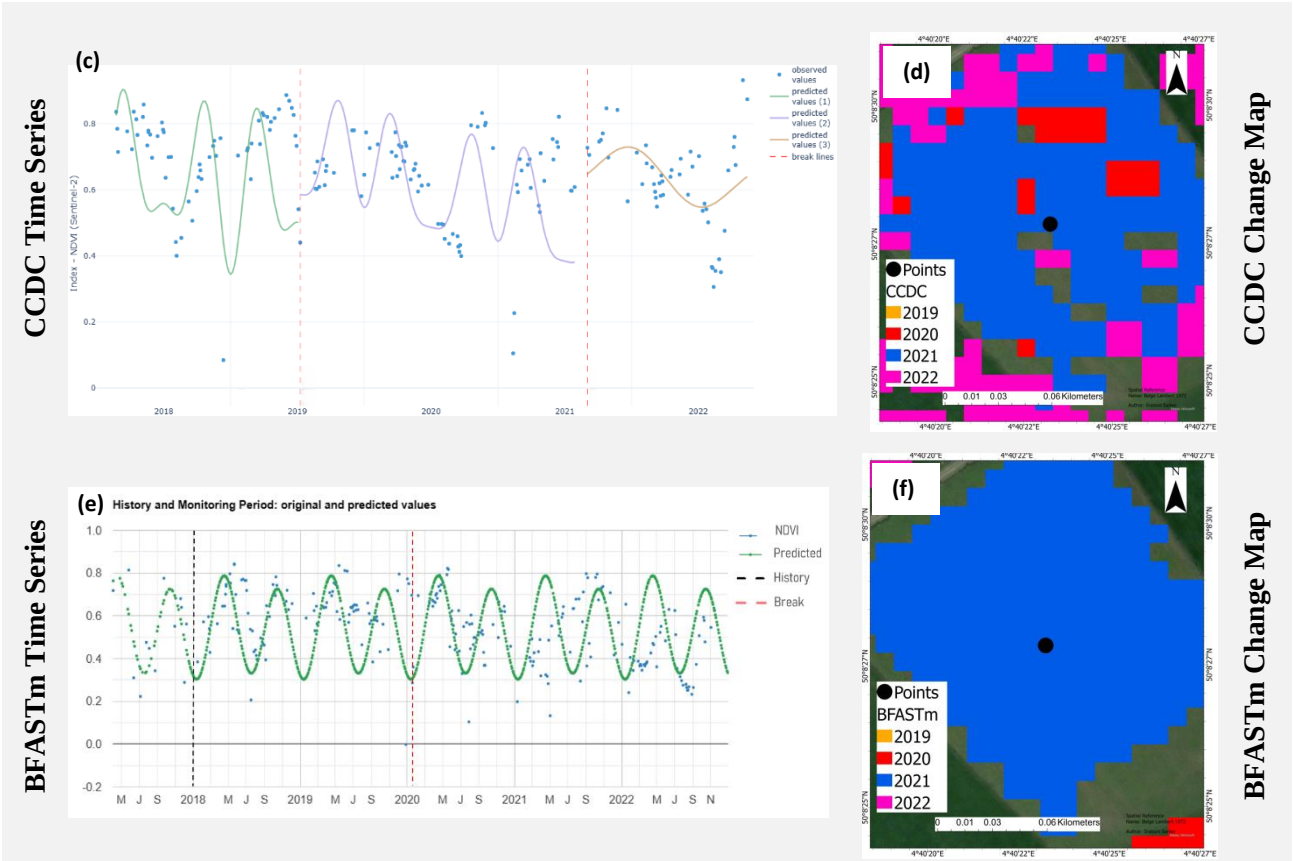

Figure 14: CCDC and BFASTm change detection algorithm comparison in cropland area based on Lifewatch data (a), sentinel – 2 images (b), CCDC time series (c) and change map (d) indicating break in 2021, BFASTm time series (e) and change map (f) indicating break in 2021

6.3.1.3. Grassland Change

In Figure 15, the transformation of grassland is depicted. In the reference maps, it is evident that the specified area remained grassland from 2018 to 2021 before transitioning to cropland in 2022. This transition is also corroborated by Sentinel-2 images. Both algorithms' time series meticulously captured this transition without error, demonstrating their robustness in detecting temporal changes in land cover. Moreover, the change maps generated by both CCDC and BFASTm algorithms accurately pinpointed the conversion to cropland in 2022. This congruence between algorithmic analysis and visual observations underscores the reliability and effectiveness of both CCDC and BFASTm methodologies in land cover change detection. Here, the CCDC model has good fit to the time series compared to BFASTm.

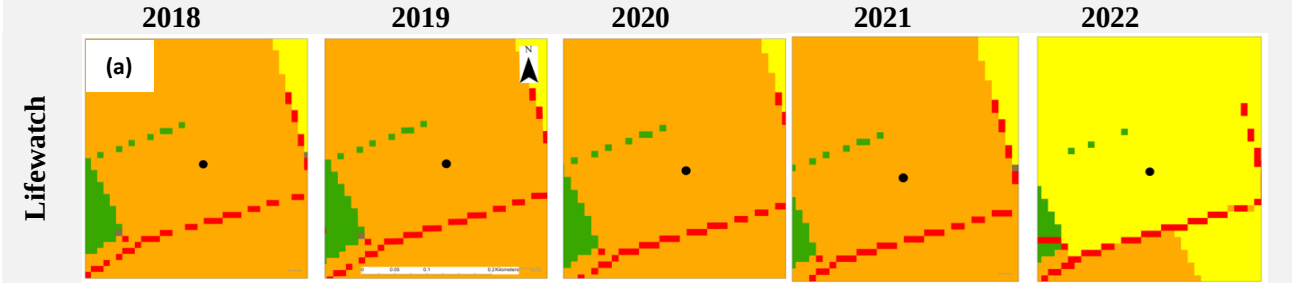

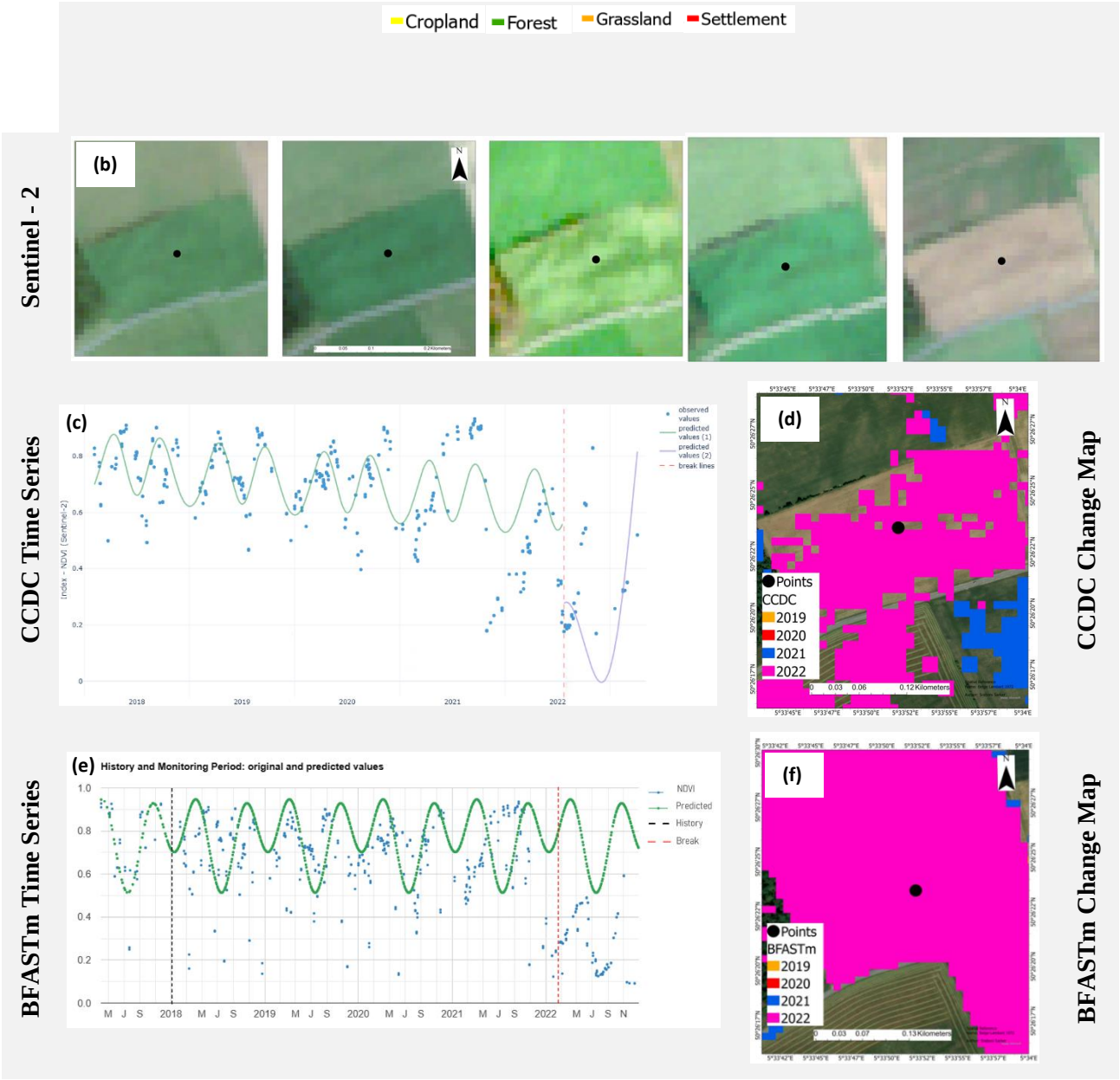

Figure 15: CCDC and BFASTm change detection algorithm comparison in grass land area based on Lifewatch data (a), sentinel – 2 images (b), CCDC time series (c) and change map (d) indicating break in 2022, BFASTm time series (e) and change map (f) indicating break in 2022

6.3.1.5. Settlement Change

The settlements within Wallonia exhibit minimal variability over time. Figure 16 illustrates the detected changes in settlements by the LULC change detection algorithm. The reference data reveals a transition from grassland areas in 2018 to other land built-up in 2020. Sentinel-2 images corroborate the initial LULC class observed in 2018 and 2019, with a subsequent change to built-up areas in 2020 (Figure 16b). Both CCDC and BFASTm algorithms accurately detected the change in 2020, aligning with the reference data. Notably, the CCDC time series impeccably identified both changes within this specific area, with the latest change clearly depicted in the map.

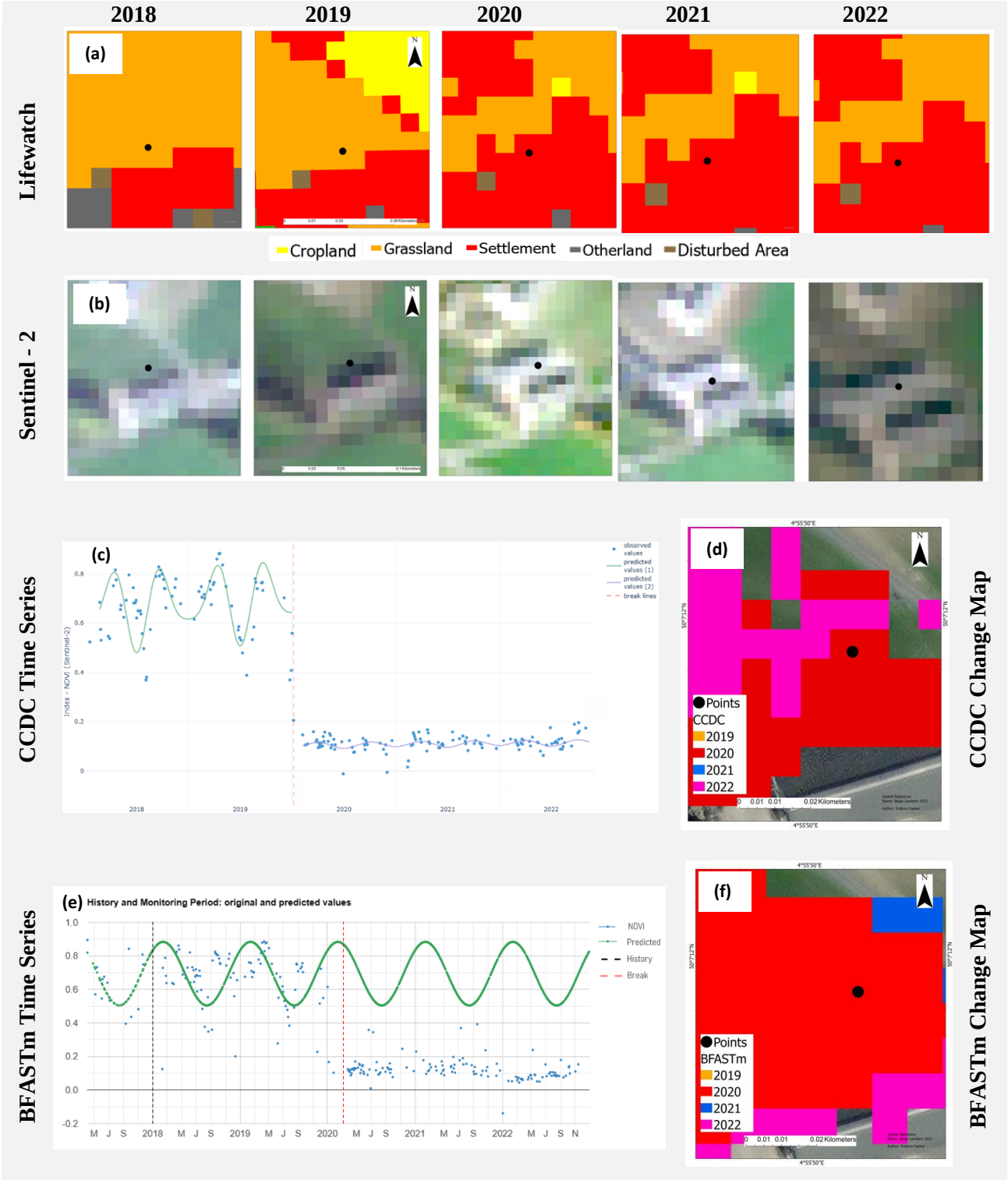

Figure 16: CCDC and BFASTm change detection algorithm comparison in settlement area based on Lifewatch data (a), sentinel – 2 images (b), CCDC time series (c) and change map (d) indicating break in 2020, BFASTm time series (e) and change map (f) indicating break in 2020

In the Wallonia region, the wetland and other land classes likely remained unchanged throughout the 5-year study period, presenting a challenge for both algorithms in detecting any changes. Instances where changes were detected in these classes by the algorithms were mostly false positives, as will be elaborated upon in the subsequent section. This underscores the importance of understanding the inherent limitations of the algorithms and carefully interpreting their outputs, particularly in areas where minimal or no change is expected.

6.3.2. Incorrect Change Detections

Each algorithm possesses its own set of limitations, contributing to instances where changes may not be accurately detected. The BFASTm algorithm, for instance, is susceptible to false positive change detection, wherein changes are erroneously identified when none have occurred. Similarly, CCDC may also exhibit false change detections, despite its robust methodology. Additionally, there are occasions where CCDC fails to detect changes within the time series data, even when changes have occurred. This section will present the non-aligned changes among Sentinel - 2, Lifewatch data, CCDC and BFASTm for seven different classes used in this study, highlighting the challenges and limitations inherent in their change detection capabilities.

6.3.2.1. Forest Land Change

Figure 17 depicts a scenario where the forest area underwent clear-cutting in 2020, as indicated by the reference dataset, and remained unchanged until 2022. However, Sentinel-2 images indicated that the change occurred in 2019. CCDC detected two changes in the time series, occurring in 2019 and 2021, respectively, whereas the change took place only once according to both the reference and satellite data. In the BFASTm time series, the particular change was observed in 2021. Both change maps identified the change year as 2021.

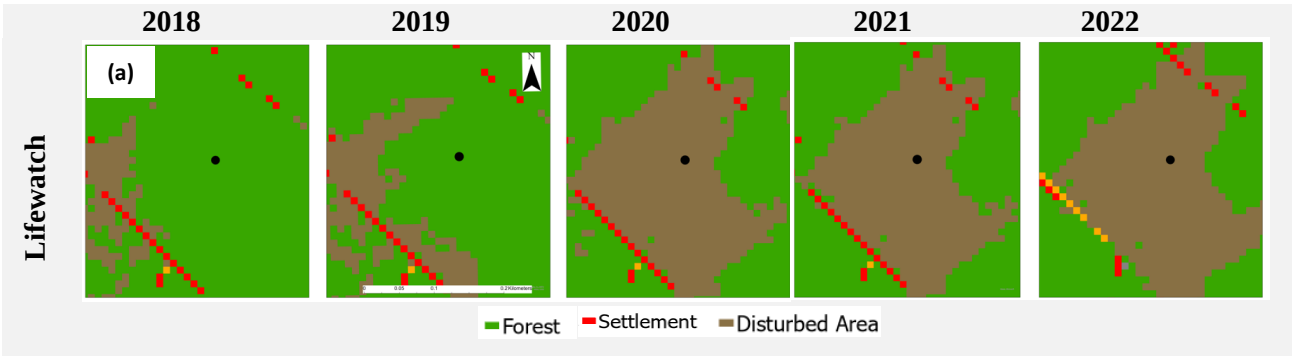

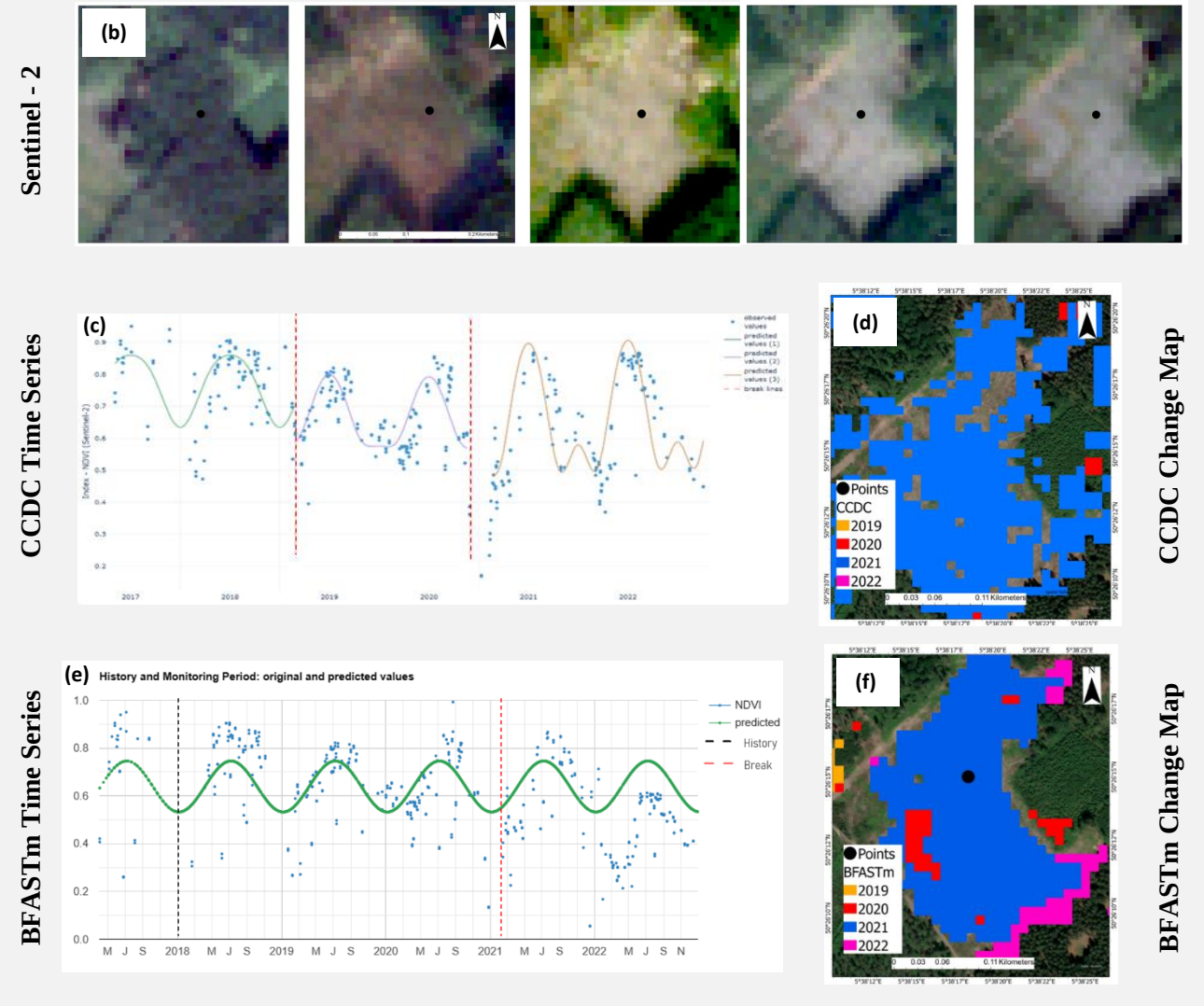

Figure 17: CCDC and BFASTm change detection algorithm comparison in forest land area based on Lifewatch data (a), sentinel – 2 images (b), CCDC time series (c) indicating two breaks in 2019 and 2021 and presenting the change on the map (d) in 2021, BFASTm time series (e) and change map (f) indicating break in 2021

6.3.2.2. Cropland Change

Figure 18 shows cropland related changes from cropland to grassland are the primary changes that occurred between the five-year time period. According to the reference data, the pixel underwent a transition from grassland to cropland in 2019, and revert to grassland by 2021 (Figure 18a). Here, CCDC successfully observed the transition for the specific pixel, with a little change detected in the surrounding area. In contrast, BFASTm accurately identified the change in 2019 in the change map (Figure 18f). Additionally, the change occurring in 2021 is evident in the BFASTm time series. The achieved results indicate the superiority of BFASTm method to CCDC in detecting real changes in cropland.

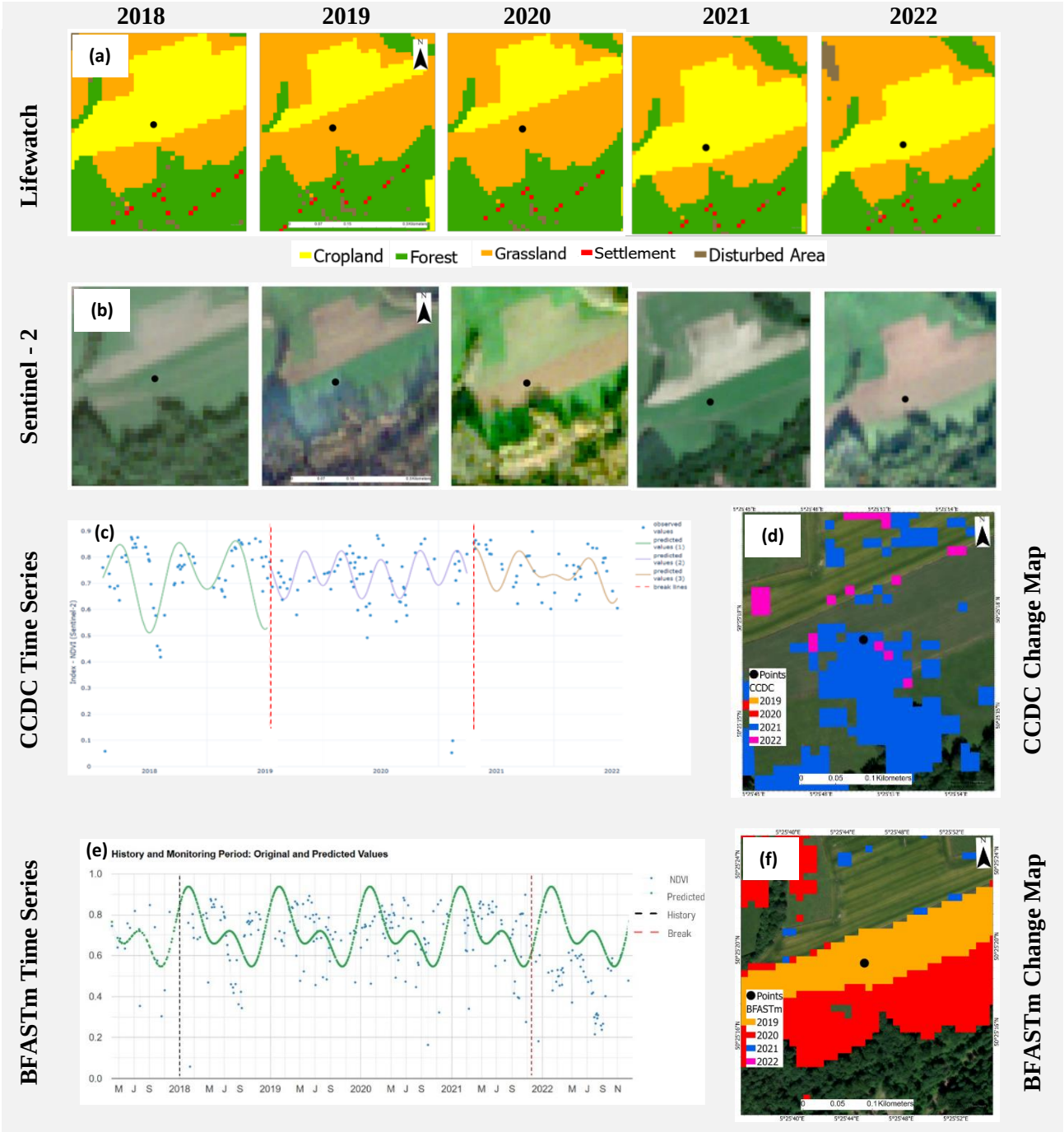

Figure 18: CCDC and BFASTm change detection algorithm comparison in cropland area based on Lifewatch data (a), sentinel – 2 images (b), CCDC time series (c) indicating two breaks in 2019 and 2021 and presenting the change on the map (d) in 2021, BFASTm time series (e) and change map (f) indicating break a in 2019

6.3.2.3. Grassland Change

Figure 19 depicts a single change occurring in grassland in 2019, where it underwent conversion to a built-up area. Both the Lifewatch dataset and Sentinel-2 images concur in detecting this change. However, in the CCDC time series analysis, the NDVI values indicate a drop in 2020 instead of 2019 (Figure 19c), which corresponds to the timing of the change. This discrepancy is also reflected in the CCDC change map (Figure 19d). In contrast, BFASTm

accurately identifies the change in 2019, aligning with both the reference dataset and Sentinel-2 images.

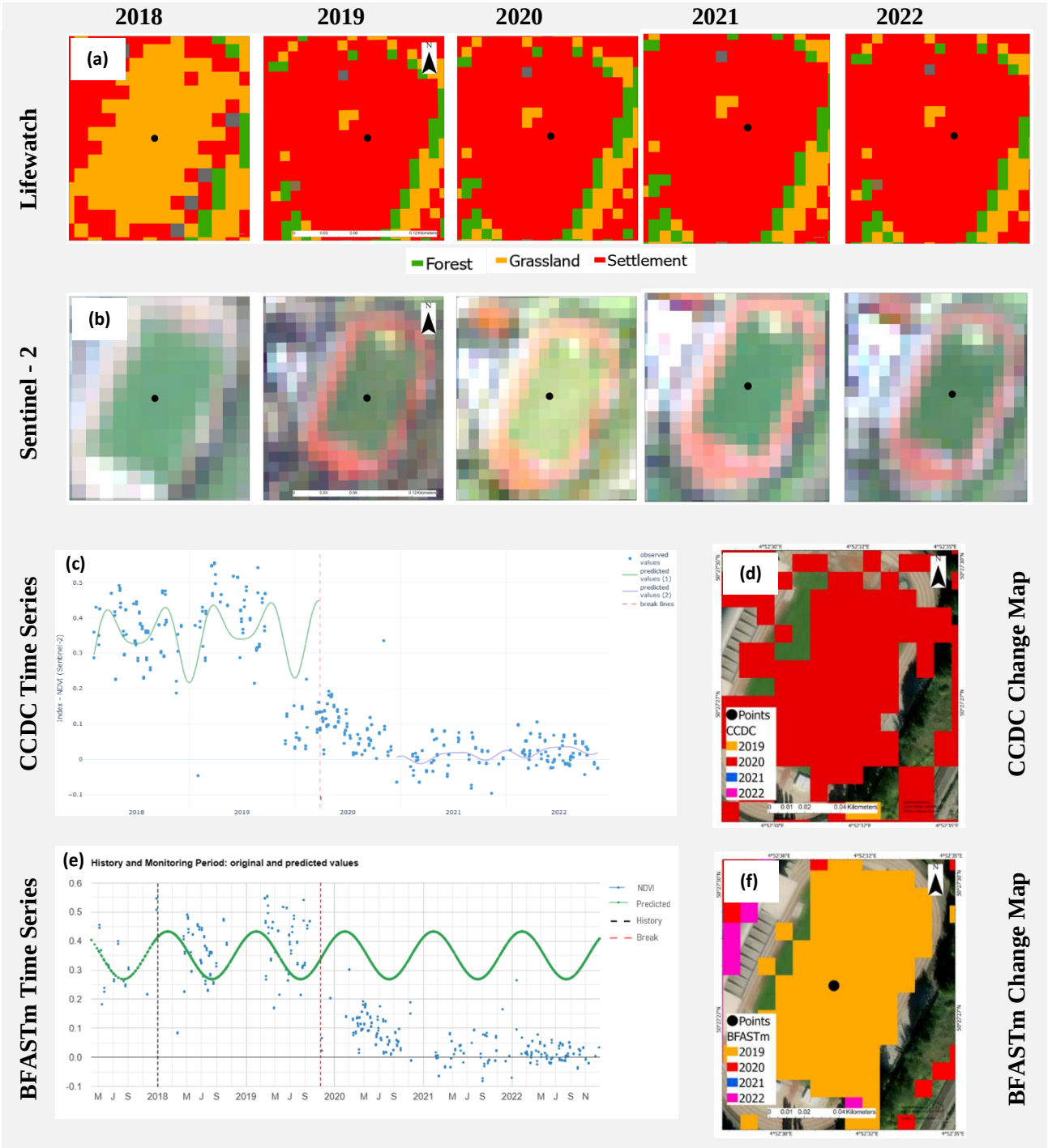

Figure 19: CCDC and BFASTm change detection algorithm comparison in grass land area based Lifewatch data (a), sentinel – 2 images (b), CCDC time series (c) and change map (d) indicating a break in 2020, BFASTm time series (e) and change map (f) indicating a break in 2019

6.3.2.5. Settlement Change

Figure 20 illustrates a change in the settlement area, transitioning to other land in 2019 and reverting to settlement areas in 2022, as indicated by the reference maps and corroborated by

Sentinel-2 images. However, CCDC failed to detect any change in the time series, despite a gradual increase in NDVI values. Additionally, the CCDC change map did not identify any changes in the specific pixel. In contrast, BFASTm successfully detected a change in 2022 in both the time series and change map.

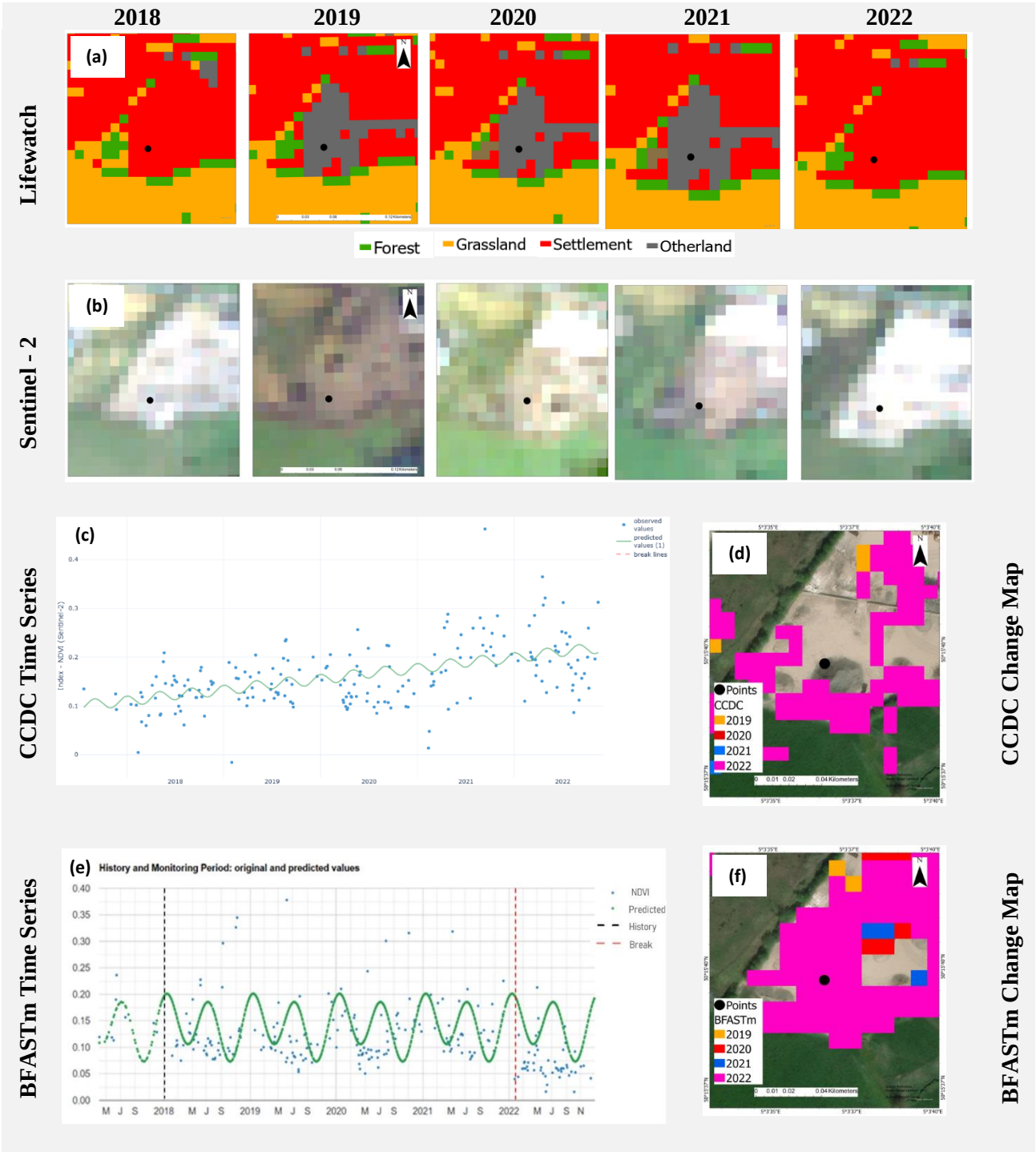

Figure 20: CCDC and BFASTm change detection algorithm comparison in settlement area based on Lifewatch data (a), sentinel – 2 images (b), CCDC time series (c) and change map (d) indicating no break in the pixel, BFASTm time series (e) and change map (f) indicating a break in 2022

6.3.2.6. Other Land Change

In this study, the "other land" category emerged as the most stable among the LULC classes. Identifying areas exhibiting any form of change within this class proved challenging. For instance, according to Lifewatch data depicted in Figure 21, a transition from "other land" to wetland is noted in 2021. However, scrutiny of Sentinel-2 imagery reveals the presence of wetland as early as 2019. Surprisingly, CCDC was unable to effectively capture any changes, resulting in no alterations in the spectral signature in the CCDC time series (Figure 21c). Consequently, the CCDC change map also failed to detect any changes in this area (Figure 21d). In the CCDC time series, Instead, CCDC generated considerable pepper and salt noise around the pixel. Conversely, BFASTm exhibited superior performance in both spatial and temporal dimensions, accurately pinpointing the change in 2019, consistent with observations from Sentinel-2 imagery. The NDVI values in the BFASTm time series exhibited a sudden decrease in 2019 when the area transitioned from other land to water bodies (Figure 21e).

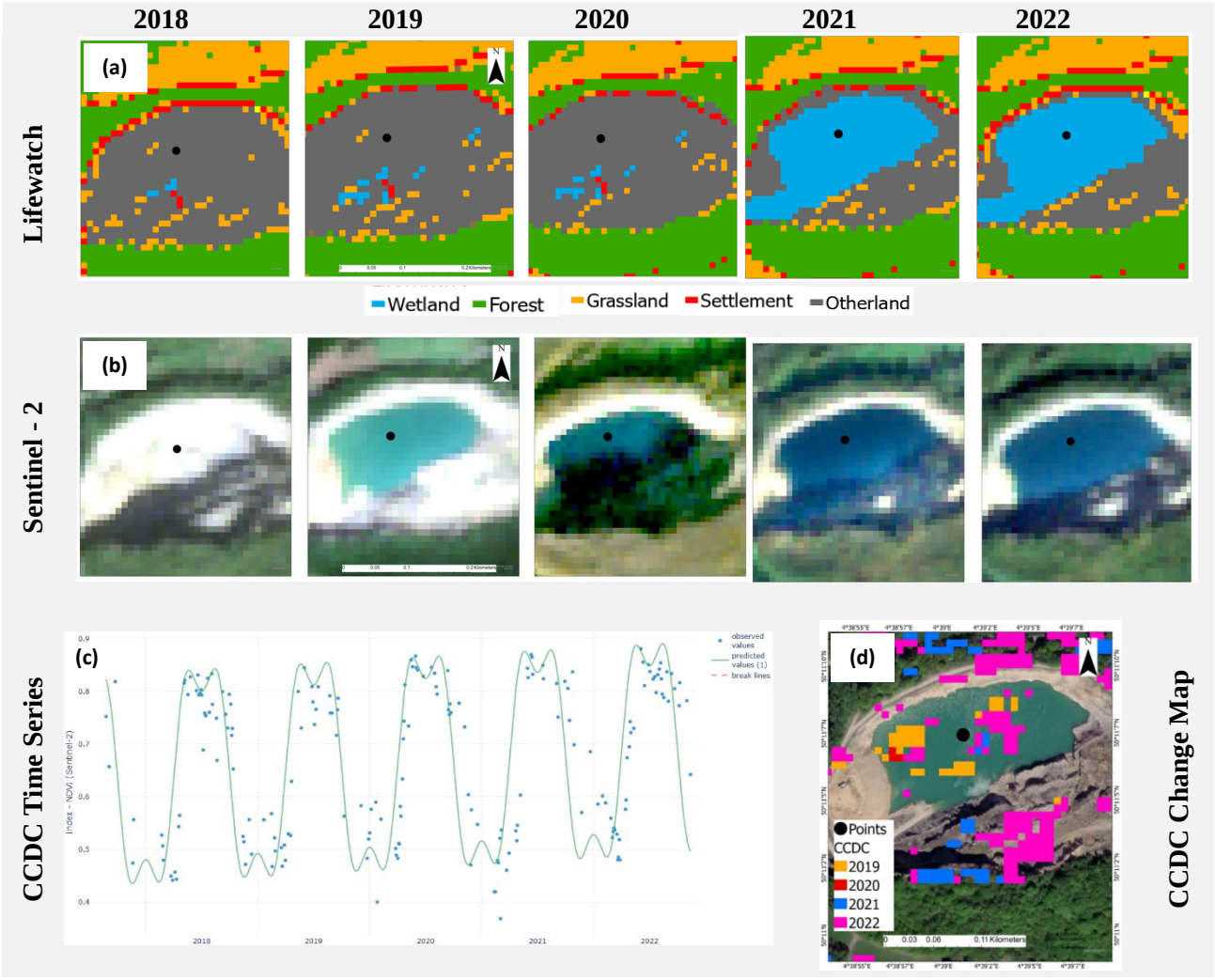

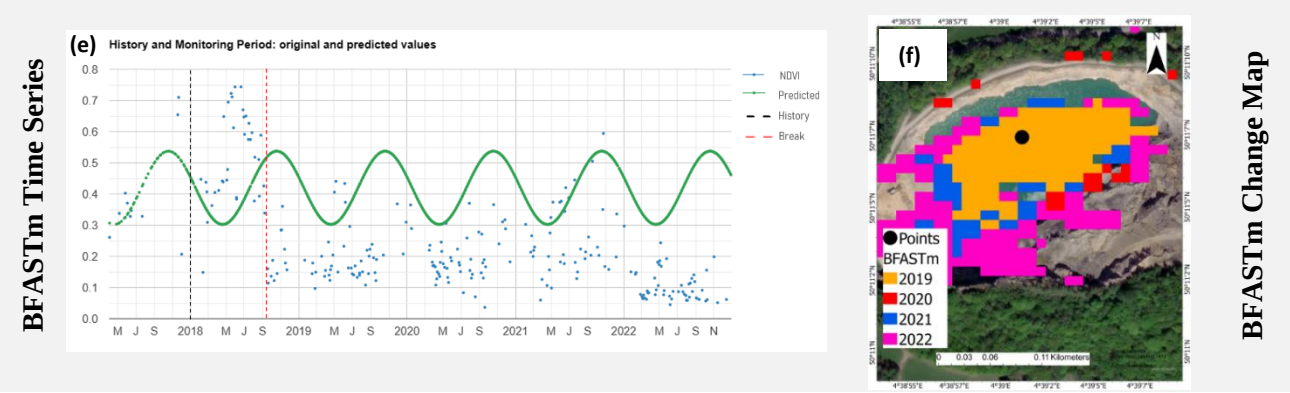

Figure 21: CCDC and BFASTm change detection algorithm comparison in other land area based on Lifewatch data (a), sentinel – 2 images (b), CCDC time series (c) and change map (d) indicating no break in the pixel, BFASTm time series (e) and change map (f) indicating a break in 2019

6.3.2.7. Disturbed Areas

In this study, disturbed vegetation is delineated as a distinct category, distinguished from other land cover types. Figure 22 illustrates the temporal evolution of disturbed areas, illustrating a progression from disturbed areas in 2018 to forest land by 2020 maintained until 2022 according to the Lifewatch dataset. These transitions observed in the reference data are further validated by Sentinel-2 images. However, in the time series of both CCDC and BFASTm, NDVI values remain unchanged despite the presence of new plantation, as evidenced by the reference dataset and Sentinel-2 images.

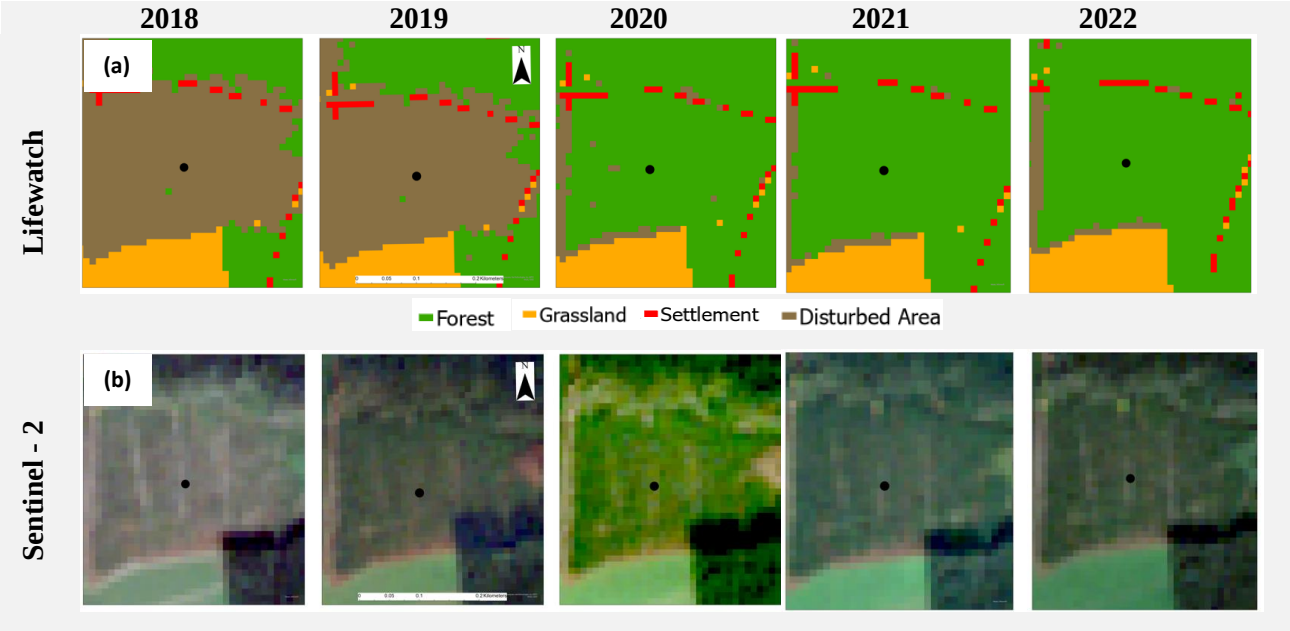

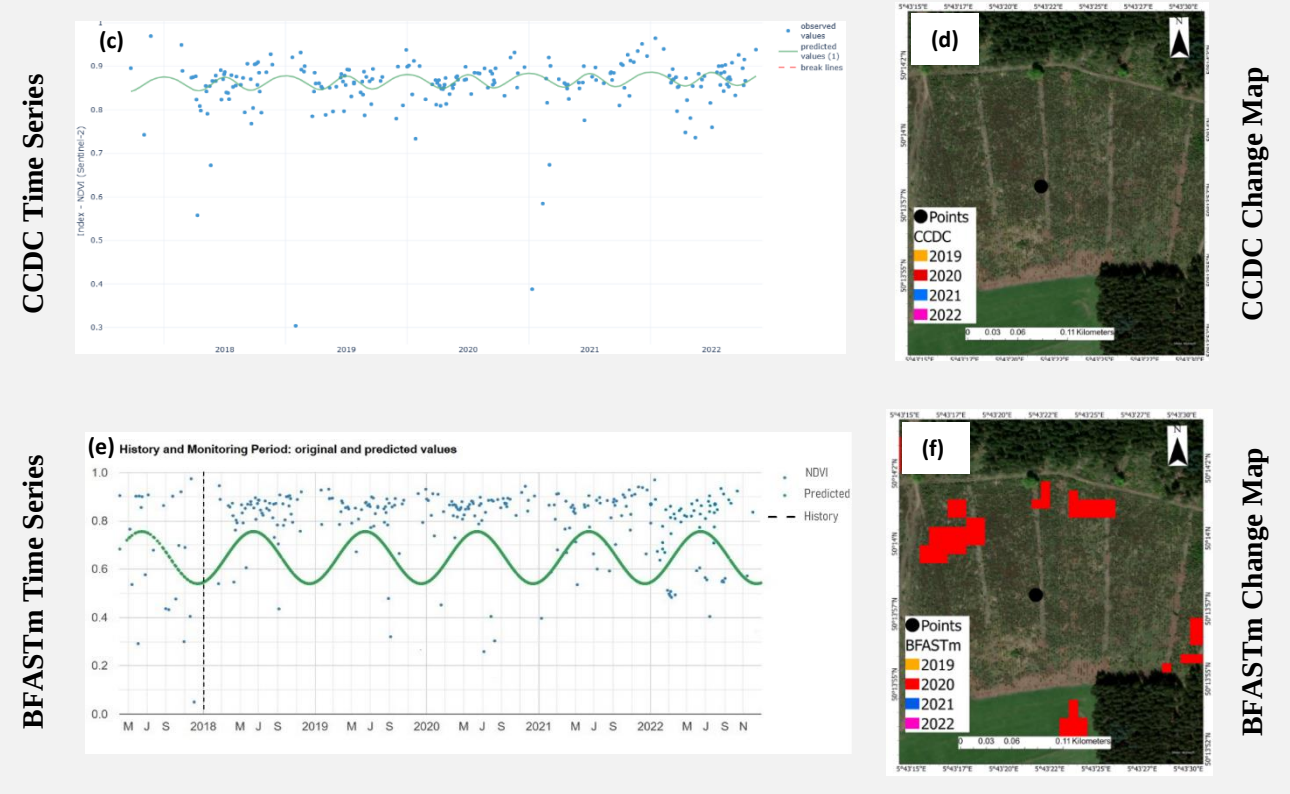

Figure 22: CCDC and BFASTm change detection algorithm comparison in other land area based on Lifewatch data (a), sentinel – 2 images (b), CCDC time series (c) and change map (d) indicating no break, BFASTm time series (e) and change map (f) indicating no break in the pixel

Although the area underwent a distinct change, both algorithms failed to detect it. Neither the time series nor the change maps yielded any detection of the change. This failure to detect changes in the disturbed area represents the most critical case among all classes examined in this section.

6.4. Validation

6.4.1. Accuracy Assessment of CCDC

Table 10 shows the summary of the CCDC algorithm performance evaluation. A stratified random approach based on change and stable samples was employed, by which OA of 60% was obtained with 44% F-score for the change pixels (Table 10). Besides, the PA of the change pixels is good (72%), and the PA of the stable pixels is comparatively low (56%).

Table 10: Error matrix of CCDC change detection algorithm

CCDC Change	Reference Change Map				
	Changed pixels	Stable pixels	Total	User's Accuracy	F-Score
Changed pixels	190	424	614	31%	44%
Stable pixels	75	539	614	88%	69%
Total	265	963	1228		

	Producer's Accuracy	72%	56%			
	Omission Error	28%	44%	**Overall Accuracy 60%**		
	Commission Error	69%	12%			

6.4.2. Accuracy Assessment of BFASTm

Table 11 provides a summary of the performance evaluation of the BFASTm algorithm. Using a stratified random sampling approach, which was based on both change and stable samples, the algorithm achieved an overall accuracy (OA) of 55% and an F-score of 37% for the changed points (Table 11). The PA for change and stable pixels remained comparatively low, at 62% and 53%, respectively.

Table 11: Error matrix of BFASTm change detection algorithm

BFASTm Change Map	**Reference Change Map**					
		Changed pixels	Stable pixels	Total	User's Accuracy	F-Score
	Changed pixels	161	452	614	26%	37%
	Stable pixels	99	515	614	84%	66%
	Total	261	967	1228		
	Producer's Accuracy	62%	53%			
	Omission Error	38%	47%	**Overall Accuracy 55%**		
	Commission Error	74%	16%			

The relatively lower UA indicates more commission errors than omission errors in detected changes. In the case of CCDC and BFASTm, commission errors primarily arise from two key factors: overfitting of the time series model and consecutive missing data points due to cloud cover. Even with a straightforward time series model, overfitting can occur, especially if certain periods consistently lack data due to cloud cover. Aside from that, cloudiness poses a significant challenge, particularly in regions like Wallonia, where cloud cover is prevalent. Cloud interference can introduce inconsistencies in the time series analysis, resulting in pseudo changes being detected by the algorithms. When cloud cover persists for three or more consecutive periods, it can erroneously trigger change identifications (Figure 25c – 25d).

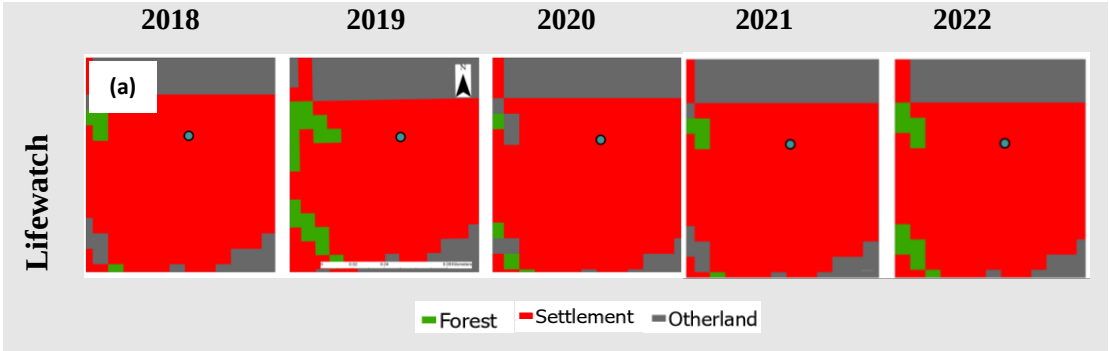

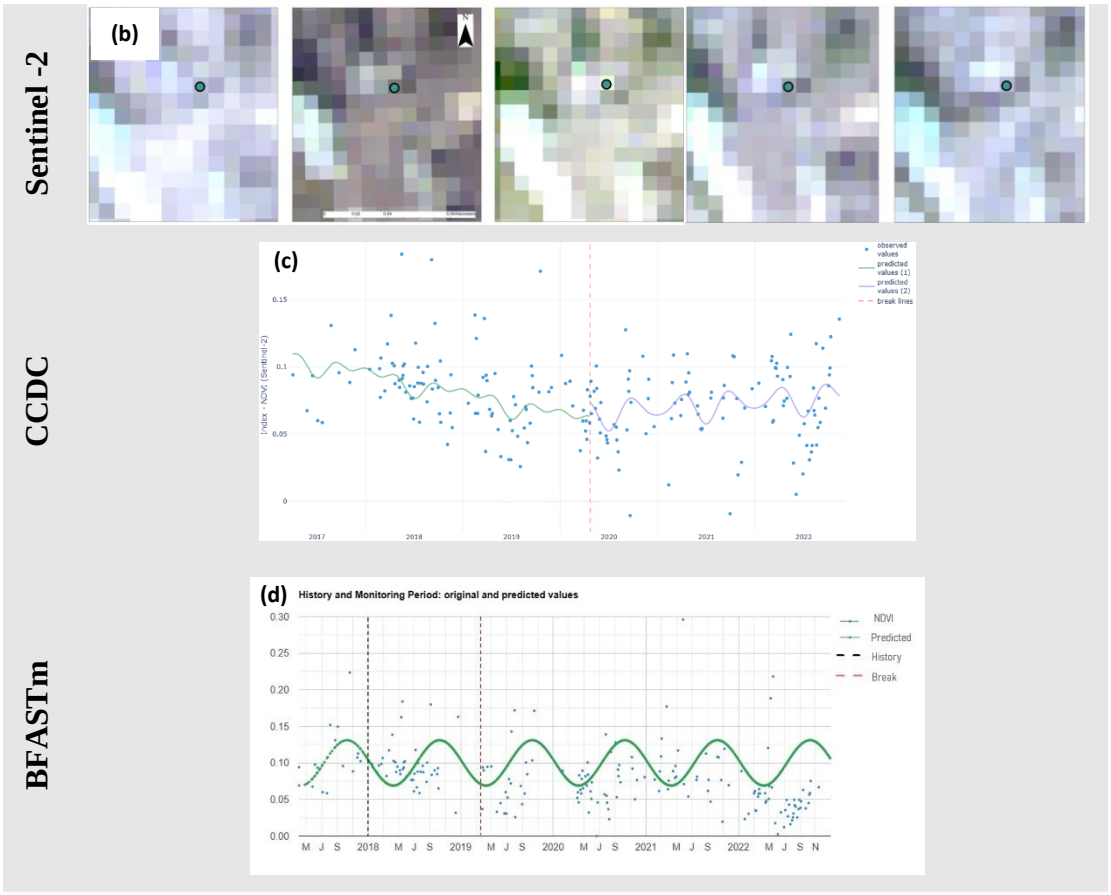

Figure 23: Commission error in change detection for CCDC (c) and BFASTm (d): clouds missed three time consecutively illustrated by NDVI time series compared with Lifewatch data (a), sentinel – 2 images (b)

Omission errors primarily occur due to partially changed pixels, which pose a significant challenge in detection. These pixels are difficult to identify because the magnitude of change depends on the proportion of change within the pixel. For instance, in Figure 26c, regrowth of grass in 2019 caused a shift in NDVI index variability, indicating a change. However, the magnitude of this change is minimal, making it challenging to detect

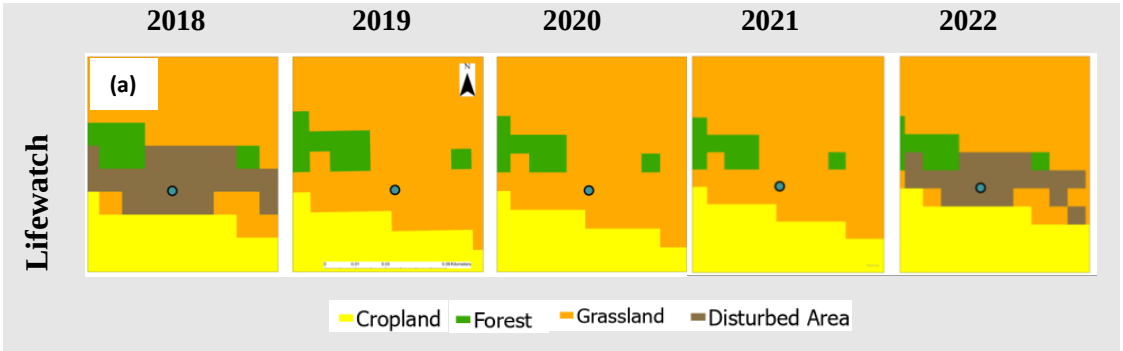

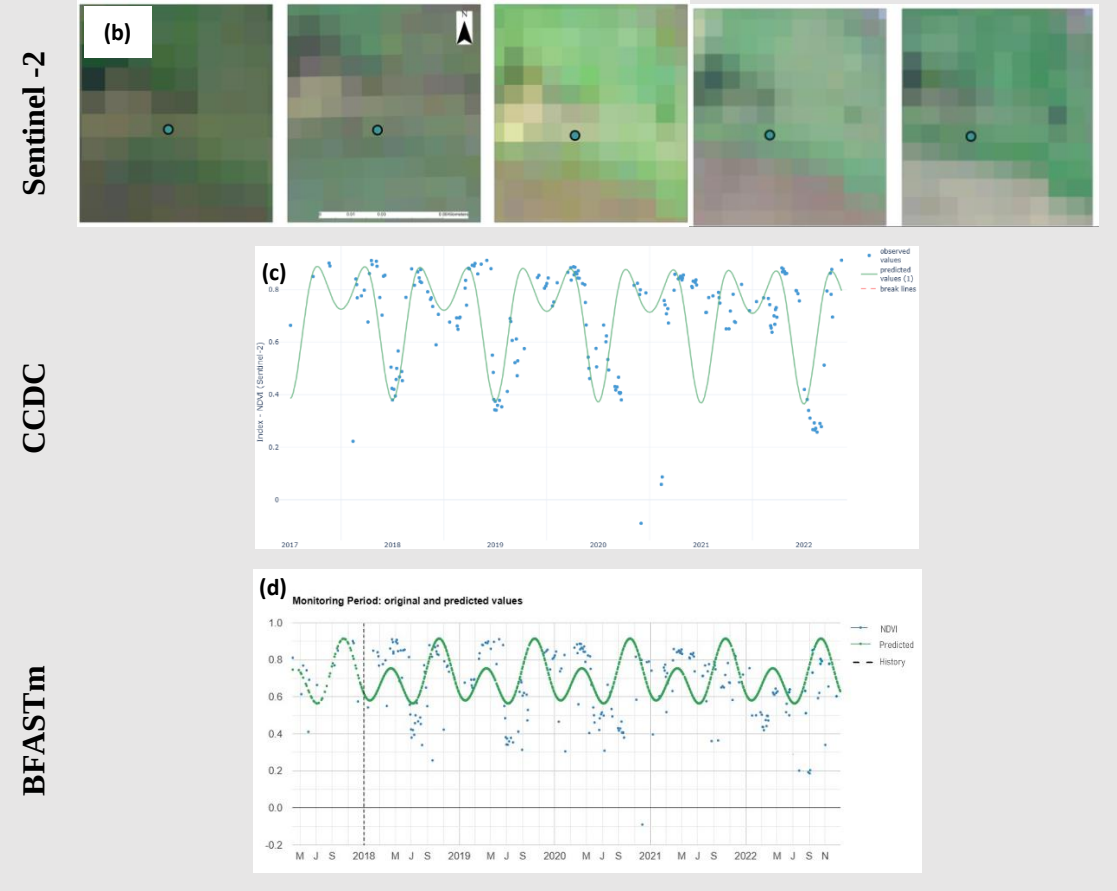

Figure 24: Omission error in change detection for CCDC (c) and BFASTm (d): partial replantation and forest cut illustrated by NDVI time series Lifewatch data (a), sentinel – 2 images (b)

A summary of the various LULC classes' performance evaluations for both algorithms is given in Table 12. Wetland and grassland obtained the lowest and highest UA, respectively, for both methodologies.

Table 12: User-specific accuracy for changed LULC Classes

LULC Class	Accuracy	
	CCDC	BFASTm
Wetland	0.0667	0.03333
Settlement	0.10256	0.12821
Cropland	0.1	0.11864
Grassland	**0.6962**	**0.35802**
Forest	0.50704	0.26397
Other land	0.37931	0.2
Disturbed area	0.29032	0.35484

Chapter 7: Discussion

This chapter will comprehensively analyze the results obtained in Chapter 6 and compare them with the previous research findings outlined in Chapter 2. Section 7.1 presents the discussion about the comparison between CCDC and BFASTm algorithms performances. Furthermore, section 7.2 discusses the limitations of the study, which can be further solved.

7.1. Comparison of CCDC and BFASTm Results

Detecting changes in land cover poses a significant challenge in remote sensing applications. Leveraging the temporal dimension of satellite data can significantly enhance the accuracy of LULC change detection. Consequently, the speed at which the CCDC algorithm identifies changes and their corresponding land cover types primarily hinges on the frequency of clear observations available. BFASTm can be used to detect significant long-term changes by exploiting the full time series while accounting for abrupt and gradual changes. In this part, the abilities of CCDC and BFASTm to detect changes in the seven LULC classes will be discussed and compared.

CCDC exhibited superior accuracy in detecting grassland transitions compared to other LULC classes with 70% UA (Table 12) and the spatial accuracy of CCDC was also promising in this regard (section 6.3). While BFASTm demonstrated only 36% UA, which is higher than other LULC classes. Grassland transitions were accurately captured because the algorithms detected harvest activities and land management processes before they were converted to cropland.

In terms of forested areas, the majority of disturbances occurred predominantly in the Northern-Eastern region of the study area, with comparatively fewer disturbances observed in the southern region. CCDC performed better in finding transformations in forest areas (Table 12). However, BFASTm failed to detect alterations correctly in this study area even though it was developed to detect forest disturbances (Verbesselt et al., 2010; Friedrich et al., 2020).

However, both algorithms encountered difficulties in detecting replantation events in disturbed areas. CCDC demonstrates limitations in effectively detecting changes within the disturbed areas class. This could be attributed to the immediate replanting of trees following forest clear-cutting, as evident from reference maps (Figure 22a). Consequently, the NDVI values may not exhibit significant changes as expected. This observation was consistent across various pixels throughout Wallonia, indicating a recurring pattern. The reference data revealed that clear-cutting occurred in small portions of land but bigger than 10*10m except thinning which is not

LULC changes. So it can potentially lead to partial changes that CCDC may struggle to detect accurately. Similarly, despite being primarily designed for forest-related assessments, BFASTm faced challenges in accurately discerning replantation or regrowth occurrences (Figure 22). Wu et al. (2020) also mentioned that the intra-annual changes, such as flooding and replantation post-deforestation, were difficult to detect by BFASTm.

In the context of monitoring cropland, both CCDC and BFASTm exhibit a tendency toward false positive change detections with only 10% UA for both algorithms (Table 12), reflecting their susceptibility to inaccuracies. According to the analysis of the reference dataset, the conversion between cropland and grassland occurs rapidly and happens mostly annually in Wallonia (Lifewatch, 2024). In this case, the transformation from cropland to grassland would be observed as a temporary alteration in land cover that occurs within the context of seasonal cycles. It must be kept in mind that the purpose of CCDC is to detect complete changes in land cover type. Zhu and Woodcock (2014) mentioned that CCDC may not be valid for land cover types with more intra-annual variation, such as agriculture.

In this study area, settlement areas were mostly unchanged during the five-year period. BFASTm captured LULC disturbances associated with settlement area establishment and expansion slightly more accurately than CCDC. Still, CCDC may not be suitable for settlement changes because settlements often exhibit gradual changes over time, which can be challenging for the algorithm to detect accurately. CCDC tends to create pseudo-changes in the entire settlements of the study area. Chen et al. (2023) mentioned that CCDC was responsible for reducing the accuracy in detecting the settlement area expansion and this is possibly because of the low quality of CCDC features related to the dense cloud cover. Nevertheless, Friedrich et al. (2020) found BFAST detecting the changes in the built-up areas robustly with higher accuracy.

In the case of other lands, the variations are insignificant. CCDC detected more accurately than other method (Table 12). For wetlands, the change throughout the study period is very negligible. There was only a very few areas were found, where any change was visible in the reference dataset. In this regard, both algorithms performed the worst in this class by creating a vast number of false positive changes.

The mention of calibrated parameter values suggests that the settings optimized for one LULC class may not be equally effective across all classes, potentially leading to errors in change

detection. It could be better to be fine-tuned based on a particular LC class. For instance, parameters suitable for detecting changes in forests might not perform well in settlement areas (Figure 25). This discrepancy is evident in the comparison between CCDC's detection of changes in forested regions versus settlements. While CCDC accurately identifies changes in forests, it tends to produce numerous pseudo changes in settlement areas when compared to Lifewatch data.

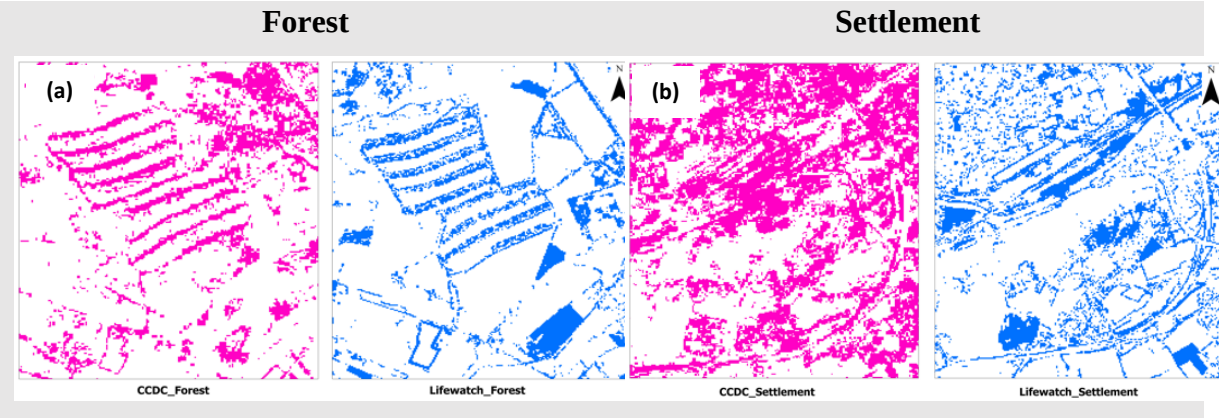

Figure 25: Comparisons of CCDC and Lifewatch change maps in forest areas (a), and in settlement area (b) based on the CCDC calibrated parameters for forest

Although CCDC was designed to detect changes across various land disturbance types, many of the research has focused on individual land cover classes rather than considering them collectively, and that was also mentioned by Zhu et al. (2022). Consequently, modifications and parameter calibrations have been tailored to each LULC class independently to optimize detection performance (Peng et al., 2021; Chen et al., 2023). Compared to CCDC's performance, BFASTm exhibited unsatisfactory effectiveness in detecting changes across all classes collectively.

In anticipation of CCDC, the results of the accuracy assessment show the PA of 72% for the change pixels and 56% for the stable pixels. The user's accuracy of change and no change pixels were 31% and 88%, respectively with an OA of 60% (Table 10). On the other hand, BFASTm has a lower overall accuracy (55%) compared to CCDC. The producer's accuracy for change pixels is 62%, while the user's accuracy is only 26%. Conversely, for stable pixels, the producer's accuracy is lower than that of change pixels, but the user's accuracy is significantly higher at 84% (Table 11). Both algorithms indicated higher omission and commission errors illustrated in Figures 23 and 24. Even so, The CCDC algorithm showed fewer commission and omission errors compared to the BFASTm algorithm.

CCDC generally provides higher overall accuracy in most studies. For example, the algorithm achieved overall accuracies of 91% (Zhu and Woodcock, 2014a) and 87% (Zhu et al., 2016) in detecting land cover changes. These higher accuracies can be attributed to using Landsat images for both the model and reference data, as well as the lower cloud cover in the study areas. Conversely, Awty-Carroll et al. (2019) found that CCDC performed the worst compared to other algorithms in an area with higher cloud cover, whereas BFASTm performed slightly better. BFASTm was the only method that improved significantly with more missing data, making it preferable in regions with high cloud cover. Both algorithms performed worse in detecting smaller magnitude changes in land cover condition. Additionally, abrupt changes in specific areas with relative stability in surrounding regions further complicate detection. Awty-Carroll et al. (2019) have also noted CCDC's tendency to detect larger magnitude changes more effectively while underestimating smaller magnitude and seasonal changes. Similarly, the BFASTm algorithm requires a significant spectral change before detection, delaying identification until the change is fully realized (Wu et al., 2020).

In this study, BFASTm was the fastest method and the most consistent in average runtime among the two algorithms. The main strength of CCDC is its ability to avoid overestimating the number of breaks. It can detect more than one break in the time series, which is one of its strengths. Evidence for this is seen in the observation that CCDC detected more breaks. Both algorithms tended to create false positive changes, but BFASTm had a lower producer's accuracy compared to CCDC due to these false positives. Nonetheless, because BFASTm detects changes on an observation-by-observation basis using the MOSUM method, it requires only a single observation to exceed a boundary for a change to be flagged. This allows for faster detection of breaks but can result in more observations being incorrectly flagged as changes. CCDC worked better with OA of 60% and BFASTm with 55%.

To quantify the uncertainty of this estimate, a 95% confidence interval for the proportion was calculated. The margin of error was found for CCDC and BFASTm to be 0.02735 and 0.0278, respectively. Hence, the actual accuracy of the CCDC algorithm is estimated to range between 57.27% and 62.73%. Similarly, the true accuracy of BFASTm spans from 52.22% to 57.78%. Still, they are preferable to other methods in regions with high quantities of missing data, such as areas with frequent cloud cover. CCDC showed comparatively consistent performance across different levels of missing data, likely because it is designed to detect land cover class changes and is less influenced by single outliers.

By analyzing all the points and error matrix, CCDC achieved superior results in Wallonia to detect changes over the five-year period from 2018 to 2022.

7.2. Study Limitations

7.2.1. Technical Challenges

7.2.1.1. Temporal Resolution Issue

In this study, the Lifewatch dataset served as the reference data for assessing land cover changes. The Lifewatch dataset is derived from ortho-photos. Consequently, changes occurring in Wallonia after the particular month of the current year observation and that month of the subsequent year are inherently inclined to be detected in the following year's dataset. This temporal lag introduces challenges in accurately capturing changes in a timely manner. Furthermore, there are instances where the reference data fails to detect changes apparent in Sentinel-2 images due to the lower temporal resolution of the reference dataset (Figure 26).

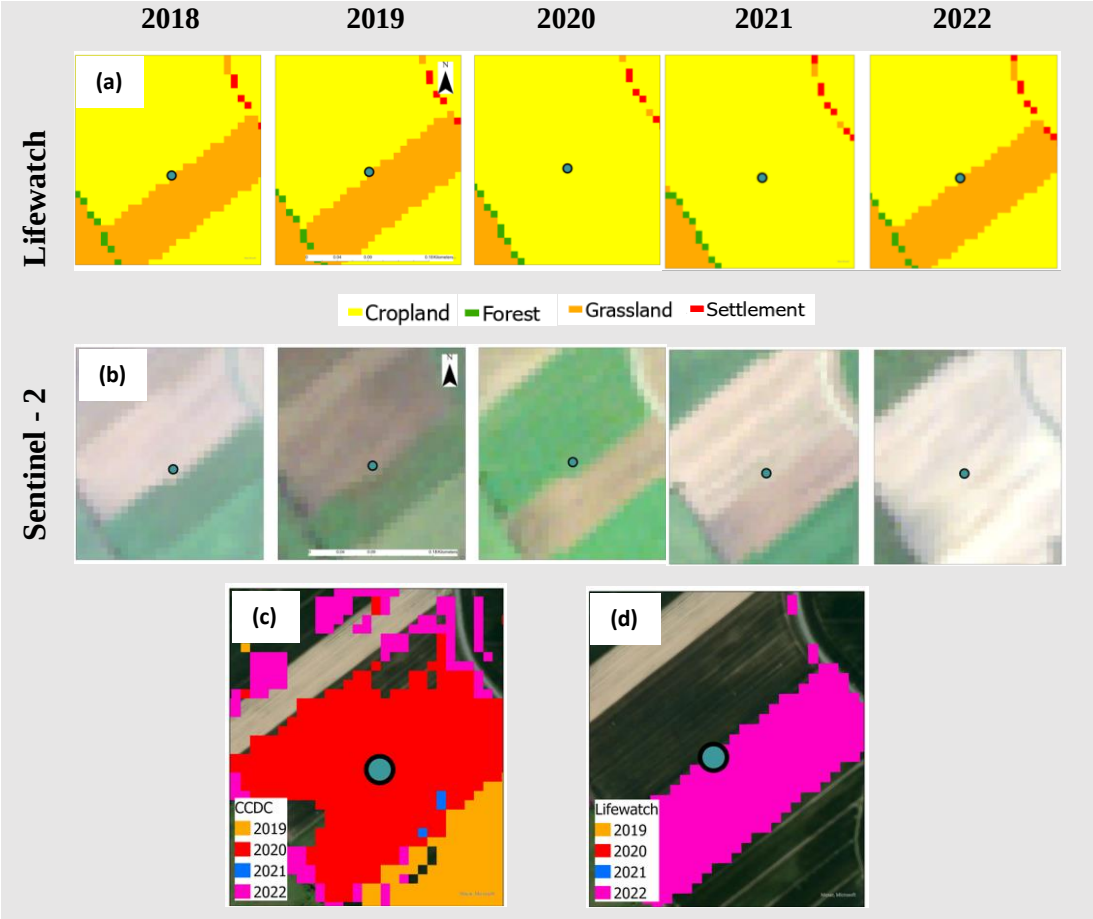

Figure 26: Temporal resolution issue in the reference data (d) compared with CCDC Change map (c) for a particular plot based on Lifewatch data (a), sentinel – 2 images (b)

7.2.1.2. Spatial Resolution Issue

Another challenge with the reference dataset is its spatial resolution, set at 2 meters, which is significantly finer than the 10-meter resolution of Sentinel-2 images. Resampling was necessary to align the resolutions, but this process resulted in the loss and misclassification of a few pixels due to resampling artefacts. Additionally, while the Lifewatch data offer high accuracy in classification, CCDC and BFASTm algorithms may occasionally miss small changes that occur within the 2m spatial resolution.

7.2.1.3. Cloudy Areas

Wallonia is one of the worst areas in Europe regarding cloudiness. It is very hard to get cloud free images in this region throughout the year. Both algorithms handled the missing values due to the clouds quite similarly with lower accuracies. However, BFASTm produced more pseudo changes than CCDC.

7.2.2. Resource Constraints

The source code utilized in this study presented certain complexities that posed challenges during implementation. Undertaking this level of analysis requires a certain level of coding expertise, as navigating through the algorithms and resolving technical hurdles demands proficiency.

7.2.3. Time Constraints

These algorithms are advanced and not widely known among students due to their complexity. Mastery of each step of the algorithms demands dedicated effort and a considerable investment of time. Furthermore, refining and optimizing different components of the algorithms to enhance their performance necessitates additional time and expertise.

Chapter 8: Conclusion

In this study, the performance of CCDC and BFASTm algorithms for LULC change detection in the Wallonia region of Belgium was assessed. This region is characterized by frequent cloud cover, which limited the number of clear satellite images available for analysis. Despite these challenges, it was found that CCDC performed better than BFASTm, achieving higher overall accuracy compared to BFASTm's.

Although higher overall accuracy was exhibited by CCDC, it did not perform well in detecting changes in cropland and wetland areas, but worked better for the grassland and forest areas. Whereas, superior performances were shown by BFASTm in grassland and disturbed areas. This discrepancy highlights the strengths and weaknesses of each algorithm in different LULC classes. The use of Lifewatch data, which provided high spatial resolution but lacked temporal precision, may have introduced some errors. The importance of accurate temporal resolution in reference data for these algorithms is emphasized, underscoring the need for high-quality, temporally accurate datasets to improve change detection accuracy.

Overall, this study underscores the effectiveness of CCDC in regions with limited clear satellite images but also points to the potential benefits of combining strengths from both algorithms to enhance LULC change detection. However, it must be acknowledged that remote sensing is not without its limitations. The limitations posed by cloud cover and lower temporal resolution in-situ data should be addressed in future research, and efforts should be made to improve the integration of these algorithms for more robust and reliable LULC monitoring. In addition, calibration of algorithm parameters for large study areas must also be approached with meticulous care to enhance results. When conducted with precision and supported by dependable in-situ datasets, the algorithms can be utilized as a decision-making tool for environmental monitoring.

References

Abd El-Kawy, O. R., Rød, J. K., Ismail, H. A., & Suliman, A. S. (2011). Land use and land cover change detection in the western Nile delta of Egypt using remote sensing data. *Applied geography*, *31*(2), 483-494. https://doi.org/10.1016/j.apgeog.2010.10.012

Ahlqvist, O. (2008). Extending post-classification change detection using semantic similarity metrics to overcome class heterogeneity: A study of 1992 and 2001 US National Land Cover Database changes. *Remote Sensing of Environment*, *112*(3), 1226-1241. https://doi.org/10.1016/j.rse.2007.08.012

Albrecht, F., Lang, S., & Hölbling, D. (2010). Spatial accuracy assessment of object boundaries for object-based image analysis. *The International Archives of the Photogrammetry, Remote Sensing and Spatial Information Sciences*, *38*(4), C7.

Anderson, J. R. (1976). A land use *and land cover classification system for use with remote sensor data* (Vol. 964). U.S. Government Printing Office. https://doi.org/10.3133/pp964

Araya, Y. H., & Hergarten, C. (2008). A comparison of pixel and object-based land cover classification: a case study of the Asmara region, Eritrea. *WIT Transactions on The Built Environment*, *100*, 233-243. https://doi.org/10.2495/geo080231

Awty-Carroll, K., Bunting, P., Hardy, A., & Bell, G. (2019). Using continuous change detection and classification of Landsat data to investigate long-term mangrove dynamics in the Sundarbans region. *Remote Sensing*, *11*(23), 2833. https://doi.org/10.3390/rs11232833.

Awty-Carroll, K., Bunting, P., Hardy, A., & Bell, G. (2021). Evaluation of the Continuous Monitoring of Land Disturbance Algorithm for Large-Scale Mangrove Classification. *Remote Sensing*, *13*(19), 3978. https://doi.org/10.3390/rs13193978

Benediktsson, J. A., Chanussot, J., & Fauvel, M. (2007). Multiple classifier systems in remote sensing: from basics to recent developments. In *International Workshop on Multiple Classifier Systems* (pp. 501-512). Berlin, Heidelberg: Springer Berlin Heidelberg. https://doi.org/10.1007/978-3-540-72523-7_50

Bontemps, S., Langner, A., & Defourny, P. (2009). Monitoring forest changes in Borneo on a yearly basis by an object-based change detection algorithm using SPOT-VEGETATION time series. *International journal of remote sensing*, *33*(15), 4673-4699. https://doi.org/10.1080/01431161.2011.638336

Breiman, L. (2001). Random forests. *Machine learning*, *45*, 5-32.

Brogna, D., Dufrêne, M., Michez, A., Latli, A., Jacobs, S., Vincke, C. and Dendoncker, N., 2018. Forest cover correlates with good biological water quality. Insights from a

regional study (Wallonia, Belgium). Journal of environmental management, 211, pp.9-21.

Brown, J. F., Tollerud, H. J., Barber, C. P., Zhou, Q., Dwyer, J. L., Vogelmann, J. E., & Rover, J. (2020). Lessons learned implementing an operational continuous United States national land change monitoring capability: The Land Change Monitoring, Assessment, and Projection (LCMAP) approach. *Remote sensing of environment*, *238*, 111356. https://doi.org/10.1016/j.rse.2019.111356.

Bruzzone, L., Cossu, R., & Vernazza, G. (2004). Detection of land-cover transitions by combining multidate classifiers. *Pattern Recognition Letters*, *25*(13), 1491-1500. https://doi.org/10.1016/j.patrec.2004.06.002

Bullock, E. L., Woodcock, C. E., & Holden, C. E. (2020). Improved change monitoring using an ensemble of time series algorithms. *Remote Sensing of Environment*, *238*, 111165. https://doi.org/10.1016/j.rse.2019.04.018.

Bunting, P., Rosenqvist, A., Lucas, R. M., Rebelo, L. M., Hilarides, L., Thomas, N., & Finlayson, C. M. (2018). The global mangrove watch—a new 2010 global baseline of mangrove extent. *Remote Sensing*, *10*(10), 1669. https://doi.org/10.3390/rs10101669

CEOS. (2023). Committee on Earth Observation Satellites. https://lpvs.gsfc.nasa.gov/LandCover/LC_home.html

Chen, J., Chen, X., Cui, X., & Chen, J. (2010). Change vector analysis in posterior probability space: A new method for land cover change detection. *IEEE Geoscience and Remote Sensing Letters*, *8*(2), 317-321. https://doi.org/10.1109/lgrs.2010.2068537

Chen, T.H.K., Pandey, B. and Seto, K.C., 2023. Detecting subpixel human settlements in mountains using deep learning: A case of the Hindu Kush Himalaya 1990–2020. *Remote Sensing of Environment*, *294*, p.113625. https://doi.org/10.1016/j.rse.2023.113625

Chen, X., Vierling, L., & Deering, D. (2005). A simple and effective radiometric correction method to improve landscape change detection across sensors and across time. *Remote Sensing of Environment, 98*(1), 63-79. https://doi.org/10.1016/j.rse.2005.05.021

Chen, Y. C., Chiu, H. W., Su, Y. F., Wu, Y. C., & Cheng, K. S. (2017). Does urbanization increase diurnal land surface temperature variation? Evidence and implications. *Landscape and Urban Planning*, *157*, 247-258. https://doi.org/10.1016/j.landurbplan.2016.06.014

Cheng, K. S., Su, Y. F., Kuo, F. T., Hung, W. C., & Chiang, J. L. (2008). Assessing the effect of landcover changes on air temperature using remote sensing images - A pilot study in northern Taiwan. *Landscape and Urban Planning*, *85*(2), 85-96. https://doi.org/10.1016/j.landurbplan.2007.09.014

Choudhary, K., Boori, M. S., & Kupriyanov, A. (2018). Spatial modelling for natural and environmental vulnerability through remote sensing and GIS in Astrakhan, Russia. *The*

Egyptian Journal of Remote Sensing and Space Science, *21*(2), 139-147. https://doi.org/10.1016/j.ejrs.2017.05.003

Chughtai, A. H., Abbasi, H., & Karas, I. R. (2021). A review on change detection method and accuracy assessment for land use land cover. *Remote Sensing Applications: Society and Environment*, *22*, 100482. https://doi.org/10.1016/j.rsase.2021.100482

Close, O., Benjamin, B., Petit, S., Fripiat, X., & Hallot, E. (2018). Use of Sentinel-2 and LUCAS database for the inventory of land use, land use change, and forestry in Wallonia, Belgium. *Land*, *7*(4), 154. https://doi.org/10.3390/land7040154

Cohen, W. B., Fiorella, M., Gray, J., Helmer, E., & Anderson, K. (1998). An efficient and accurate method for mapping forest clearcuts in the Pacific Northwest using Landsat imagery. *Photogrammetric engineering and remote sensing*, *64*(4), 293-299.

Cohen, W. B., Yang, Z., Healey, S. P., Kennedy, R. E., & Gorelick, N. (2018). A LandTrendr multispectral ensemble for forest disturbance detection. *Remote sensing of environment*, *205*, 131-140. https://doi.org/10.1016/j.rse.2017.11.015

Copernicus. (2023). Copernicus Programme. https://www.copernicus.eu/en/copernicus-services/land

Dara, A., Baumann, M., Kuemmerle, T., Pflugmacher, D., Rabe, A., Griffiths, P., & Hostert, P. (2018). Mapping the timing of cropland abandonment and recultivation in northern Kazakhstan using annual Landsat time series. *Remote Sensing of Environment*, *213*, 49-60. https://doi.org/10.1016/j.rse.2018.05.005

Desclée, B., Bogaert, P., & Defourny, P. (2006). Forest change detection by statistical object-based method. *Remote sensing of environment*, *102*(1-2), 1-11. https://doi.org/10.1016/j.rse.2006.01.013

DeVries, B., Decuyper, M., Verbesselt, J., Zeileis, A., Herold, M., & Joseph, S. (2015). Tracking disturbance-regrowth dynamics in tropical forests using structural change detection and Landsat time series. *Remote Sensing of Environment*, *169*, 320-334. http://dx.doi.org/10.1016/j.rse.2015.08.020.

Dewan, A. M., & Yamaguchi, Y. (2009). Using remote sensing and GIS to detect and monitor land use and land cover change in Dhaka Metropolitan of Bangladesh during 1960–2005. *Environmental monitoring and assessment*, *150*, 237-249. https://doi.org/10.1007/s10661-008-0226-5

Dutrieux, L. P., Verbesselt, J., Kooistra, L., & Herold, M. (2015). Monitoring forest cover loss using multiple data streams, a case study of a tropical dry forest in Bolivia. *ISPRS Journal of Photogrammetry and Remote Sensing*, *107*, 112-125. http://dx.doi.org/10.1016/j. isprsjprs.2015.03.015.

Dye, M., Mutanga, O., & Ismail, R. (2011). Examining the utility of random forest and AISA Eagle hyperspectral image data to predict Pinus patula age in KwaZulu-Natal, South

Africa. *Geocarto International*, *26*(4), 275-289. https://doi.org/10.1080/10106049.2011.562308

EEA. (2017). European environment Agency. Country fact sheet, Belgium. https://www.bing.com/search?q=belgium+has+one+of+the+lowest+mean+annual+land+cover+rates+in+all+of+europe.&gs_lcrp=EgZjaHJvbWUqBwgAEEUYwgMyBwgAEEUYwgMyBwgBEEUYwgMyBwgCEEUYwgMyBwgDEEUYwgMyBwgEEOwHGEAyBwgFEOwHGEAyBwgGEOwHGEAyBwgHEOwHGEDSAQsyMTA1MzY1ajBqMagCBLACAQ&FORM=ANNTA1&PC=HCTS

ESA. (2015). User handbook. *ESA Standard Document*, *64*(2), 64. https://sentinel.esa.int/documents/247904/685211/Sentinel-2_User_Handbook

FAO - Food and Agriculture Organization, (2024). https://www.fao.org/geospatial/our-work/what-we-do/land-cover-and-land-use/en/#:~:text=Land%20cover%20is%20defined%20as%20the%20observed%20physical,cover%20type%20to%20produce%2C%20change%2C%20or%20maintain%20it. Retrieved on 12th May, 2024.

Fichera, C. R., Modica, G., & Pollino, M. (2012). Land Cover classification and change-detection analysis using multi-temporal remote sensed imagery and landscape metrics. *European journal of remote sensing*, *45*(1), 1-18. https://doi.org/10.5721/eujrs20124501

Fonji, S. F., & Taff, G. N. (2014). Using satellite data to monitor land-use land-cover change in North-eastern Latvia. *Springerplus*, *3*, 1-15. https://doi.org/10.1186/2193-1801-3-61

Fragal, E. H., Silva, T. S. F., & Novo, E. M. L. D. M. (2016). Reconstructing historical forest cover change in the Lower Amazon floodplains using the LandTrendr algorithm. *Acta Amazonica*, *46*, 13-24. https://doi.org/10.1590/1809-4392201500835

Franklin, S. E., Ahmed, O. S., Wulder, M. A., White, J. C., Hermosilla, T., & Coops, N. C. (2015). Large area mapping of annual land cover dynamics using multitemporal change detection and classification of Landsat time series data. *Canadian Journal of Remote Sensing*, *41*(4), 293-314. http://dx.doi.org/10.1080/07038992.2015.1089401.

Friedl, M. A., Woodcock, C. E., Olofsson, P., Zhu, Z., Loveland, T., Stanimirova, R. & Souza Jr, C. (2022). Medium spatial resolution mapping of global land cover and land cover change across multiple decades from landsat. *Frontiers in Remote Sensing*, *3*, 894571. https://doi.org/10.3389/frsen.2022.894571.

Friedrich, H.K. and Van Den Hoek, J., 2020. Breaking ground: automated disturbance detection with landsat time series captures rapid refugee settlement establishment and growth in North Uganda. *Computers, Environment and Urban Systems*, *82*, p.101499. https://doi.org/10.1016/j.compenvurbsys.2020.101499

GEE – Google Earth Engine Documentation, (2024). https://developers.google.com/earth-engine/apidocs/ee-algorithms-temporalsegmentation-ccdc. Retrieved on 21st February, 2024.

Giannetti, F., Pecchi, M., Travaglini, D., Francini, S., D'Amico, G., Vangi, E. & Chirici, G. (2021). Estimating VAIA windstorm damaged forest area in Italy using time series Sentinel-2 imagery and continuous change detection algorithms. *Forests*, *12*(6), 680. https://doi.org/10.3390/f12060680

Gislason, P. O., Benediktsson, J. A., & Sveinsson, J. R. (2006). Random forests for land cover classification. *Pattern recognition letters*, *27*(4), 294-300. https://doi.org/10.1016/j.patrec.2005.08.011

Gorelick, N., Hancher, M., Dixon, M., Ilyushchenko, S., Thau, D., & Moore, R. (2017). Google Earth Engine: Planetary-scale geospatial analysis for everyone. Remote Sensing of Environment.

Halimi, M., Sedighifar, Z., & Mohammadi, C. (2018). Analyzing spatiotemporal land use/cover dynamic using remote sensing imagery and GIS techniques case: Kan basin of Iran. *GeoJournal*, *83*, 1067-1077. https://doi.org/10.1007/s10708-017-9819-2

Halmy, M. W. A., Gessler, P. E., Hicke, J. A., & Salem, B. B. (2015). Land use/land cover change detection and prediction in the north-western coastal desert of Egypt using Markov-CA. *Applied Geography*, *63*, 101-112. https://doi.org/10.1016/j.apgeog.2015.06.015

Hamad, R. (2020). An assessment of artificial neural networks, support vector machines and decision trees for land cover classification using sentinel-2A data. *Sciences*, *8*(6), 459-464. https://doi.org/10.12691/aees-8-6-18

Hansen, M. C., Potapov, P. V., Moore, R., Hancher, M., Turubanova, S. A., Tyukavina, A. & Townshend, J. (2013). High-resolution global maps of 21st-century forest cover change. *science*, *342*(6160), 850-853. https://doi.org/10.1126/science.1244693.

Hayes, M. M., Miller, S. N., & Murphy, M. A. (2014). High-resolution landcover classification using Random Forest. *Remote sensing letters*, *5*(2), 112-121. https://doi.org/10.1080/2150704x.2014.882526

Hermosilla, T., Wulder, M. A., White, J. C., & Coops, N. C. (2022). Land cover classification in an era of big and open data: Optimizing localized implementation and training data selection to improve mapping outcomes. *Remote Sensing of Environment*, *268*, 112780. https://doi.org/10.1016/j.rse.2021.112780.

Hernando, A., Tiede, D., Albrecht, F., & Lang, S. (2012). Spatial and thematic assessment of object-based forest stand delineation using an OFA-matrix. *International Journal of Applied Earth Observation and Geoinformation*, *19*, 214-225. https://doi.org/10.1016/j.jag.2012.05.007

Hilker, T., Wulder, M. A., Coops, N. C., Linke, J., McDermid, G., Masek, J. G., ... & White, J. C. (2009). A new data fusion model for high spatial-and temporal-resolution mapping of forest disturbance based on Landsat and MODIS. *Remote Sensing of Environment*, *113*(8), 1613-1627. https://doi.org/10.1016/j.rse.2009.03.007

https://maps.elie.ucl.ac.be/download/ecotopes_documentation_en_v4-18.pdf

Huang, C., Goward, S. N., Masek, J. G., Thomas, N., Zhu, Z., & Vogelmann, J. E. (2010). An automated approach for reconstructing recent forest disturbance history using dense Landsat time series stacks. *Remote Sensing of Environment*, *114*(1), 183-198. https://doi.org/ 10.1016/j.rse.2009.08.017.

Jia, B., Luo, X., Cai, X., Jain, A., Huntzinger, D.N., Xie, Z., Zeng, N., Mao, J., Shi, X., Ito, A. and Wei, Y., 2020. Impacts of land use change and elevated CO 2 on the interannual variations and seasonal cycles of gross primary productivity in China. *Earth System Dynamics*, *11*(1), pp.235-249. https://doi.org/10.5194/esd-11-235-2020

Jin, S., Homer, C., Yang, L., Xian, G., Fry, J., Danielson, P., & Townsend, P. A. (2013). Automated cloud and shadow detection and filling using two-date Landsat imagery in the USA. *International Journal of Remote Sensing*, *34*(5), 1540-1560. https://doi.org/10.1080/01431161.2012.720045.

Jin, Y., Liu, X., Chen, Y., & Liang, X. (2018). Land-cover mapping using Random Forest classification and incorporating NDVI time-series and texture: A case study of central Shandong. *International journal of remote sensing*, *39*(23), 8703-8723. https://doi.org/10.1080/01431161.2018.1490976

Kennedy, R. E., Yang, Z., & Cohen, W. B. (2010). Detecting trends in forest disturbance and recovery using yearly Landsat time series: 1. LandTrendr—Temporal segmentation algorithms. *Remote Sensing of Environment*, *114*(12), 2897-2910. https://doi.org/10.1016/j.rse.2010.07.008.

Khatami, R., Mountrakis, G., & Stehman, S. V. (2016). A meta-analysis of remote sensing research on supervised pixel-based land-cover image classification processes: General guidelines for practitioners and future research. *Remote sensing of environment*, *177*, 89-100. https://doi.org/10.1016/j.rse.2016.02.028

Kusimi, J. M. (2008). Assessing land use and land cover change in the Wassa West District of Ghana using remote sensing. *GeoJournal*, *71*(4), 249-259. https://doi.org/ 10.1007/s10708-008-9172-6.

Kusimi, J.M., 2008. Assessing land use and land cover change in the Wassa West District of Ghana using remote sensing. *GeoJournal*, *71*(4), pp.249-259.

Lein, J. K., & Lein, J. K. (2012). Object-based analysis. *Environmental sensing: analytical techniques for earth observation*, 259-278. https://doi.org/10.1007/978-1-4614-0143-8_11

Lifewatch-FWB: UCL- Geomatics, (2024). https://maps.elie.ucl.ac.be/Lifewatch/ecotopes_wal.html?lang=en&year=2018. Retrieved on 15th February, 2024.

Liu, C., Frazier, P., & Kumar, L. (2007). Comparative assessment of the measures of thematic classification accuracy. *Remote sensing of environment*, *107*(4), 606-616. https://doi.org/10.1016/j.rse.2006.10.010

Liu, X., Huang, Y., Xu, X., Li, X., Li, X., Ciais, P., & Zeng, Z. (2020). High-spatiotemporal-resolution mapping of global urban change from 1985 to 2015. *Nature Sustainability*, *3*(7), 564-570. https://doi.org/10.1038/s41893-020- 0521-x.

Lu, D., Mausel, P., Brondizio, E., & Moran, E. (2004). Change detection techniques. *International journal of remote sensing*, *25*(12), 2365-2401. https://doi.org/10.1080/0143116031000139863

Lunetta, R. S., Knight, J. F., Ediriwickrema, J., Lyon, J. G., & Worthy, L. D. (2022). Land-cover change detection using multi-temporal MODIS NDVI data. In *Geospatial Information Handbook for Water Resources and Watershed Management, Volume II* (pp. 65-88). CRC Press. https://doi.org/10.1201/9781003175025-5

MapBiomass. (2018). MapBiomas General "Handbook". Algorithm Theoretical Basis Document (ATBD). Collection 8-Version 1. https://brasil.mapbiomas.org/en/download-dos-atbds-com-metodo-detalhado/

Masiliūnas, D., Tsendbazar, N.E., Herold, M. and Verbesselt, J., 2021. BFAST lite: a lightweight break detection method for time series analysis. *Remote Sensing*, *13*(16), p.3308. https://doi.org/10.3390/rs13163308

Maxwell, A. E., & Warner, T. A. (2020). Thematic classification accuracy assessment with inherently uncertain boundaries: An argument for center-weighted accuracy assessment metrics. *Remote Sensing*, *12*(12), 1905. https://doi.org/10.3390/rs12121905

McInerney, D. O., & Nieuwenhuis, M. (2009). A comparative analysis of k NN and decision tree methods for the Irish National Forest Inventory. *International Journal of Remote Sensing*, *30*(19), 4937-4955. https://doi.org/10.1080/01431160903022936

Mellor, A., Haywood, A., Stone, C., & Jones, S. (2013). The performance of random forests in an operational setting for large area sclerophyll forest classification. *Remote Sensing*, *5*(6), 2838-2856. https://doi.org/10.3390/rs5062838

Mugiraneza, T., Nascetti, A. and Ban, Y., 2020. Continuous monitoring of urban land cover change trajectories with landsat time series and landtrendr-google earth engine cloud computing. *Remote Sensing*, *12*(18), p.2883. https://doi.org/10.3390/rs12182883

Mugiraneza, T., Nascetti, A., & Ban, Y. (2020). Continuous monitoring of urban land cover change trajectories with landsat time series and landtrendr-google earth engine cloud computing. *Remote Sensing*, *12*(18), 2883. https://doi.org/10.3390/rs12182883

Nagarajan, M., & Basil, G. (2014). Remote sensing-and GIS-based runoff modeling with the effect of land-use changes (a case study of Cochin corporation). *Natural hazards*, *73*, 2023-2039. https://doi.org/10.1007/s11069-014-1173-9

Nomura, K., & Mitchard, E. T. (2018). More than meets the eye: Using Sentinel-2 to map small plantations in complex forest landscapes. *Remote Sensing*, *10*(11), 1693. https://doi.org/10.3390/rs10111693

Olofsson, P., Foody, G. M., Herold, M., Stehman, S. V., Woodcock, C. E., & Wulder, M. A. (2014). Good practices for estimating area and assessing accuracy of land change. *Remote sensing of Environment*, *148*, 42-57. https://doi.org/10.1016/j.rse.2014.02.015

Peng, J., Liu, S., Lu, W., Liu, M., Feng, S. and Cong, P., 2021. Continuous change mapping to understand wetland quantity and quality evolution and driving forces: a case study in the Liao River estuary from 1986 to 2018. *Remote Sensing*, *13*(23), p.4900. https://doi.org/10.3390/rs13234900

Pérez-Cutillas, P., Pérez-Navarro, A., Conesa-García, C., Zema, D.A. and Amado-Álvarez, J.P., 2023. What is going on within google earth engine? A systematic review and meta-analysis. *Remote Sensing Applications: Society and Environment*, *29*, p.100907.https://doi.org/10.1016/j.rsase.2022.100907

Petit, C., Scudder, T., & Lambin, E. (2001). Quantifying processes of land-cover change by remote sensing: resettlement and rapid land-cover changes in south-eastern Zambia. *International Journal of Remote Sensing*, *22*(17), 3435-3456. https://doi.org/10.1080/01431160010006881

Phiri, D., Simwanda, M., Salekin, S., Nyirenda, V. R., Murayama, Y., & Ranagalage, M. (2020). Sentinel-2 data for land cover/use mapping: A review. *Remote Sensing*, *12*(14), 2291. https://doi.org/10.3390/rs12142291

Prabu, P., & Dar, M. A. (2018). Land-use/cover change in Coimbatore urban area (Tamil Nadu, India)—a remote sensing and GIS-based study. *Environmental monitoring and assessment*, *190*, 1-14. https://doi.org/10.1007/s10661-018-6807-z

Qian, J., Zhou, Q., & Hou, Q. (2007, August). Comparison of pixel-based and object-oriented classification methods for extracting built-up areas in arid zone. In *ISPRS workshop on updating Geo-spatial databases with imagery & the 5th ISPRS workshop on DMGISs* (Vol. 8, pp. 163-171). China: Urumchi, Xingjizng. https://doi.org/10.1007/978-3-030-72896-0_76

Quintero-Gallego, M. E., Quintero-Angel, M., & Vila-Ortega, J. J. (2018). Exploring land use/land cover change and drivers in Andean mountains in Colombia: A case in rural Quindío. *Science of The Total Environment*, *634*, 1288-1299. https://doi.org/10.1016/j.scitotenv.2018.03.359

R Documentation, 2024. https://www.rdocumentation.org/packages/bfast/versions/1.5.7/topics/bfastmonitor. Retrieved on 12th March, 2024.

Radoux, J., Bourdouxhe, A., Coppée, T., De Vroey, M., Dufrêne, M., & Defourny, P. (2022). A consistent land cover map time series at 2 m spatial resolution—the Lifewatch 2006-2015-2018-2019 Dataset for Wallonia. *Data*, *8*(1), 13. https://doi.org/10.3390/data8010013

Radoux, J., De Vroey, M., Coppée, T., Bourdouxhe, A., Dufrêne, M. and Defourny, P., Lifewatch-WB geodatabase (v3. 14): attribute description.

Rahman, A., Kumar, S., Fazal, S., & Siddiqui, M. A. (2012). Assessment of land use/land cover change in the North-West District of Delhi using remote sensing and GIS techniques. *Journal of the Indian Society of Remote Sensing*, *40*, 689-697. https://doi.org/10.1007/s12524-011-0165-4

Rawat, J. S., & Kumar, M. (2015). Monitoring land use/cover change using remote sensing and GIS techniques: A case study of Hawalbagh block, district Almora, Uttarakhand, India. *The Egyptian Journal of Remote Sensing and Space Science*, *18*(1), 77-84. https://doi.org/10.1016/j.ejrs.2015.02.002

reforestACTION, (2024). https://www.reforestaction.com/en/magazine/diversified-forest-wallonia. Retrieved on 2nd March, 2024.

Reiche, J., Verbesselt, J., Hoekman, D., & Herold, M. (2015). Fusing Landsat and SAR time series to detect deforestation in the tropics. *Remote Sensing of Environment*, *156, 276-293*. http://dx.doi.org/10.1016/j.rse.2014.10.001.

Reid, R. S., Kruska, R. L., Muthui, N., Taye, A., Wotton, S., Wilson, C. J., & Mulatu, W. (2000). Land-use and land-cover dynamics in response to changes in climatic, biological and socio-political forces: the case of southwestern Ethiopia. *Landscape Ecology*, *15*, 339-355. https://doi.org/10.1016/j.ecoser.2021.101338

Rodriguez-Galiano, V. F., Ghimire, B., Rogan, J., Chica-Olmo, M., & Rigol-Sanchez, J. P. (2012). An assessment of the effectiveness of a random forest classifier for land-cover classification. *ISPRS journal of photogrammetry and remote sensing*, *67*, 93-104. https://doi.org/10.1016/j.isprsjprs.2011.11.002

Rollins, M. G. (2009). LANDFIRE: a nationally consistent vegetation, wildland fire, and fuel assessment. *International Journal of Wildland Fire*, *18*(3), 235-249. https://doi.org/10.1071/WF08088.

Rondeux, J., Sanchez, C., & Latte, N. (2010). Belgium (Walloon Region). *National Forest Inventories: Pathways for Common Reporting*, 73-87. https://doi.org/10.1007/978-3-319-44015-6_8

Rosenfield, G. H., & Fitzpatrick-Lins, K. (1986). A coefficient of agreement as a measure of thematic classification accuracy. *Photogrammetric engineering and remote sensing*, *52*(2), 223-227. https://doi.org/10.14358/pers.72.7.823

Saxena, R., Watson, L. T., Wynne, R. H., Brooks, E. B., Thomas, V. A., Zhiqiang, Y., & Kennedy, R. E. (2018). Towards a polyalgorithm for land use change detection. *ISPRS journal of photogrammetry and remote sensing*, *144*, 217-234. https://doi.org/10.1016/j.isprsjprs.2018.07.002

Schneibel, A., Stellmes, M., Röder, A., Frantz, D., Kowalski, B., Haß, E., & Hill, J. (2017). Assessment of spatio-temporal changes of smallholder cultivation patterns in the Angolan Miombo belt using segmentation of Landsat time series. *Remote sensing of Environment*, *195*, 118-129. https://doi.org/10.1016/j.rse.2017.04.012

Sentinel Online, 2024. https://sentinel.esa.int/web/sentinel/user-guides/sentinel-2-msi/processing-levels/level2#:~:text=The%20Scene%20Classification%20%28SCL%29%20algorithm%20allows%20the%20detection,cloud%20shadows%2C%20vegetation%2C%20not%20vegetated%2C%20water%20and%20snow. Retrieved on 28th March, 2024.

SEPAL Cookbook, (2024). https://docs.sepal.io/en/latest/cookbook/ccdc.html. Retrieved on 28th February, 2024

Shelestov, A., Lavreniuk, M., Kussul, N., Novikov, A., & Skakun, S. (2017). Exploring Google Earth Engine platform for big data processing: Classification of multi-temporal satellite imagery for crop mapping. *frontiers in Earth Science*, 17. https://doi.org/10.3389/feart.2017.00017

Shen, P., Zhang, J., & Su, Z. (2011). The Application of Remote Sensing in the Extraction of Urban Iand Use Changes. *Procedia Environmental Sciences*, *10*, 1589-1594. https://doi.org/10.1016/j.proenv.2011.09.252

Shukla, P.R., Skeg, J., Buendia, E.C., Masson-Delmotte, V., Pörtner, H.O., Roberts, D.C., Zhai, P., Slade, R., Connors, S., Van Diemen, S. and Ferrat, M., 2019. Climate Change and Land: an IPCC special report on climate change, desertification, land degradation, sustainable land management, food security, and greenhouse gas fluxes in terrestrial ecosystems.

Stehman, S. V., Pengra, B. W., Horton, J. A., & Wellington, D. F. (2021). Validation of the US geological survey's land change monitoring, assessment and projection (LCMAP) collection 1.0 annual land cover products 1985–2017. *Remote sensing of environment*, *265*, 112646. https://doi.org/10.1016/j.rse.2021.112646

Svoboda, J., Štych, P., Laštovička, J., Paluba, D., & Kobliuk, N. (2022). Random Forest Classification of Land Use, Land-Use Change and Forestry (LULUCF) Using Sentinel-2 Data - A Case Study of Czechia. *Remote Sensing*, *14*(5), 1189. https://doi.org/10.3390/rs14051189

Tollerud, H. J., Zhu, Z., Smith, K., Wellington, D. F., Hussain, R. A., & Viola, D. (2023). Toward consistent change detection across irregular remote sensing time series observations. *Remote Sensing of Environment*, *285*, 113372. https://doi.org/10.1016/j.rse.2022.113372.

Verbesselt, J., Hyndman, R., Newnham, G., & Culvenor, D. (2010). Detecting trend and seasonal changes in satellite image time series. *Remote sensing of Environment*, *114*(1), 106-115. https://doi.org/10.1016/j.rse.2009.08.014

Verbesselt, J., Zeileis, A., & Herold, M. (2012). Near real-time disturbance detection using satellite image time series. *Remote Sensing of Environment*, *123*, 98-108. https://doi.org/10.1016/j.rse.2012.02.022

Weiss, M., Baret, F., & Jay, S. (2020). S2ToolBox Level 2 products: LAI, FAPAR, FCOVER.

Weng, Q. (2001). A remote sensing? GIS evaluation of urban expansion and its impact on surface temperature in the Zhujiang Delta, China. *International journal of remote sensing*, *22*(10), 1999-2014. https://doi.org/10.1080/713860788

Weng, Q., 2001. A remote sensing? GIS evaluation of urban expansion and its impact on surface temperature in the Zhujiang Delta, China. *International journal of remote sensing*, *22*(10), pp.1999-2014. https://doi.org/10.1080/713860788

Wessels, K. J., Prince, S. D., Frost, P. E., & Van Zyl, D. (2004). Assessing the effects of human-induced land degradation in the former homelands of northern South Africa with a 1 km AVHRR NDVI time-series. *Remote sensing of environment*, *91*(1), 47-67. https://doi.org/10.1016/j.rse.2004.02.005

Wu, L., Li, Z., Liu, X., Zhu, L., Tang, Y., Zhang, B., & Liu, B. (2020). Multi-type forest change detection using BFAST and monthly landsat time series for monitoring spatiotemporal dynamics of forests in subtropical wetland. *Remote Sensing*, *12*(2), 341. https://doi.org/10.3390/rs12020341

Wulder, M. A., Masek, J. G., Cohen, W. B., Loveland, T. R., & Woodcock, C. E. (2012). Opening the archive: How free data has enabled the science and monitoring promise of Landsat. *Remote Sensing of Environment*, *122*, 2-10. https://doi.org/10.1016/j.rse.2012.01.010

Yan, J., Wang, L., Song, W., Chen, Y., Chen, X., & Deng, Z. (2019). A time-series classification approach based on change detection for rapid land cover mapping. *ISPRS Journal of Photogrammetry and Remote Sensing*, *158*, 249-262. https://doi.org/10.1016/j.isprsjprs.2019.10.003

Yang, Y., Erskine, P. D., Lechner, A. M., Mulligan, D., Zhang, S., & Wang, Z. (2018). Detecting the dynamics of vegetation disturbance and recovery in surface mining area via Landsat imagery and LandTrendr algorithm. *Journal of Cleaner Production*, *178*, 353-362. https://doi.org/10.1016/j.jclepro.2018.01.050

Ye, S., Zhu, Z., & Cao, G. (2023). Object-based continuous monitoring of land disturbances from dense Landsat time series. *Remote Sensing of Environment*, *287*, 113462. https://doi.org/10.1016/j.rse.2023.113462

Yuan, F., Sawaya, K.E., Loeffelholz, B.C., Bauer, M.E., 2005. Land cover classification and change analysis of the twin cities (Minnesota) metropolitan area by multitemporal Landsat remote sensing. Remote Sens. Environ. 98, 317–328. https://doi.org/10.1016/j.rse.2005.08.006

Zhao, F., Huang, C., Goward, S. N., Schleeweis, K., Rishmawi, K., Lindsey, M. A. & Michaelis, A. (2018). Development of Landsat-based annual US forest disturbance history maps (1986–2010) in support of the North American Carbon Program (NACP). *Remote sensing of environment*, *209*, 312-326. https://doi.org/10.1016/j.rse.2018.02.035.

Zhu, L., Liu, X., Wu, L., Tang, Y., & Meng, Y. (2019). Long-term monitoring of cropland change near Dongting Lake, China, using the LandTrendr algorithm with Landsat imagery. *Remote Sensing*, *11*(10), 1234. https://doi.org/10.3390/rs11101234

Zhu, Z. (2017). Change detection using Landsat time series: A review of frequencies, preprocessing, algorithms, and applications. *ISPRS Journal of Photogrammetry and Remote Sensing*, *130*, 370-384. https://doi.org/10.1016/j.isprsjprs.2017.06.013

Zhu, Z., & Woodcock, C. E. (2014). Continuous change detection and classification of land cover using all available Landsat data. *Remote sensing of Environment*, *144*, 152-171. https://doi.org/10.1016/j.rse.2014.01.011.

Zhu, Z., Fu, Y., Woodcock, C.E., Olofsson, P., Vogelmann, J.E., Holden, C., Wang, M., Dai, S., Yu, Y., 2016. Including land cover change in analysis of greenness trends using all available Landsat 5, 7, and 8 images: a case study from Guangzhou, China (2000–2014). Remote Sens. Environ. 185, 243–257. http://dx.doi.org/10.1016/j.rse.2016.03.036

Zhu, Z., Qiu, S., & Ye, S. (2022). Remote sensing of land change: A multifaceted perspective. *Remote Sensing of Environment*, *282*, 113266. https://doi.org/10.1016/j.rse.2022.113266

Zhu, Z., Zhang, J., Yang, Z., Aljaddani, A. H., Cohen, W. B., Qiu, S., & Zhou, C. (2020). Continuous monitoring of land disturbance based on Landsat time series. *Remote Sensing of Environment*, *238*, 111116. https://doi.org/10.1016/j.rse.2019.03.009

Appendix

I. Definition of Six Different IPCC Land Categories

Types	Definitions
Forest land	This category includes all land with woody vegetation consistent with thresholds used to define forest land in the national GHG inventory, sub-divided into managed and unmanaged, and also by ecosystem type as specified in the IPCC Guidelines3. It also includes systems with vegetation that currently fall below, but are expected to exceed, the threshold of the forest land category.
Cropland	This category includes arable and tillage land, and agro-forestry systems where vegetation falls below the thresholds used for the forest land category, consistent with the selection of national definitions.
Grassland	This category includes rangelands and pasture land that is not considered as cropland. It also includes systems with vegetation that fall below the threshold used in the forest land category and are not expected to exceed, without human intervention, the threshold used in the forest land category. The category also includes all grassland from wild lands to recreational areas as well as agricultural and silvi-pastural systems, subdivided into managed and unmanaged consistent with national definitions.
Wetlands	This category includes land that is covered or saturated by water for all or part of the year (e.g., peatland) and that does not fall into the forest land, cropland, and grassland or settlements categories. The category can be subdivided into managed and unmanaged according to national definitions. It includes reservoirs as a managed sub-division and natural rivers and lakes as unmanaged sub-divisions.
Settlements	This category includes all developed land, including transportation infrastructure and human settlements of any size, unless they are already included under other categories. This should be consistent with the selection of national definitions.
Other land	This category includes bare soil, rock, ice, and all unmanaged land areas that do not fall into any of the other five categories. It allows the total of identified land areas to match the national area, where data are available.

II. Sample points

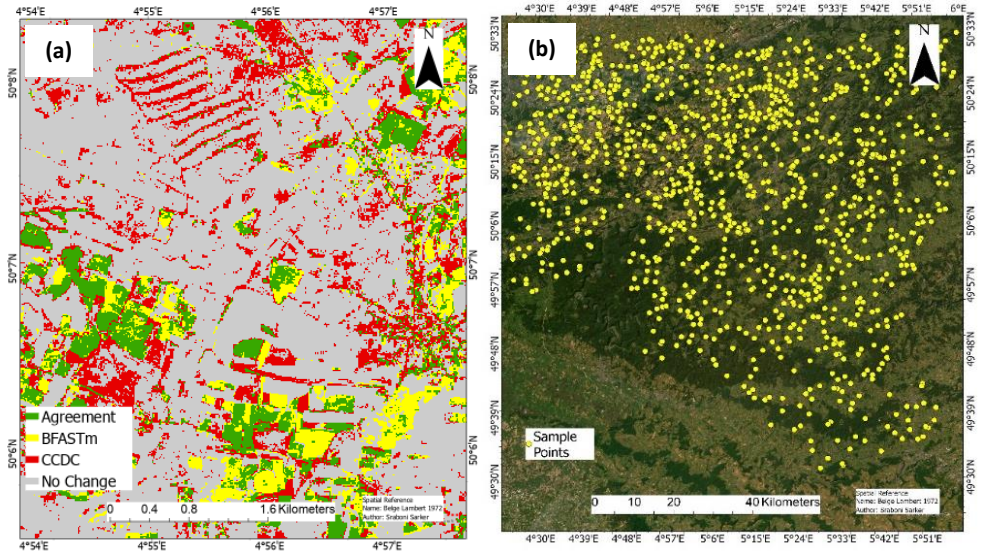

Figure 27: Map showing four different stratum (a), and sample points (b) for validation

Figure 27 shows 1228 sample points in four different stratum: 'Agreement' for both algorithms, 'BFASTm', 'CCDC' and 'No Change'.

III. Forest Land Change in Different Bands

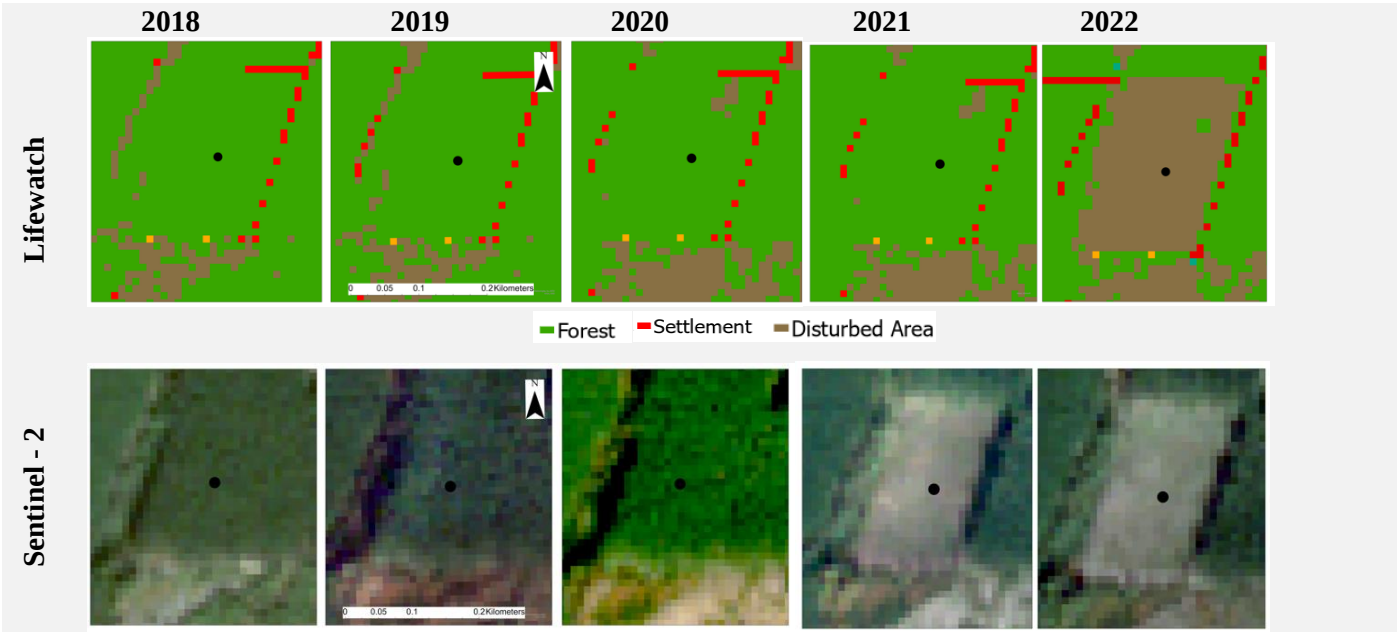

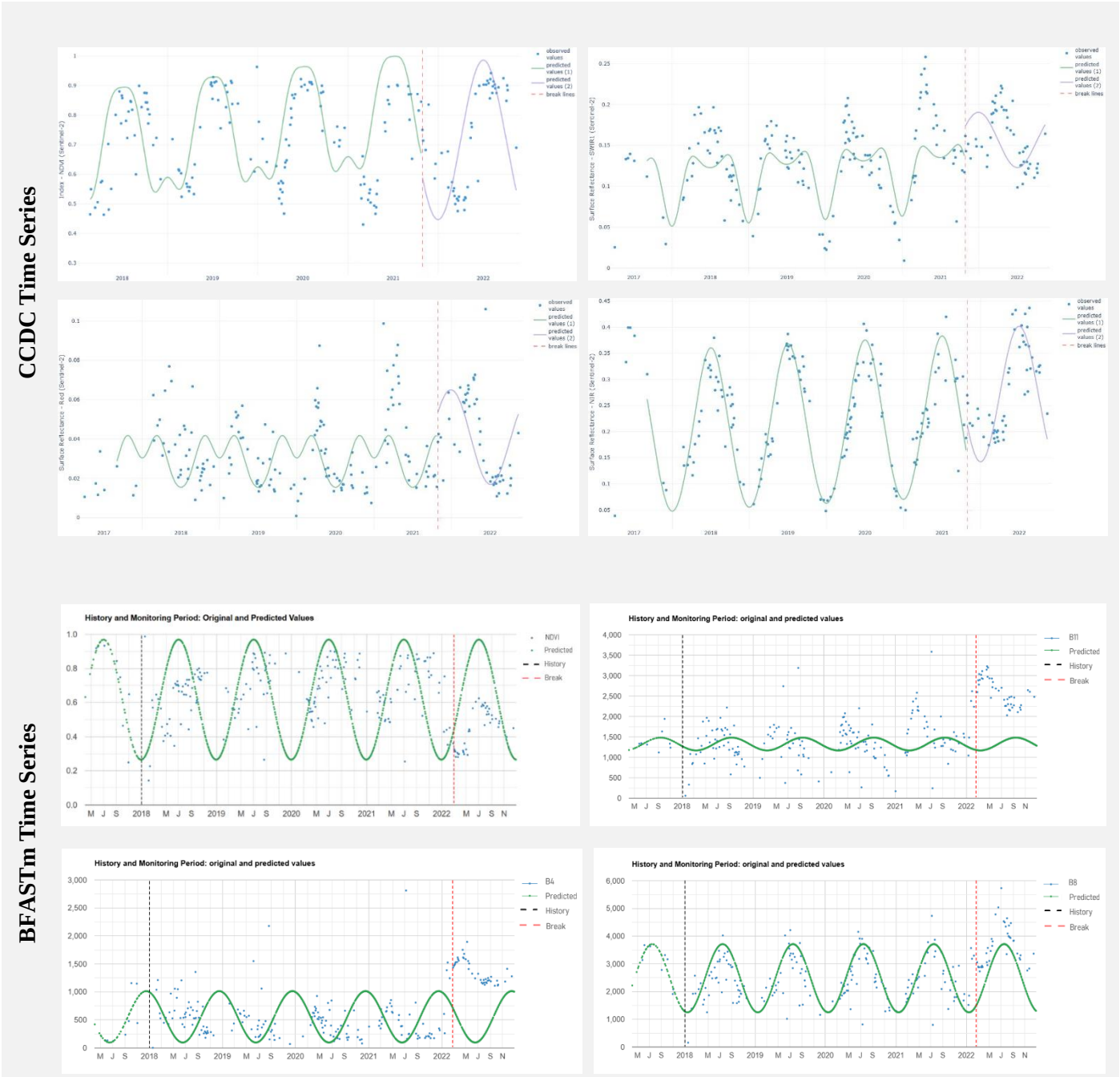

Figure 28: CCDC and BFASTm change detection algorithm comparison in cropland area based on Lifewatch data, Sentinel – 2 images, CCDC and BFASTm time series indicating a break in four different bands (NDVI, B4, B8, B11)

Assessing Land Use/Land Cover Change Detection Algorithms using Sentinel-2 Satellite Time Series from 2018 to 2022

Sraboni Sarker

Land Use and Land Cover (LULC) change detection algorithms are essential for monitoring environmental changes. This study evaluates the performance of two prominent algorithms, Continuous Change Detection and Classification (CCDC) and Breaks For Additive Season and Trend Monitor (BFASTm), in the Wallonia region of Belgium. All available Sentinel-2 images acquired between 2017 and 2022 were used. Changes were detected and analyzed across seven different LULC classes. A random stratified sample design was used for assessing the change detection accuracy with 1228 sample pixels. The performance of both algorithms was assessed using Lifewatch data from 2018 to 2022 as the reference dataset. CCDC proved to be effective for detecting changes in almost all land cover classes. It achieved a higher overall accuracy of 60%, accurately identifying true changes in 31% of cases. Conversely, BFASTm identified true changes in 26% of cases, with an overall accuracy of 55%. Both algorithms demonstrated strong performance in detecting changes in grassland areas while exhibiting the poorest performance in wetland regions. The two methods experienced a decline in performance due to high cloud cover, resulting in producing higher commission errors for change pixels, and temporal constraints related to the reference dataset. This study underscores the challenges of achieving high accuracy in cloud-prone regions like Wallonia and emphasizes the need to refine these algorithms to better handle the complexities of LULC change detection.

UNIVERSITÉ CATHOLIQUE DE LOUVAIN

Faculté des bioingénieurs

Croix du Sud, 2bte L7.05.01, 1348 Louvain-La-Neuve, Belgique | www.uclouvain.be/agro